ABSTRACT

Title of Thesis:	BIOELECTRONIC SENSOR FOR CELLULAR ASSAYS USING POLYELECTROLYTE MULTILAYER-MODIFIED ELECTRODES
	Geraldine Isabel Mijares, Master of Science, 2008
Thesis Directed By:	Associate Professor Donald L. DeVoe Department of Mechanical Engineering

Cell-based impedance biosensors provide non-invasive, quantitative, and instantaneous detection of cellular responses to applied stimuli. Extracellular matrix proteins, which degrade over time, are commonly used as cell adhesion promoters on planar electrodes, but decrease the lifetime of biosensors. In this work, the feasibility of using non-biological polyelectrolyte multilayers (PEMs) to facilitate cell attachment on titanium-tungsten alloy/gold electrodes for cell assays is investigated. The PEMs-modified electrode system is modeled as an equivalent electrical circuit and the addition of cells to the system is defined by their electrical properties. Electrode performance is characterized by cyclic voltammetry and impedance spectroscopy. The electrodes are found to have the ability to specifically probe non-faradaic processes and show a 15% increase in impedance due to cell proliferation. This thesis work demonstrates the use of PEMs-modified electrodes for the continuous monitoring of cell proliferation and for the future application of probing cell confluency in microfluidic cytotoxicity assays.

BIOELECTRONIC SENSOR FOR CELLULAR ASSAYS USING POLYELECTROLYTE MULTILAYER-MODIFIED ELECTRODES

By

Geraldine Isabel Mijares

Thesis submitted to the Faculty of the Graduate School of the
University of Maryland, College Park, in partial fulfillment
of the requirements for the degree of
Master of Science
2008

Advisory Committee:
Associate Professor Donald L. DeVoe, Chair
Professor William E. Bentley
Dr. Michael Gaitan

DEDICATION

To my family, for always giving me guidance and instilling in me the willingness to strive for the best. To my loved ones and friends, for their great support and encouragement.

ACKNOWLEDGEMENTS

I would like to thank my advisor, Professor Don L. DeVoe, for providing me the opportunity to be a part of the Maryland Microfluidics Laboratory and to complete this thesis work under his guidance. Thanks are also extended to Dr. Michael Gaitan and Dr. Jon Geist of the Semiconductor Electronics Division (SED) at the National Institute of Standards and Technology (NIST), for providing their expertise and technical insights during the duration of this work.

I would like to thank my friends and colleagues at NIST, especially Dr. Darwin R. Reyes, for the endless guidance and support throughout the years. Also, many thanks to Dr. Brian J. Polk, Dr. Jayna J. Shah, Dr. Pierre-Alain Auroux, Dr. Kristen L. Steffens, Dr. Kimberly A. Briggman, Dr. Louis P. Hromada, Jr., Angel Rivera, Dr. Christina A. Hacker, and Jennifer S. Hong, for all of the valuable discussions, efforts, or words of encouragement.

This work was supported by the NIST Innovations in Measurement Science Cellular Biometrology Program and the Electronics and Electrical Engineering Laboratory (EEEL) Director's Reserve Program for Bioelectronics.

TABLE OF CONTENTS

List of Tables vi

List of Figures vii

1 Introduction 1

1.1 Thesis Objective and Motivation 2

1.2 Conventional Cell Culture Techniques 4

1.2.1 Surface Biocompatibility 6

1.3 Cell Culture in Microfluidics 8

1.4 Thesis Organization 9

2 Background 11

2.1 Impedance Spectroscopy 12

2.2 Electrical Properties of the Cell 15

2.3 Measure of Cell Confluence Using Impedance Spectroscopy 18

2.4 Previous Work 21

2.5 Conclusion 24

3 Cell Confluence Detector 26

3.1 Fabrication of Electrodes 28

3.2 Cell Cultivation 29

3.3 Electrode Surface Preparation for Biocompatibility 31

3.3.1 Polyelectrolyte Multilayer Formation 31

3.3.2 Surface Treatment Characterization 33

3.3.3 Cellular Response to PEMs versus Bare Gold 38
3.4 Electrical Equivalent Circuit 41
3.5 Electrode Characterization 46
3.5.1 Electrode Performance versus Ionic Concentration 47
3.5.2 Interbatch and Intrabatch Variability 50
3.5.3 Cyclic Voltammetry 52
3.6 Conclusion 60

4 Cellular Proliferation Measurements 62
4.1 Impedance Monitoring 62
4.1.1 Determination of Optimal Frequency 64
4.2 Quantification of Cells 65
4.3 Cell Confluency Monitoring 68
4.3.1 Impedance Data Normalization 75
4.3.2 Comparison with Electrical Equivalent Circuit Model 78
4.3.3 Correlation of Impedance with Cell Confluency 84
4.4 Conclusion 86

5 Conclusions and Future Work 89
5.1 Significant Contributions 92
5.2 Future Work 93

A Biocompatible Electrode Materials 95

B Student's *t*-Test Calculations 100

LIST OF TABLES

3.1 Summary of contact angle measurements obtained from various surface treatments……..37

3.2 Summary of measured DMEM double layer capacitance values of forward and reverse CV scans on unmodified and PEMs-modified electrodes……54

3.3 Anodic and cathodic peak potentials of $[Fe(CN)_6]^{3-/4-}$ for unmodified and PEMs-modified electrodes……...59

4.1 Parameter values obtained by fitting the impedance data of cell-free DMEM to the equivalent circuit…….82

4.2 CPE parameter values obtained by fitting the impedance data of unmodified electrodes with DMEM + cells over time to the equivalent circuit……..…83

4.3 CPE parameter values obtained by fitting the impedance data of PEMs-modified electrodes with DMEM + cells over time to the equivalent circuit……..84

B.1 Example calculations of *t*-test difference values for a factor-of-two change in ionic solution concentration measured with PEMs-modified electrodes at low frequencies……..101

B.2 Summary of calculated *t*-values for unmodified and PEMs-modified electrode performance in solutions with varying ionic concentration differences……102

B.3 Summary of calculated *t*-values for unmodified electrode variability within the same and fabrication batches……..…103

B.4 Table of selected *t*-distributions……..…104

LIST OF FIGURES

1.1 Overview of bioelectronics……...2

1.2 An example of conventional cell culture techniques utilized for cell assays…...5

2.1 Bode plot of a purely resistive element……...13

2.2 Bode plot of a purely capacitive element……....14

2.3 Bode plot of a purely inductive element……...…..14

2.4 Diagram of altered current flow from cells and aqueous gaps as a result of focal adhesions…….16

2.5 Equivalent electrical circuit of the impedance sensor with cells on sensor surface…..……..……..18

2.6 Illustration of the basic concept of impedance spectroscopy as a means to measure cell confluence……...…….……..19

3.1 Top-down view of the electrode design…….…….27

3.2 3-D schematic and photograph of fabricated device……...……27

3.3 Fabrication schematic for device fabrication……..30

3.4 PEMs formation for gold electrode surface biofunctionalization……...…31

3.5 Chemical structures of polyelectrolytes, PEI, PSS, and PAH……32

3.6 Two-dimensional AFM height measurements…….…...34

3.7 Transmission IR spectra of gold surfaces with adsorbed PEI and adsorbed PEI(PSS/PAH)$_5$…….…..36

3.8 Viability assay results of NIH-3T3 fibroblast cells 72 hours after inoculation……..…….39

3.9 Cell spreading and nuclear morphology comparison of NIH-3T3 fibroblast cells……..…….……..41

3.10 Equivalent electrical circuit for a two-electrode system immersed in an electrolyte solution…….…….42

3.11 Reduced equivalent electrical circuit of cell confluence detector in cell-free media……...43

3.12 Equivalent electrical circuit of the cell confluence detector in cell-free media.……..……44

3.13 Equivalent electrical circuit of the cell confluence detector with the addition of cells in media……..……45

3.14 Equivalent electrical circuit that takes into account the electrical properties of the addition of PEMs……..46

3.15 Magnitude of impedance as a response to air, deionized water, and solutions with varying ionic concentrations…….…..49

3.16 Magnitude of impedance and phase shift of six devices filled with a physiological concentration of PBS to test for interbatch and intrabatch variability……51

3.17 Cyclic voltammograms of electrodes in DMEM at room temperature……...53

3.18 Determination of double layer capacitance of electrodes in DMEM at room temperature…….....55

3.19 Electrode active area region configuration at two stages of PEM film growth…….56

3.20 Cyclic voltammograms of electrodes in PBS and $[Fe(CN)_6]^{3-/4-}$ in PBS with respect to Ag/AgCl (sat. KCl) or gold reference electrodes at a scan rate of 50 mV/sec……..…..58

4.1 Example Bode plot of the impedance of cell-free media and cells that began to flatten onto the electrode surface four hours after inoculation……...…63

4.2 NIH-3T3 fibroblast cells growing 48 hours after inoculation……66

4.3 Cell density graphs of NIH-3T3 fibroblast cells…….67

4.4 Impedance analyzer instrumentation and setup for the characterization of cell confluence detector device…….….69

4.5 Phase contrast images of NIH-3T3 fibroblast cells on the device prior to and after exposure to 0.25% trypsin……..71

4.6 Magnitude of impedance of NIH-3T3 fibroblast cell growth at 1000 Hz……..72

4.7 Normalized magnitude of impedance against t = 0 hours at 1000 Hz……76

4.8 Reproducibility of three different unmodified and PEMs-modified electrode devices each……77

4.9 Bode plot of theoretical equivalent circuit model data fitted against recorded experimental data of unmodified electrode devices in cell-free media and with NIH-3T3 fibroblast cells at t = 72 hours……...…..79

4.10 Bode plot of theoretical equivalent circuit model data fitted against recorded experimental data of PEMs-modified electrode devices in cell-free media and with NIH-3T3 fibroblast cells at t = 96 hours…….....80

4.11 Normalized magnitude of impedance as a function of NIH-3T3 fibroblast cell density…….....85

A.1 XPS spectra of sample surface analysis……..96

A.2 Differential interference contrast images……..……..97

A.3 Effect of metal adhesion layer for Au electrodes……97

A.4 Impedance measurements at 10 Hz of mammalian cell growth until 48 hours after inoculation……..98

CHAPTER 1

INTRODUCTION

Bioelectronics is an interdisciplinary field of study that combines the areas of biology, chemistry, physics and engineering. It is a very broad research subject that has scientific and practical importance in medicine, high-tech industry, military, and homeland security applications [1]. The study of biosensors alone plays its part in health care, pharmaceuticals, food and process control, environmental monitoring, and defense and security [2]. Bioelectronic platforms integrate biological materials, such as proteins, enzymes, antigens and antibodies, DNA, and whole cells, with electronic elements, such as electrodes, field-effect transistors, and piezoelectric crystals [3], as illustrated in Figure 1.1. This interfacing of biomolecules with electronic devices is used to transduce biological signals into electronically readable signals. For that to be accomplished, it is essential that the interface between the biological and electronic systems is effective with the immobilization of the biocomponents onto the surface of the electronic device in order to produce an effective electron transfer between biomolecules and a conductive support [1].

Lab-on-a-chip (LOC) devices are used to study the characteristics of single cells or a group of cells and their responses to different stimuli and therefore, advances the field of bioelectronics [4-9]. LOC devices are utilized as micro total analysis systems to increase the speed and efficiency of biological and chemical assays while reducing sample and reagent consumption [10-12] by minimizing the losses by incorporating multiple process steps in series [13-16]. Examples of increased speed and efficiency of

LOC developments include advancements in capillary electrophoresis [17, 18], liquid chromatography [10, 19], PCR [20], and DNA analysis [21, 22]. With a decrease in sample and reagent consumption and shorter fluid transport times due to length scales on the order of micrometers or nanometers, high-throughput performance are achieved.

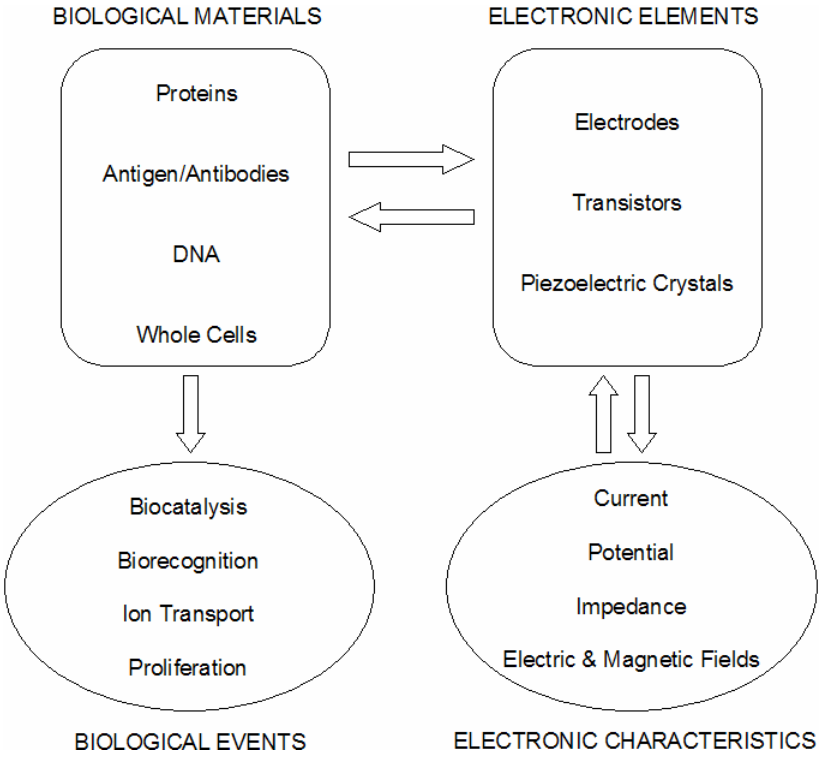

Figure 1.1 Overview of Bioelectronics. It is essential to properly interface biological materials with electronic elements to monitor biological events by the interpretation of applied and recorded electronic characteristics. Adapted from [3].

1.1 Thesis Objective and Motivation

The main objective of this thesis work is the design, fabrication, and characterization of a cell confluence detector consisting of underlying optically-transparent titanium-tungsten/gold (TiW/Au) electrodes to monitor cell growth by

measuring impedance. The surface of this microscale cell culture chamber is modified with polyelectrolyte multilayers (PEMs) in order to promote increased cell adhesion throughout the entire chamber. The use of these PEMs is investigated for its feasibility in obtaining impedance measurements during cell growth. As cells attach to and proliferate on the surface of the electrodes within a PDMS reservoir, the magnitude of the impedance increases. Optically-transparent electrodes allow for the continuous monitoring of cell growth with the use of an inverted microscope with cell incubation abilities.

The development of a cell confluence detector within a microfluidic system will aid in the design of a LOC for the purposes of cellular assays, such as cytotoxicity assessments. It will provide a closed environment for culturing and isolating single cells or a small group of cells and will also provide a fine control over the microenvironment surrounding the cells. It is envisioned that after one culture pass, some of the cells will flow into another microchamber to continue the cell culture for future assays on the same microfluidic chip. When incorporated onto a platform for single cell or cell colony assays, a microscale cell culture chamber with an electronic cell confluence detector will allow for more rapid testing and high-throughput results. This is achieved through the integration of cell sample preparation and analysis on a single automated platform instead of handling the cells on the traditional, macroscale level with their addition to a microsystem manually.

1.2 Conventional Cell Culture Techniques

The cultivation of cells *in vitro*[1] offers a way to study the responses of particular cells types to stimuli of interest. Cellular biological studies provide information on intracellular activity [23], intracellular flux [24], environmental interaction [25], cell-cell interaction [26], and genetics [27]. These investigations provide important information that leads to significant contributions in medical research towards the production of antiviral vaccines, in pharmaceuticals with the reduction of animal use in the cytotoxicity and screening of pharmaceutics, cosmetics, etc., and in human genetics [28].

Current cell biological studies are carried out in traditional Petri dishes, culture flasks, or on microscope slides. Traditional cell culture methods are well-established protocols that require large, specialized equipment to provide the correct aseptic physicochemical environment. An incubator provides an environment where temperature, humidity, and carbon dioxide (CO_2) levels are controlled to the optimal conditions that support cell growth. Conventional cell culture techniques also require a laminar-flow hood to carry out procedures aseptically during cell passage or harvesting. Once the cells are ready for passage or harvesting, a centrifuge is used to isolate the cells detached from the substrate in the supporting media. Along with the necessary, yet bulky, equipment, traditional techniques also require cell cultures to have the correct physiological environment by receiving a supplementation of media and growth factor-containing serum to provide the essential nutrients to the cells.

In order to study the responses of a cell to certain stimuli, an understanding of how the cellular components, e.g. organelles or large molecules, respond as a function of

[1] *In vitro*, which literally means "within the glass," refers to performing a technique in a controlled environment outside of a living organism.

that stimulus is required and accomplished through biochemical analysis. Most biochemical procedures utilize conventional cell culture techniques (Figure 1.2) and require obtaining large number of cells and then physically disrupting them to isolate their components. Another way to study the cellular response is to view the cells under a microscope, usually with a fluorescent dye to visualize viability or cellular metabolism, while the effects of adding or removing specific molecules or stimuli is examined. Therefore, conventional cell culturing techniques for cell assays require the handling and treatment of cell cultures combined with the use of large specialized equipment. This leads to a laborious line of procedural tasks, all of which results in cellular analysis being very time consuming.

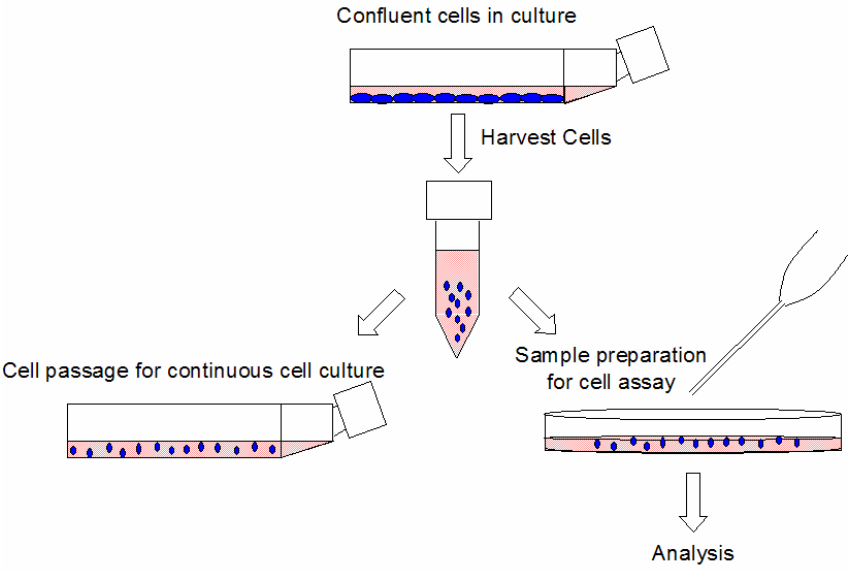

Figure 1.2 An example of conventional cell culture techniques utilized for cell assays. Cells are cultured until a confluent layer is achieved, at which point they are harvested to either continue the cell culture or to be chemically prepared for the desired cell assay. The analysis of the test is completed at a desired time point.

In particular, there are cytotoxicity assays that utilize numerous laboratory tools and a laborious procedure to investigate and assess whether or not the exposure of a compound, e.g. drugs, cosmetics, or food additives, results in direct cellular damage or negative systemic and/or physiological effects at the cellular level. An estimation of viability can be assessed by, for example, the use of a microtitration assay, which requires the cultivation of cells onto multiwell plates and the addition of a drug or toxin at certain concentrations for a specified amount of time. The toxin is then removed and the cells are allowed to recover before the survival estimation is determined. One specific example of a cytotoxicity assay is the MTT (3-[4, 5-dimethyl-thiazol-2-yl]-2, 5-diphenyl-tetrazolium bromide) reduction, which requires a fluorescence microscope. MTT is a yellow water-soluble tetrazolium dye that is reduced by live cells to produce a purple formazan product that is insoluble in aqueous solutions. This MTT assay is an example of a lengthy procedure that employs conventional cell culturing techniques for cellular assays.

1.2.1 Surface Biocompatibility

Along with providing the correct physicochemical and physiological environments to the cells to ensure cell survival and to support normal cell growth, it is essential that the substrate the cells attach to be biocompatible and promote cell adhesion. Adhesion begins with the secretion of extracellular matrix (ECM) proteins and proteoglycans. They are then recognized by specific cell surface receptors, i.e. integrins. The ECM adheres to a charged substrate, and the cells, in turn, bind to the matrix via cell surface receptors, which ties the matrix to the cytoskeleton of the cell [28, 29].

Single-use sterile polystyrene culture dishes or flasks are routinely used in conventional cell culture techniques. As manufactured, polystyrene is hydrophobic and is not a suitable surface for cell growth. Therefore, tissue culture plastics are treated in various ways to produce a charged, wettable surface. This is accomplished by subjecting the substrate to γ-irradiation, an electric ion discharge, chemically, or by treating the surface with a constituent of the ECM [28, 30]. Therefore, any substrate, whether glass or plastic, that is pretreated with ECM constituents, such as fibronectin, collagen, elastin, laminin, or other derivatives, provides a surface to facilitate cell attachment and proliferation.

The problem with using matrix proteins to render substrates biocompatible is their ability to degrade over time due to the biological peptide bonds. This can be remedied with the use of polyelectrolyte multilayers (PEMs), which are stable non-biological thin film layers. They are assembled by a simple aqueous process involving the alternate adsorption of oppositely-charged, non-biological polymers through electrostatic interactions [31]. PEMs are used in a large number of systems including those for *in vivo*[2] biomedical applications [32], biosensors for immunosensing [33, 34], electroosmotic flow control in microfluidics [35, 36], and selective cell patterning [37-39]. Polyelectrolyte multilayers are excellent for modifying a surface to promote cell adhesion because of its ability to control the thickness of the films and their molecular architecture with pH and ionic concentration. PEMS are also excellent to incorporate biomolecules, such as proteins or enzymes, into the layers without the loss of their functionality.

[2] *In vivo*, which literally means "within the living," refers to performing a technique within a living organism.

1.3 Cell Culture in Microfluidics

There are several advantages for culturing cells for cellular assays in a microfluidic environment versus traditional methods. Conventional cell culture technology essentially requires large cell culture surfaces, bulky and expensive equipment, large fluid volumes, and an extensive amount of human labor. If cellular assays are performed wholly on an LOC device, the time required for cellular analysis is greatly reduced because of the ability of the cells to be cultured, manipulated, and analyzed all on-chip. This decrease in the time for cell handling, sample preparation, and analysis allows small cell populations or single cells to be probed inexpensively and at high-throughput. In addition, low sample size and reagent usage within a microfluidic system is another benefit to increase the efficiency and productivity of results, as well as reducing process costs. The use of microfluidic platforms also allows for the discerning control of the microenvironment surrounding the cells by defining precise solute concentrations and volumes, flow rates of media and other solutions, and the specific delivered location of nutrients or toxins within the microchannel network [40]. Also, these platforms can finely control the addition of ECM proteins or other cell adhesive materials for selective cell patterning [41].

Microfabrication techniques commonly used in the semiconductor industry, such as photolithography and micromachining, allow for the development of miniaturized bioanalytical devices [42, 43] to make electrical measurements [44] and electrochemical detections [45] on biological systems. Other examples of bioelectronic applications include bioaffinity interaction assays [46, 47] and DNA amplification and electrophoretic separations [48-50].

Since some of the substrates of microfabricated devices are bioinert materials commonly used in the microelectronics industry, it is necessary to modify the surfaces to make them biocompatible to allow for cell attachment, growth, and survival. Such processes to render surfaces biocompatible are the same as in conventional cell culture techniques. Examples of these processes include the application of cell adhesion proteins [51, 52], or other non-biological materials, such as polyelectrolyte multilayers (PEMs) [37, 39] onto the substrate surface to induce cell adherence by mimicking the natural ECM. Small populations of cells or single cells can then attach, proliferate, and survive on the treated surfaces of various substrates while biological or electronic analysis is conducted.

1.4 Thesis Organization

This thesis is organized into five chapters and two appendices. Chapter 1 provides a brief introduction to the field of BioMEMS and LOC devices involving bioelectronic measurements. It also describes conventional cell culturing and surface biocompatibility techniques for cellular assays, culturing cells in microfluidic networks for cellular assays, and an introduction to this thesis work. Chapter 2 introduces the concept of electrical impedance measurements by providing general information on impedance spectroscopy and the electrical properties of the cell that make it susceptible to impedance measurements. The third chapter presents a bioelectronic cell confluence detector utilizing optically-transparent electrodes to be incorporated within a microscale cell culture chamber for the goal of performing analysis on a group of cells or single cells. The polyelectrolyte multilayer formation on the electrode surface is introduced and

a comparison of cell viability and morphology on the PEMs-modified device versus a traditional cell culture flask is completed. The chapter also includes a discussion on the equivalent electrical circuit of the system including the cells with and without a PEMs layer. In addition, the performances of unmodified and PEMs-modified electrodes are characterized by impedance spectroscopy and cyclic voltammetry. The fourth chapter presents the results of the cellular proliferation measurements recorded by the fabricated electrodes. A procedure for monitoring impedance, as well as the quantification of the cells growing on the surface, is introduced. Also, the impedance data is fitted to and compared with the equivalent electrical circuit model proposed in the previous chapter. Finally, Chapter 5 includes concluding remarks, significant contributions, and suggestions for future work.

CHAPTER 2

BACKGROUND

When biological cells are cultured with the necessary nutrients and environmental conditions, they properly attach to the surface and normal cell function is able to occur. The goal of studying cells and their reactions is to gain a complete understanding of what takes place in a cell as it responds to its environment and/or interacts with neighboring cells. Continuous observation under a microscope can be made or the cells can be analyzed biochemically in order to examine the effects of adding or removing specific molecules, such as toxins or hormones.

A cell-based assay that is of particular interest today is one that tests for cytotoxicity. It is essential to determine and detect the functional characteristics of the drugs, pathogens, or toxicants being tested. This is accomplished in a number of techniques, such as metabolic assays that measure dehydrogenase activity or DNA, RNA, or protein synthesis, survival assays that measure the long-term retention of the capacity of the cells to regenerate, and short-term toxicity assays, otherwise known as viability tests, which examines the immediate cellular response to the change in environment [28]. The quick, convenient, and easy viability assays reveal cells that are dead at the time of the assay and normally rely on the breakdown in membrane integrity that is determined either by the uptake of a dye normally impermeable or the release of a dye normally taken up and metabolized by viable cells.

The use of cell-based impedance biosensors is an alternative way to detect cell viability by monitoring cell attachment and surface coverage when cells proliferate. If

cells are subjected to an internal or external stimulus that alters their health and function negatively, then the adherent cells will begin to detach from the surface they are cultured on. Cell-based impedance biosensors interface living biological cells with electrodes and utilize them as a non-invasive, quantitative, and instantaneous way to detect and analyze cellular responses and physiological changes caused by a chemical, biological or other type of applied stimuli [53]. To detect changes in cell behavior, the impedance is measured as a change in the electrical signal at the contact between an adherent cell and the electrode. This results in the observation of cellular mechanisms, such as attachment, spreading, growth, motility, and death, due to the effect of external agents on the cells.

2.1 Impedance Spectroscopy

Electrical resistance is the ability of a circuit element to resist the flow of a direct electrical current. It is defined by Ohm's law as the ratio of voltage (V) to the flow of current (I) allowed (Equation 2.1). This measure of resistance is limited to the one circuit element of an ideal resistor. An ideal resistor follows Ohm's law at all current and voltage levels, its value is independent of frequency, and AC current and voltage signals through a resistor are in phase with each other [54].

$$R = \frac{V}{I} \qquad \text{(Equation 2.1)}$$

However, non-ideal circuit elements exhibit more complex behavior. Thus, impedance is used and is a measure of the apparent resistance to the flow of an alternating current applied to an electrical circuit. Unlike resistance, impedance is not limited by the properties listed in the previous paragraph.

Impedance is commonly measured in the frequency domain by applying a single-frequency voltage to the electrical circuit and measuring the phase shift and amplitude, or the real and imaginary parts, of the resulting current at that frequency [55]. The voltage and current of the circuit is expressed as a complex number having a specific magnitude and phase angle measured relative to the input signal of the circuit. This is used to represent the real physical value of voltage or current [42]. The complex impedance values of a resistor, capacitor, and inductor in a circuit is shown in Equations 2.2, 2.3, and 2.4, respectively, where R = resistance, $j = \sqrt{-1}$, ω = frequency, C = capacitance, and L = inductance.

$$Z_R = R \qquad \text{(Equation 2.2)}$$

$$Z_C = \frac{1}{j\omega C} \qquad \text{(Equation 2.3)}$$

$$Z_L = j\omega L \qquad \text{(Equation 2.4)}$$

The impedance of a resistor is independent of frequency and has only a real component. Since there is no imaginary impedance, the current through the resistor has a phase shift of 0° with respect to the voltage (Figure 2.1).

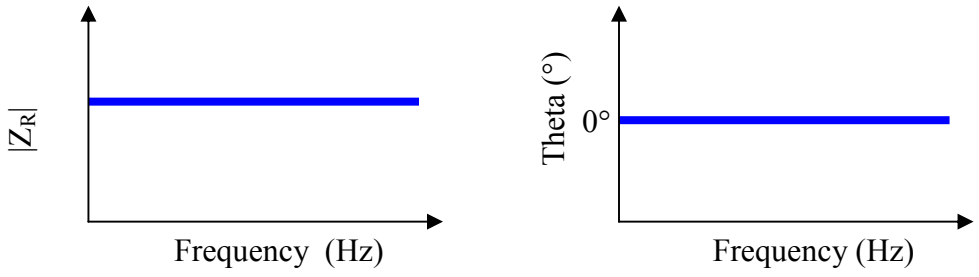

Figure 2.1 The corresponding Bode plot of a purely resistive element.

The impedance of a capacitor decreases as frequency increases. Capacitors only have an imaginary impedance component. The current through a capacitor has a phase shift of –90° with respect to the voltage (Figure 2.2).

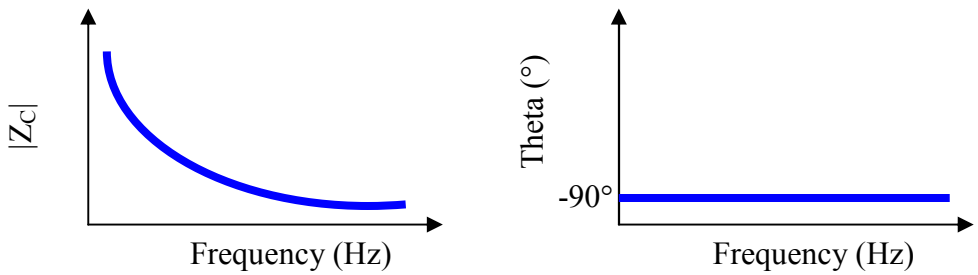

Figure 2.2 The corresponding Bode plot of a purely capacitive element.

The impedance versus frequency behavior of an inductor is opposite to that of a capacitor, in that it increases as the frequency increases. Inductors also only have an imaginary impedance component and, as a result, its current has a phase shift of 90° with respect to voltage (Figure 2.3).

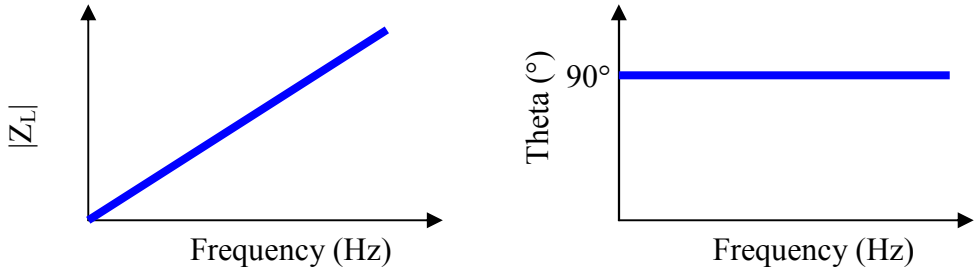

Figure 2.3 The corresponding Bode plot of a purely inductive element.

The data from impedance measurements are represented by a Bode plot that graphs the magnitude of impedance vs. frequency ($|Z(j\omega)|$ vs. f) and the phase angle vs. frequency ($\angle Z(j\omega)$ vs. f). A Nyquist plot is constructed by plotting the real and imaginary parts of impedance in the complex plane using frequency as a plotting parameter.

2.2 Electrical Properties of the Cell

An immobilized cell on an electrode impedes the electrical current flow from the electrode and into the bulk electrolyte [56]. This occurs because the cell anchors itself to the electrode surface via transcellular membrane proteins. As shown in Figure 2.4, The current flow is dispersed through any narrow cell-substrate junctions, in addition to any spaces in between neighboring cells [57]. An individual cell or group of cells can be expressed in terms of electrical impedance elements, in particular resistors and capacitors, because of its influence to impede current flow, thereby affecting the resulting measured electrical signal.

Impedance measurements conducted on living cells depend on the properties of the cell membrane. The cell membrane is the essential component that provides a barrier for the cell and its surroundings, which are very different from each other in terms of composition, structure, and electric potential. It is, therefore, the origin of the principle of the bioelectric effects of the cell [58].

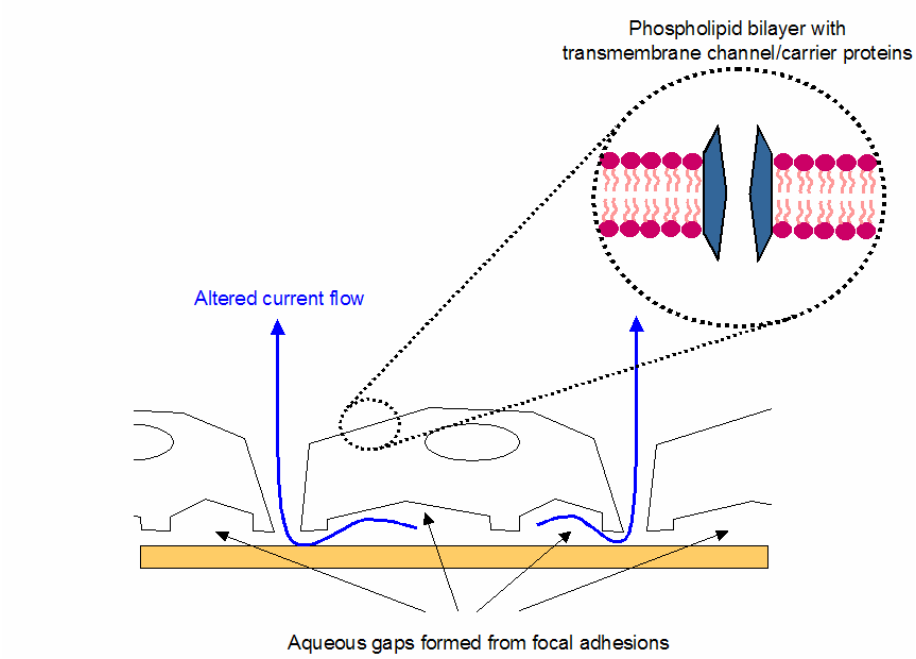

Figure 2.4 Diagram of altered current flow from cells and aqueous gaps as a result of focal adhesions. The inset picture illustrates the cell plasma membrane, which consists of a phospholipid bilayer with embedded proteins to allow the transport of molecules across the cell surface.

Cells exhibit excellent insulating properties at low frequencies. This insulating property is due to their ability to act as dielectrics because of the cell membrane phospholipid bilayer configuration [59]. This configuration consists of a lipid bilayer with proteins embedded within it, as shown in Figure 2.4. The polar hydrophilic lipid head groups are charged and are in contact with the surrounding medium, while the non-polar hydrophobic tails of each layer are uncharged. The association of these two components together creates the lipid bilayer and allows it to act as an electrical dielectric insulator.

In addition, biological cells are very poor conductors at low frequencies below 10 kHz and, therefore, force electrical currents to bypass them [60]. This resistance to

current flow occurs because, as illustrated in Figure 1.2, cells attach to the electrode surface via transmembrane surface receptors, i.e. integrins, which bind to ECM proteins. The ECM proteins are either secreted by the cell or added to the substrate surface to make it susceptible for cell adhesion. The binding of the receptor proteins to the ECM creates focal adhesion areas [29], and as a result, an aqueous gap between the cell membrane and substrate is produced. These gaps allow electric current to flow underneath the cell from the electrode and into the bulk electrolyte.

At higher frequencies greater than 10 kHz, the cells are represented as resistive elements. This is due to the current capacitively coupling through individual cell membranes [61] and, as a whole, through the cell layer by the way of transcellular pathways [62]. A function of the cell membrane is to allow the transport of essential ions in and out of the cell for its survival. The ability of ion permeability suggests that cell membranes offer a conductance, or resistive, contribution to impedance measurements. The resting potential and the conductance of the membrane are both functions of the ion permeability [58].

A whole cell can be represented as the simple equivalent circuit shown in Figure 2.5. Because of the dielectric properties of cell membranes resulting in a capacitive characteristic, the capacitor element is placed in the equivalent circuit. The capacitor represents the phospholipid bilayer and intracellular volume of the cell exposed to an applied AC signal with an intermediate frequency range between 10 Hz and 10 kHz. A resistive component is in parallel with the capacitor. The resistance is due to integrins creating pockets of culture media, which is the conducting electrolyte in the system, as a result of the presence of focal adhesion areas. These aqueous gaps allow electrical

current to flow in between the electrode surface and the cell, where the flow of ionic current into the bulk electrolyte is inhibited.

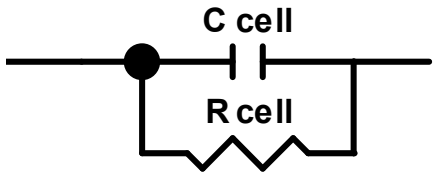

Figure 2.5 Equivalent electrical circuit of the impedance sensor with cells on sensor surface. C_{cell} represents the capacitance due to the cell membrane. R_{cell} represents the resistance of current flow due to the focal adhesions producing aqueous gaps in between the electrode and cell surfaces.

2.3 Measure of Cell Confluence Using Impedance Spectroscopy

The basis of using impedance spectroscopy on living cells depends on the electrical properties of their cell membranes at the intermediate frequencies between 10 Hz and 10 kHz. In this frequency range, the cells are regarded as insulating elements that restrict the resulting AC current flow to areas underneath and in between the cells. This hindrance of flow changes the effective electrode impedance. As a result of culturing cells over electrode contacts, cell adhesion, spreading, and mortality are monitored and therefore, utilized for cytotoxicity assays.

Figure 2.6 illustrates the basic concept of using impedance spectroscopy as a tool to measure cell confluence with a constant applied AC potential. As shown in Figure 2.6A, when cells are absent, the AC signal flows unhindered from the working electrode (WE) and into the bulk electrolyte, where the signal is detected by the counter electrode (CE). However, when cells are seeded onto the device and allowed to adhere, grow and multiply over the electrode surface (Figure 2.6B), the electrode begins to become covered

by the cells. This results in the applied signal being restricted to flow in the areas underneath and in between the cell layer. The altered flow from the working electrode to the bulk electrolyte is detected by the counter electrode as an increase in the overall impedance value.

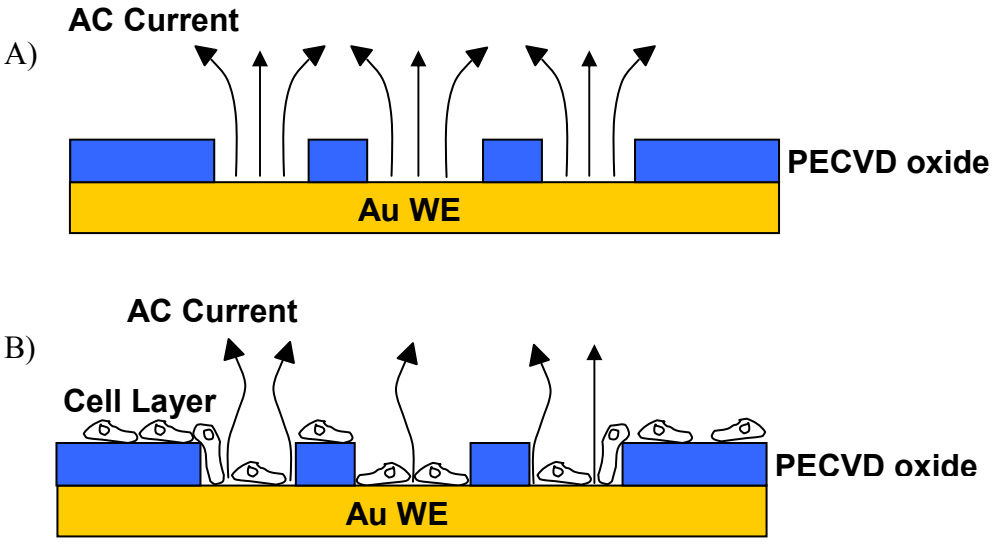

Figure 2.6 Illustration of the basic concept of impedance spectroscopy as a means to measure cell confluence. A) Unhindered AC signal flow due to the absence of cells on the electrode surface. B) Altered signal flow due to the presence of cells on the electrode. The cells cause the current to flow underneath and in between neighboring cells. Diagram not drawn to scale. Adapted from Applied Biophysics, Inc.

Impedance measurements conducted at the proper intermediate frequency for the designed electrode system (how to choose the correct frequency is discussed in Chapter 4) must follow the following requirements:

1. A difference between live and dead cells, more specifically attached and unattached cells, must be observable;

2. If the cells are subjected to any applied stimulus that affects cell growth either negatively or positively, then it should be detected due to changes in cell shape or attachment;
3. Any change in the media composition resulting from cellular metabolism, i.e. pH, dissolved O_2, or ion concentration, should be minimal when compared to the direct effects of the cell layer influence;
4. Any influence from the adsorption of serum components specifically adhering onto the surface of the electrode should be minimal; and
5. For the total impedance of the system to be determined by the electrical properties of the working electrode covered by the cells, its active area must be significantly smaller than the counter electrode active area in order to ensure that the largest current density is found on the WE, where the desired changes in cell viability is probed.

It is also important to note that different adherent cell lines will produce their own characteristic impedance curve over time as the cells proliferate on the electrode surface. This is because some cells adhere more tightly onto the surface than others, thereby affecting the size of the aqueous gap. The gap has a direct influence on impedance measurements and ranges between 15-35 nm for close contacts and 150-170 nm for other parts of the cell that make cell-substrate contact [63]. In particular, embryonic 3T3 mouse fibroblasts attach closely to surfaces with a typical cell-surface distance of approximately 15 nm [64].

2.4 Previous Work

A primary challenge to developing LOC cellular assays is the development of a miniaturized culture system with electrodes to track the growth of cells electronically, instead of optically, for the use in a microfluidic system. The need for this new technology is based on the desire to increase the efficiency for high-throughput, parallel experimentation strategies and to maintain a sterile environment for cell-based tests, such as functional genomic studies or drug candidate testing.

Currently, a commercialized product by Applied Biophysics, Inc. allows for the monitoring of cell adhesion, spreading, motility, growth, and death through impedance measurements. The system employs 8 culture wells made from the same material as tissue culture dishes, e.g. polystyrene. Integrated gold electrodes measure cellular response changes through Electric Cell-Substrate Impedance Sensing (ECIS) [65, 66]. Although this developing technology is quite promising, it is presently hindered by its inability to effectively incorporate itself within a closed microfluidic system. Moreover, the system setup only allows an assay to be performed in a single well and does not permit the cultured cells to be moved to another part of the chip for continuous culturing or to be subjected to another assay. This device also suffers from the use of a single or a set of 250 μm, 100 μm, 50 μm, or 25 μm diameter working electrodes placed in the center of the chamber. This arrangement allows an average measurement of cell coverage to take place in the immediate center of the chamber. On the other hand, it is more beneficial to have the WE active areas spread out over the majority of the culture chamber. This arrangement allows for a more accurate average of cell coverage for the entire growth chamber instead of limiting it to within the immediate center.

Additional impedance sensing employs the ECIS device and technology developed by Applied Biophysics, Inc. with the primary difference of using various surface preparations to promote cell adhesion at the detecting electrode. The dependence of the coating proteins, such as fibronectin and ovalbumin, on the relationship of the number of cells attached on the working electrode was investigated [67]. It was also reported that the impedance increased linearly as cells covered the electrode. Other ECM proteins can be physically adsorbed onto electrode surfaces to induce the secretion of cell adhesion molecules that result in adhesive interactions [68, 69]. However, it is not possible to employ a self-assembled monolayer (SAM) of an alkanethiol or, in fact, any other molecule that is held in a solvent-based solution, desired to functionalize the surface of the Applied Biophysics commercial device. This is because the passivation layer used to coat their devices dissolves when it comes into contact with any chemical solvent.

Impedance spectroscopy with the Applied Biophysics, Inc. device were used in many applications, such as monitoring the spreading [61, 70], motility [71, 72], and viability [62, 73] of cells through electrical detection. Changes in impedance were correlated to the attachment and motion of cells on electrodes [57, 65, 67, 74], as well as cell shape changes [66]. Other applications of the ECIS technology included its use in cytotoxicity from detergents [75] or chemical inhibitors [73, 76] and electroporation/wound healing [77, 78] assays.

The combination of optical and electrical impedance monitoring was demonstrated for the determination of cell confluence. ECIS technology was modified to allow simultaneous microscopic readings of attachment, growth and motility for the

correlation of impedance over periods of time up to 40 hours with cell confluence on small gold electrodes [79]. Although this technique demonstrates that impedance measured with the ECIS technique is a good quantitative measure of cell confluence, the system employs the use of a 1 cm-thick Plexiglas block for culture wells, which makes it difficult to incorporate it onto a LOC device. It also does not investigate its use with a coating material to promote cell adhesion in order to mimic the normal cellular physiological environment.

Other biosensors were fabricated that utilize impedance spectroscopy for cell assays. For example, microelectrode arrays were used to probe cell attachment and response to protein inhibitors that result in the loss of focal adhesions [80, 81]. Alternatively, interdigitated electrode structures [60, 82] were used to determine the influence of toxic compounds on a confluent cell layer. Electrodes made of materials other than gold, such as indium tin oxide electrodes, were also other examples that could either investigate cell attachment and spreading [83] or sense ion permeability changes within cell membranes as a biosensing platform for glucose detection [59]. However, the modification of these systems with proteins or other coating materials to promote cell adhesion was not investigated. The use of cell adhesion coatings on planar electrodes is essential in trying to recreate the proper physiological environment the cells are accustomed to within the body. Normally, cells grow and form a 3-D conformational structure. Such configurations are not possible with conventional planar electrode set-ups. However, microfluidic devices provide solutions to establish 3-D matrices for cell growth.

It is necessary to develop microfluidic cell culture systems to provide a stable microenvironment for the growth of cells to be utilized in cellular assays [84, 85]. Such devices include microchamber arrays with the ability to continuously perfuse medium [86, 87], microfluidic channel networks that support short-term and long-term perfusion [88], and poly(dimethylsiloxane) (PDMS) chips that are comprised of a cell cultivation chamber and microfluidic channels [89]. While these devices are successful in the microcultivation of cells, they lack the ability to monitor cell growth within the cell chambers by means other than optical observation.

2.5 Conclusion

The theory of impedance spectroscopy and the electrical properties of cells, as they pertain to bioelectrical measurements, are presented in this chapter. It is possible to electrically measure the presence and abundance of cells on an electrode surface through impedance measurements. As the cells begin to attach, spread, and proliferate on the surface of the electrodes, the resulting current flow from the applied potential is hindered. The effective area of the electrode available for current flow is altered due to focal cell adhesions and the resulting aqueous gaps, which produces an increase in impedance. The electrical properties of the cells are a result of the cell membrane being in a phospholipid bilayer configuration. This configuration leads the cell to act as a dielectric because of the capability of the membrane to exhibit insulating properties at low frequencies. As a result, an individual cell can be modeled as a capacitor and resistor in parallel in an equivalent electrical circuit diagram.

The ability to develop a miniaturized platform for the use in "cell-culture-on-a-chip" applications was explored. The demonstrated technologies were confined to separate applications of impedance measurements or optical observations on cell microcultivations to monitor growth. Although there was one demonstration of combining the techniques to provide a quantitative measurement of cell confluence, the system is unable to be incorporated within a microfluidic network as an LOC device or as a part of a platform to perform continuous cell-based assays. Additionally, a commercially available device exists for cell proliferation monitoring, however, it also does not allow for investigation to take place on an LOC device. Moreover, they cannot be customized with solvent-based coatings. Other systems are limited to a 2-D surface, whereas cells naturally exist in a 3-D environment. To address these issues, the experimental research was conducted to realize the use of optically-transparent, PEMs-modified TiW/Au electrodes embedded within a micro cell culture chamber to detect cell growth with the well-established ECIS measurement techniques instead of optical observations. The use of a microenvironment with PEMs can better replicate the 3-D environment optimal for cell culture. The experimental steps consisted of fabricating a two-electrode system to sense impedance changes, preparing the surface of those electrodes with PEMs to promote cell adhesion, and to correlate the measured impedance with cell confluence.

CHAPTER 3

CELL CONFLUENCE DETECTOR

The first phase of research consisted of experimentation on optically-transparent TiW/Au electrodes. The focus of the initial work was to demonstrate the effectiveness of the overall electrode design and the feasibility of using polyelectrolyte multilayers (PEMs) to promote cell attachment for impedance measurements. The design, fabrication, and process for the surface modification of the electrodes are described. An equivalent electrical circuit was proposed to describe the effects of the PEMs and the attached cells on the electrode system. Finally, the performance of the PEMs-modified electrodes were characterized by cyclic voltammetry and impedance spectroscopy and compared to unmodified electrodes.

The device was designed with a working electrode (WE) surrounded by a counter electrode (CE) for impedance measurements (Figure 3.1). The electrode pattern involved several traditional microfabrication steps to form the device: photolithography, DC sputtering, and metal lift-off to form the TiW/Au electrodes; plasma enhanced chemical vapor deposition (PECVD) to form a passivation layer over the electrodes; and reactive ion etching (RIE) to open the active areas over the working and counter electrodes. Finally, as shown in Figure 3.2, a PDMS reservoir and coverplate was sealed around the electrode pattern to create a well for cell culturing.

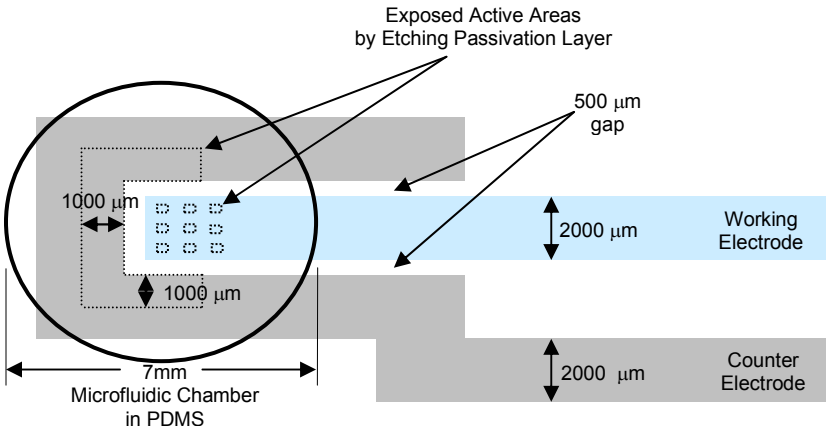

Figure 3.1 Top-down view of the electrode design consisting of a WE (total area = $51x10^6$ μm^2) surrounded by a CE (total area = 90.5 μm^2). The blue-colored electrode is the WE and the gray-colored electrode represents the CE. The total active area of the counter electrode is $9.5x10^6$ μm^2 and each working electrode active area is 200μm x 200μm for a total WE active area of $0.36x10^6$ μm^2.

A)

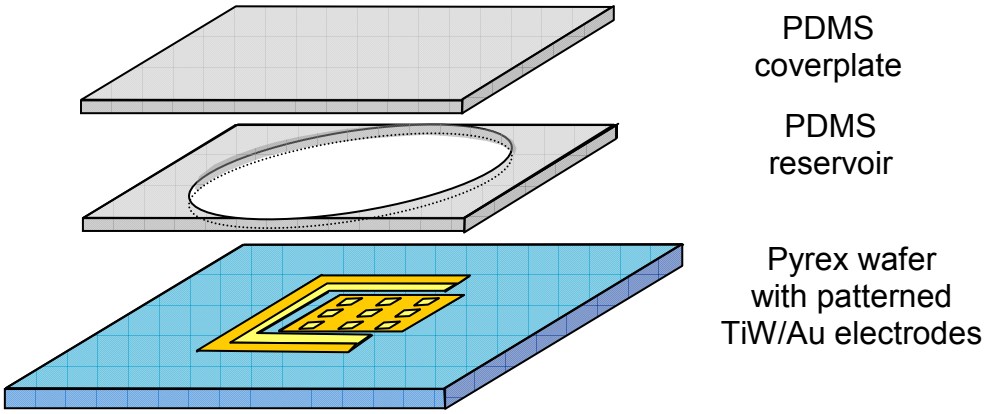

B)

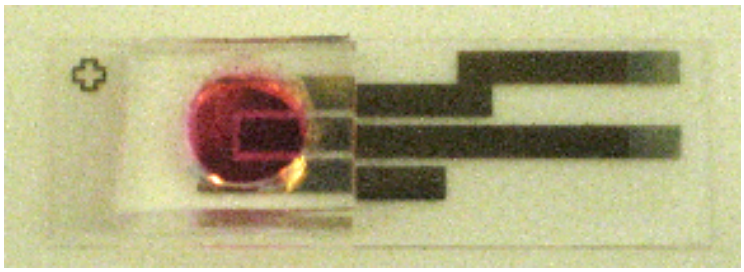

Figure 3.2 A) 3-D schematic and B) Photograph of fabricated device with a 7mm diameter PDMS reservoir surrounding the electrode design. The PDMS reservoir is filled with cell culture media and sealed with a PDMS coverplate.

3.1 Fabrication of Electrodes

The device fabrication was completed at the National Institute of Standards and Technology Center for Nanoscale Science and Technology Nanofabrication Facility. The process steps are detailed in Figure 3.3. The cell culture chamber electrodes were first patterned on 7.62 cm diameter Pyrex glass wafers. After photolithographic lift-off-resist patterning of the working and counter electrodes were performed on the wafer, a 47.5 nm-thick gold layer in between two 3.0 nm-thick titanium tungsten (TiW 90/10 wt%, Kurt J. Lesker, Co., Pittsburg, PA) adhesion layers was sputtered with DC power onto the patterned wafer. The rationale behind the choice of utilizing a TiW adhesion layer is discussed in Appendix A. A metal lift-off process was completed to produce the working and counter electrodes. A passivation layer was deposited using PECVD at 300 °C for 8.5 minutes to form 400 nm of silicon oxide. The pattern for the etching of the active areas of the working and counter electrodes was accomplished by using standard photolithographic techniques. Reactive ion etching for 14 minutes opened the active electrode areas, and 6:1 buffered hydrofluoric acid completed the etching process to expose the underlying TiW layer. The top layer of TiW was etched away from the electrode active areas to expose the underlying gold layer by immersing the wafer into chromium etchant (CR-7) [90] for 15 minutes.

The active area of the working electrode consisted of nine 200 μm x 200 μm squares (total active area = 0.36×10^6 μm^2) that are in direct contact with the supporting electrolyte. It was essential that this area be significantly less than the counter electrode active area, which is 9.5×10^6 μm^2, in order for the working electrode to have the largest

current density. This results in an electronic response for probing the events occurring on the working electrode surface.

Finally, a PDMS reservoir was used to form the cell culture chamber environment. It was sealed with another piece of PDMS as a coverplate. The PDMS well and coverplate were cleaned with 100% ethanol and DI water and then blown dry with nitrogen gas before the addition of cell culture media and biological cells. The chamber was aligned and sealed to surround the electrodes.

3.2 Cell Cultivation

The immortalized NIH-3T3 mouse embryonic fibroblast cell line used in this study was grown in Dulbecco's Modification of Eagle's Medium (DMEM, ATTC, Manassas, VA) with L-glutamine (4mM), glucose (4500mg/L), and sodium bicarbonate (1500mg/L). Additionally, the DMEM was supplemented with newborn bovine serum (Invitrogen Corporation, Carlsbad, CA). The cell cultures were incubated at 37 °C in 5% (v/v) CO_2. DMEM was changed every other day and the cells were allowed to proliferate until approximately 80% confluency[3] was reached.

[3] Confluency refers to the approximate coverage of cells on a substrate surface.

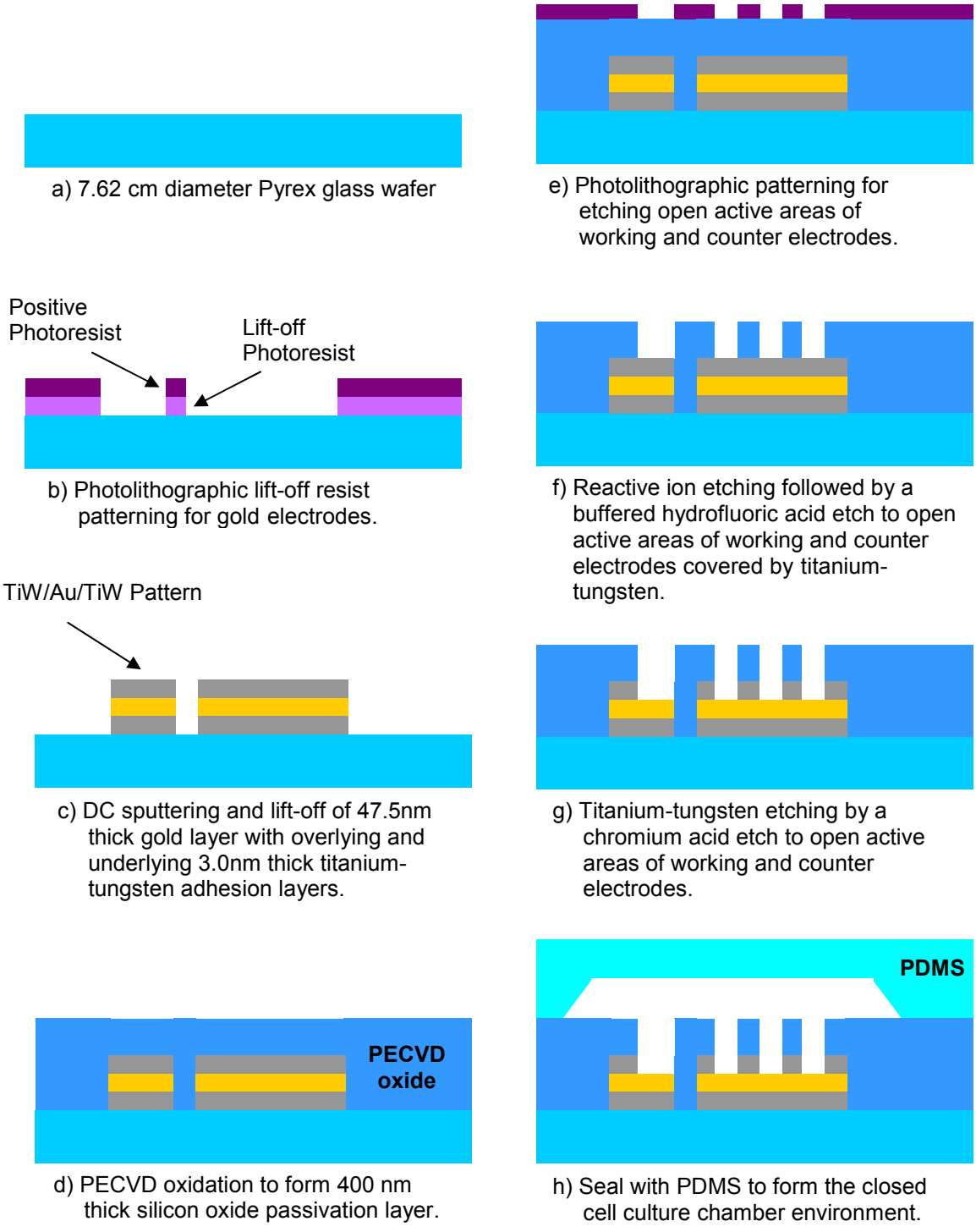

Figure 3.3 Fabrication schematic for device fabrication.

3.3 Electrode Surface Preparation for Biocompatibility

The exposed gold electrode surfaces were modified by the deposition of polyelectrolyte multilayers for cell adhesion promotion and growth within the microchamber. The first polycation oriented itself and bound onto the bare gold surface [91]. A polyanion then was electrostatically bound to the polycation, and so forth, until a final polycation layer was rendered as the top layer to promote cell attachment. The schematic for the surface preparation through multilayer formation is shown in Figure 3.4.

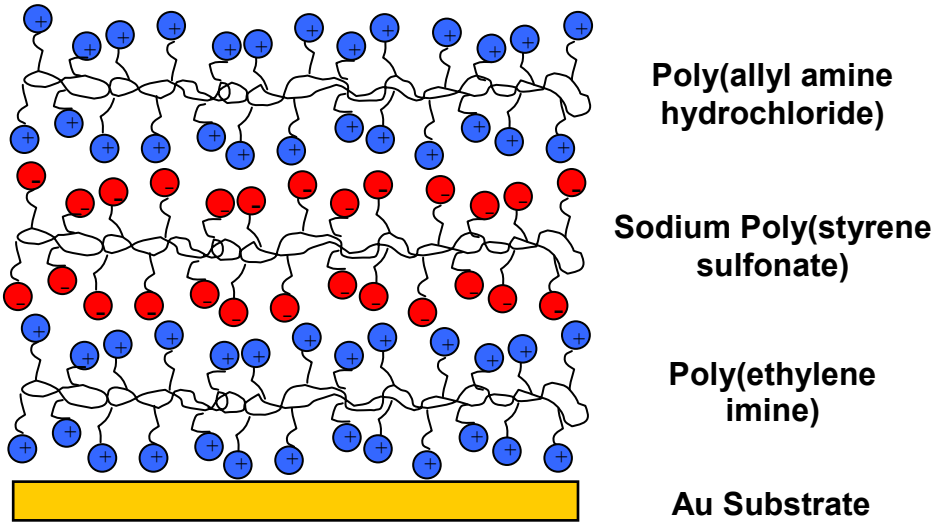

Figure 3.4 PEMs formation for gold electrode surface biofunctionalization.

3.3.1 Polyelectrolyte Multilayer Formation

Aqueous polyelectrolyte solutions of poly(ethyleneimine) (PEI, Polysciences, Inc., 70 000 MW), sodium polystyrene sulfonate (PSS, Polysciences, Inc., 70 000 MW), and poly(allylamine hydrochloride) (PAH, Scientific Polymer Products, Ontario, NY, 70

000 MW) were prepared using 18.2 MΩ Milli-Q water (Millipore Corp., Bedford, MA). The structures of PEI, PSS, and PAH are shown in Figure 3.5. Sodium chloride (Mallinkrodt Baker, Inc., Phillipsburg, NJ) was added to the 1 mM polyelectrolyte solutions to produce a salt concentration of 0.1M NaCl. Altering the ionic concentration of the PEMs solutions allowed for the control of layer thickness and surface roughness [92]. A low ionic concentration of 0.1M NaCl produced thin, smooth PEMs layers [39]. The pH levels of the polyelectrolyte solutions were adjusted so that the degree of ionization of the functional groups was appropriate for the formation of the polyelectrolyte layers [32]. This was accomplished by either adding 0.1M NaOH or 0.1M HCl until the pHs were adjusted to 4.8-5.0, 6.0, and 5.0 for PEI, PSS, and PAH, respectively. Any particulates found in solution were removed from the solution by filtering with 0.20 μm Millex-GN syringe driven nylon filter units (Millipore Corp.).

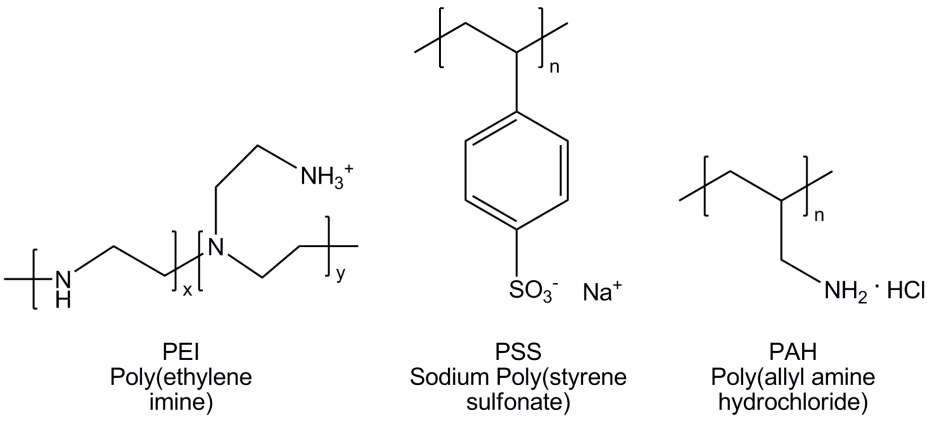

Figure 3.5 Chemical structures of polyelectrolytes, PEI, PSS, and PAH.

The PEI polycation was deposited onto the electrode surface by pipetting 200 μL of the solution into the PDMS reservoir and allowed it to sit for 25 minutes to form the

initial PEI monolayer. PEI must be used as the anchoring layer because of its ability to adsorb onto a gold surface [91]. Followed by three deionized water rinsing steps to remove any non-bonded PEI, 200 μL of PSS was added to the system and allowed to sit for five minutes to form the first polyanion layer. The device was rinsed again and PAH was added, allowed to sit for five minutes, and was followed by a rinsing step. The formed PSS/PAH layer makes up one bilayer. Polyelectrolyte multilayers of PSS and PAH were alternately deposited onto the substrate until the desired number of five bilayers were formed. Five bilayers of PSS/PAH [$(PSS/PAH)_5$] was appropriate to mask the functional group of PEI, which was shown to inhibit cell adhesion [93].

3.3.2 Surface Treatment Characterization

The deposition of the PEMs was confirmed by atomic force microscopy (AFM, Figure 3.6). Height measurements were determined by using a Veeco Nanoscope IIIa scanning probe microscope and stage controller (Digital Instruments, Santa Barbara, CA) and visualized with the Nanoscope 5.30rl software (Digital Instruments). AFM scans were conducted in tapping mode in air with a standard etched silicon cantilever tip (NanoDevices, Inc., Santa Barbara, CA) with a spring constant of 40 N/m exhibiting a resonance frequency of 300 kHz ± 20%. Measurements were performed at amplitude setpoints of 0.6723V and 0.2617V for PEI and PEI/$(PSS/PAH)_5$, respectively and was operated at a scan rate of 0.219 Hz to visualize the surface of planar microelectrodes before and after surface modification and functionalization.

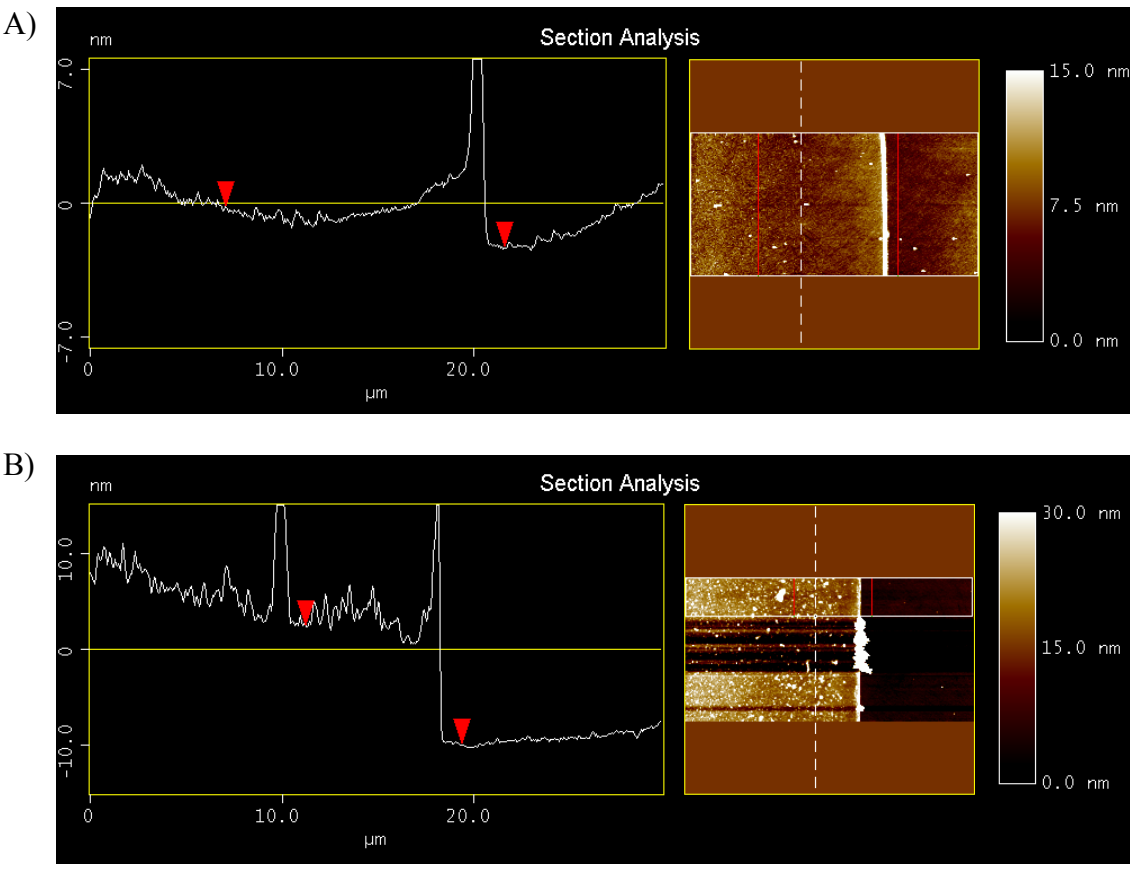

Figure 3.6 Two-dimensional AFM height measurements of A) adsorbed PEI on Au and B) adsorbed PEI/$(PSS/PAH)_5$ on Au.

The section analysis of PEI and PEI/$(PSS/PAH)_5$ produced an average step height of 2.080 nm and 12.343 nm, respectively. This verified the deposition of PEMs on the surface of gold and was in accordance with the generalization that an individual polyelectrolyte layer is approximately 1-2 nm in height [32, 39].

In addition to the AFM height measurements, Fourier Transform Infrared Spectroscopy (FTIR) was used to verify the adsorption of PEI and the PSS/PAH bilayers on the surface of the gold electrodes. IR spectroscopy provided an excellent probe of functional groups present as long as they were present in sufficient amounts. FTIR was

accomplished by utilizing a Thermo Nicolet Nexus 670 FT-IR Spectrometer and OMNIC v6.2 software (Thermo Electron Corporation). The spectra were obtained by running 256 scans in a range of 4000-725 cm^{-1} with a resolution of 2 cm^{-1}. Absorbance changes were detected by a mercury cadmium telluride detector.

The spectra in Figure 3.7 revealed that PEI and the PSS/PAH bilayers were deposited onto the gold surface. Samples containing PEI on gold (band A) and $(PSS/PAH)_5$ on PEI on gold (band B) were scanned with respect to a bare gold sample and corrected for any water vapor in the chamber. CO_2 peaks were apparent in both bands at 2400-2300 cm^{-1} and above 3600 cm^{-1}, all of which can be ignored because it was always present in the detecting chamber. Band A showed only CH_2 groups for PEI with peaks just below 3000 cm^{-1} and at around 1700 cm^{-1}. The 1°, 2°, or 3° amine functional groups were probably not detected due to the fact that they were not present in a sufficient amount in this single layer. Band B showed more CH_2 groups on the surface when compared to band A and a large shoulder at the higher energy tail. This shoulder was due to aromatic CH stretches in PSS or CH stretches next to charged species in both PSS and PAH. The broadness of the peaks indicated an inhomogeneity or a wide range of differing CH stretches. In addition, there were also a number of peaks at the low frequency, or fingerprint, region (1400-990 cm^{-1}) due to the aromatics and amine functional groups of the polyelectrolytes.

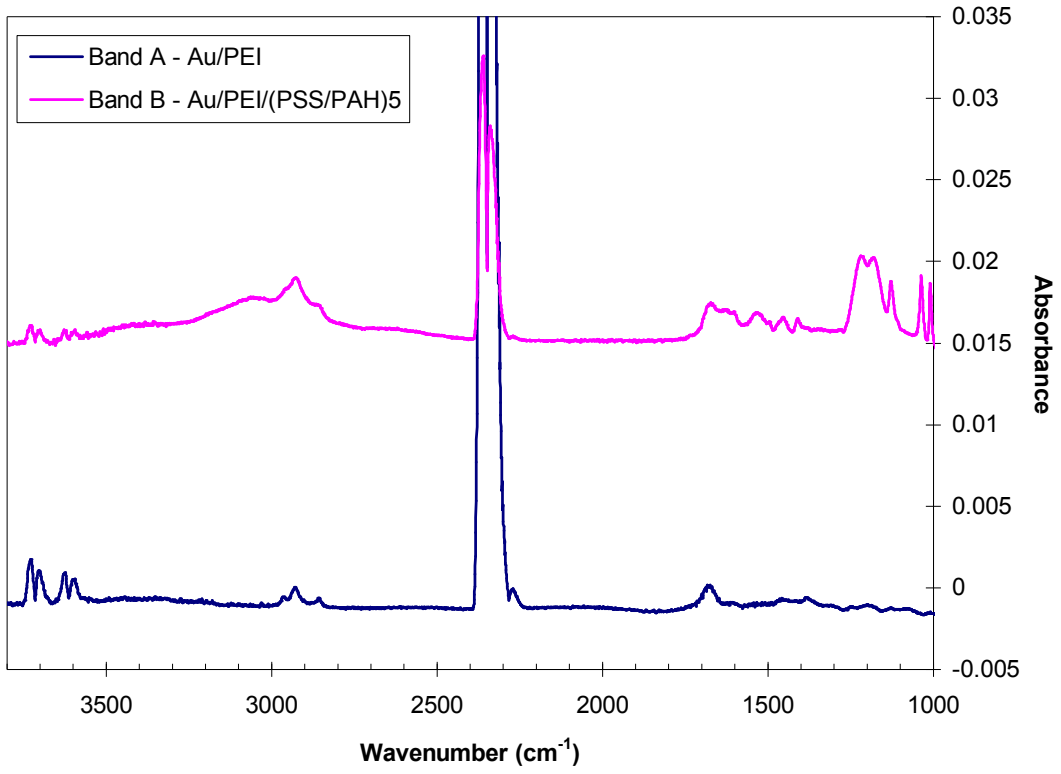

Figure 3.7 Transmission IR spectra of gold surfaces with deposited PEI (Band A) and PEI(PSS/PAH)$_5$ (Band B) using bare gold as a reference. The peaks around 3000 cm^{-1} and between 1700-1400 cm^{-1} were due to CH, CH_2, and CH_3 groups in each polyelectrolyte, or aromatic CHs found in PSS. The peaks around 3400-3200 cm^{-1} and in the fingerprint region arose from amine functional groups present in PAH. The CO_2 peaks at 2400-2300 cm^{-1} and above 3600 cm^{-1} were ignored.

An easy way to distinguish the surface properties of molecular films was to perform contact angle measurements [94, 95]. Contact angle data provided information on the hydrophobicity or hydrophilicity of the surface, and allowed for an immediate indication of differences in molecular organization and surface coverage between dissimilar surface treatments. Water contact angle measurements were performed using FTA Video Drop Shape Analysis v2.0 software (First Ten Angstroms, Portsmouth, VA) to analyze the captured image of a sessile water drop from an APPRO B/W camera (Approtech, Inc.,

Sunnyvale, CA). The reported values were the average of three measurements of 18.2 MΩ•cm deionized water on each surface treatment.

Table 3.1 Summary of Contact Angle Measurements Obtained From Various Surface Treatments

Surface Treatment	CA (°)
Untreated Polystyrene Dish	84.22 ± 0.70
Treated Polystyrene Cell Culture Dish	66.71 ± 0.51
Bare Au	88.86 ± 0.47
Au/PEI	67.29 ± 1.23
Au/PEI/$(PSS/PAH)_5$	46.86 ± 0.66

Cells preferentially adhered to a charged, wettable surface. As shown in Table 3.1, untreated polystyrene plastic was normally hydrophobic and unsuitable for cell culture until it was treated to create a hydrophilic surface. A bare gold surface had a contact angle similar to that of untreated polystyrene plastic. Adding PEMs to the surface of bare gold created a hydrophilic surface, more so than the traditional treated polystyrene culture dish. The addition of the PSS/PAH bilayers had an increased hydrophilicity than PEI alone, which had a contact angle similar to that of a treated cell culture dish. This hydrophilic property, which was demonstrated with contact angle measurements, allowed cells to attach, grow, spread, and proliferate onto PEMs-modified surfaces.

3.3.3 Cellular Response to PEMs versus Bare Gold

Viability visualization was essential to confirm that the 3T3 cells were alive and functioning properly during the duration of the culturing and impedance measurement process. Viability was assessed by using of 6-carboxy-2', 7'-dichloro-dihydrofluorescein diacetate (DCFDA, Molecular Probes, Eugene, OR). The cells were incubated in 10 μM DCFDA in DMEM for 20 min at 37 °C in the absence of light. Fluorescent-viable cells were visualized using an Axiovert 40 CFL microscope (Zeiss, Thornwood, NY) equipped with an AxioCam MRm camera (Zeiss) with a fluorescein isothiocyanate (FTIC) filter with excitation and emission wavelengths of 450-490 nm and 500-550 nm, respectively. Figure 3.8 shows the images acquired by AxioVision software v.4.5 for the comparison of viability assays completed 72 hours after inoculation on an unmodified Au electrode surface, PEMs-modified electrode surface, as well as a polystyrene culture flask.

In viable cells, DCFDA was taken up by the cells, where it underwent intracellular oxidation. The cleaved byproduct of this oxidation process was carboxydichlorofluorescein and was observed fluorescently. Figure 3.8A shows the viability of NIH-3T3 fibroblast cells on a conventional polystyrene cell culture flask 72 hours after seeding. Images from a bare gold electrode surface (Figure 3.8B) and a PEMs-modified electrode surface (Figure 3.8C) showed that fibroblast cells were also viable on these surfaces 72 hours after inoculation. Therefore, cell attachment, spreading, and proliferation were supported with both unmodified and PEMs-modified gold surfaces.

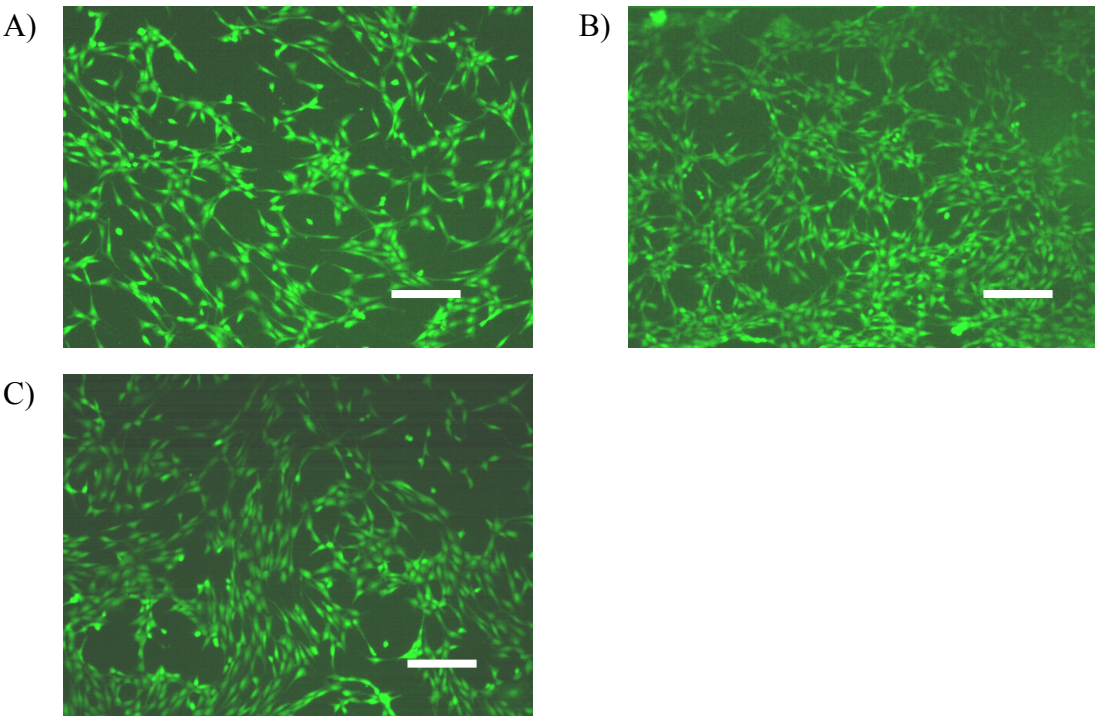

Figure 3.8 Viability assay results of NIH-3T3 fibroblast cells 72 hours after inoculation in A) a polystyrene cell culture flask, B) on a bare gold electrode surface, and C) on an electrode surface modified with PEI/$(PSS/PAH)_5$. All scale bars are 200 μm.

Cell spreading and nucleus morphology were also compared to that displayed by cells grown in a polystyrene cell culture flask (Figure 3.13). This was accomplished by performing cytoskeleton and nuclear staining at room temperature on cells that were cultured for 72 hours on a polystyrene culture flask, bare gold electrodes, and PEMs-modified electrodes. The cells were rinsed with Dulbecco's phosphate-buffered saline (DPBS, Mediatech, Inc., Herndon, VA) and then underwent fixation by using 4% w/v paraformaldehyde (Electron Microscopy Sciences, Hatfield, PA) for 10 minutes. The cells were washed twice with phosphate-buffered saline (PBS, Mediatech, Inc., Herndon, VA) before the addition of 0.1% Triton-X 100 (Sigma-Aldrich, St. Louis, MO) for 3-5 minutes. After washing twice with PBS, 1% bovine serum albumin (BSA, Sigma-

Aldrich, St. Louis, MO) was added to the samples for 20-30 minutes and rinsed again with PBS. For cytoskeleton staining, 5 units/mL of alexa fluor 568 phalloidin (Molecular Probes, Eugene, OR) was added to the cells for 20 minutes, at which point, the cells were washed twice with PBS.

After staining the cytoskeleton of the cell, nuclear staining was performed at room temperature. The cells were exposed to a 5 mg/mL 4', 6-diamidino-2-2-phenylindole (DAPI) solution for 3-5 minutes, rinsed two times with PBS, and viewed in PBS. The cytoskeletal and nuclear stained cells were visualized using the same microscope equipment and software as used with the viability assay, except for using filters with excitation wavelengths of 542 nm and 358 nm, and emission wavelengths of 565 nm and 463 nm, for phalloidin and for DAPI, respectively.

The cell spreading and nuclear morphology of the fibroblast cells were investigated to see if the cellular structure integrity was preserved. The cytoskeleton structural proteins are the actin filaments, which were stained red in Figure 3.9. The nuclei of the cells were stained blue. Figure 3.9A shows the morphology of 3T3 cells grown in a polystyrene cell culture flask and was compared to show a similar cell spreading and nuclear morphology on both bare gold (Figure 3.9B) and PEMs-modified electrodes (Figure 3.9C).

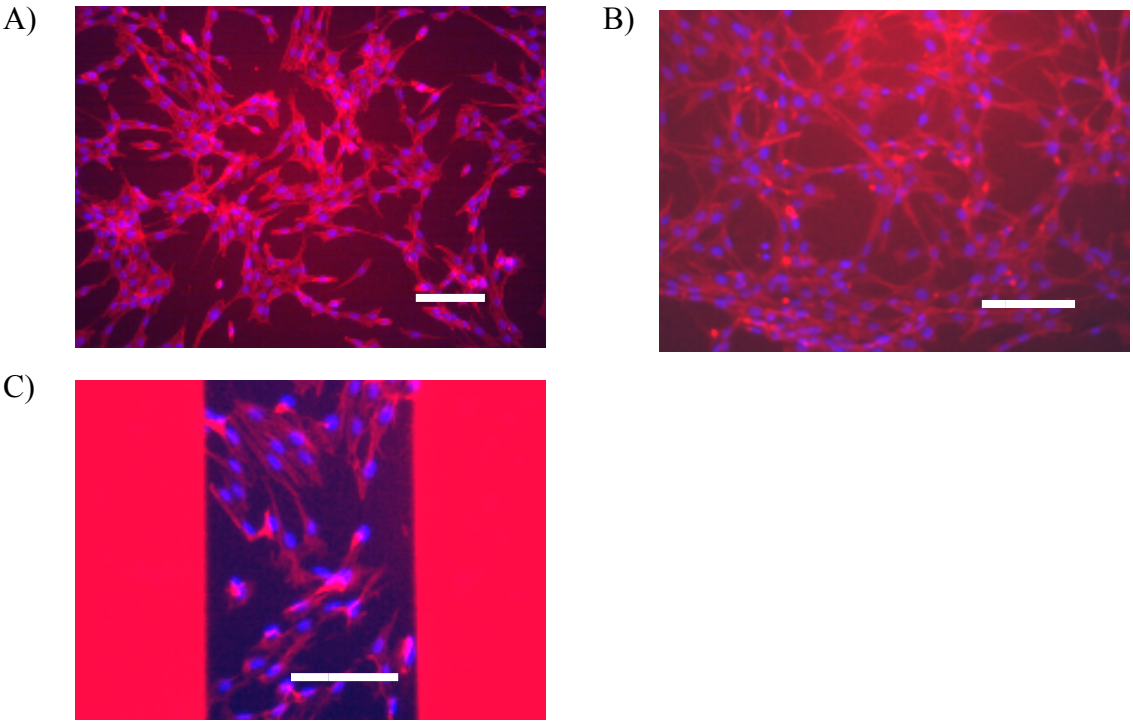

Figure 3.9 Cell spreading and nuclear morphology comparison of NIH-3T3 fibroblast cells grown A) in a polystyrene cell culture flask, B) on a bare gold electrode surface, and C) on a PEMs-modified electrode surface. All scale bars are 200 μm.

3.4 Equivalent Electrical Circuit

The performance of the two-electrode system is represented as an equivalent electrical circuit. A pair of electrodes immersed in an electrolytic solution is represented by the equivalent circuit model in Figure 3.10 [60], where R_s represents the resistance of the electrolyte solution. This spreading resistance is encountered as the current flows, or spreads out, from the working electrode and into the surrounding bulk electrolyte solution [96], and the electrode is able to sense the conductivity of the solution, which is represented by the resistor in series.

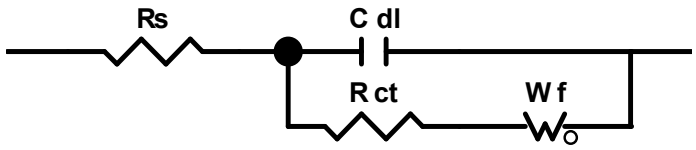

Figure 3.10 Equivalent electrical circuit for a two-electrode system immersed in an electrolyte solution.

In series to R_s are the electrical components that take into account the contributions due to non-faradaic and faradaic processes occurring at the electrode-solution interface. C_{dl} represents the capacitance of the electrical double layer at the interface. This non-faradaic contribution is a result of the accumulation of charge occurring at the metal surface. The structure formed is the electrical double layer, which exhibits dielectric properties.

Faradaic processes, which are associated with electron transfer across the interface and lead to the reduction and oxidation of species present at the interface, are represented by the remaining two electrical components, R_{ct} and Z_w. Some charge is allowed to leak across the double layer due to electrochemical reactions taking place at the electrode-solution interface. This leakage experiences an electron charge transfer resistance, R_{ct}. The Warburg impedance, Z_w, or interfacial impedance, is an important component that accounts for the changes in the electrolyte concentration gradient at the interface [97] and results from limited mass diffusion from the electrode surface to the solution due to electrochemical reactions. Mass transport processes are responsible for bringing species present in a bulk solution to the electrode surface in order to become reduced or oxidized. However, since there are no faradaic processes (i.e. electrochemical reactions) occurring in the cell confluence detector system, the circuit elements that

represent faradaic process can be eliminated, resulting in the reduced equivalent electrical circuit for cell-free media represented in Figure 3.11.

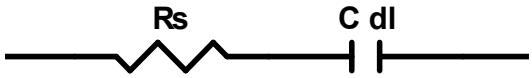

Figure 3.11 Reduced equivalent electrical circuit of cell confluence detector in cell-free media.

When ideal elements, such as resistors and capacitors, do not fit the measured spectra in a satisfactory way, constant phase elements (CPEs) can replace them. CPEs are used when there are inhomogeneities present on a surface. Thus, the ideal capacitive element can then be replaced by a CPE (Figure 3.12). The CPE is given by the following empirical expression [98]:

$$Z_{CPE} = \frac{1}{(j\omega Q)^p} \qquad \text{(Equation 3.1)}$$

where Q is the measure of the magnitude of Z_{CPE}, p is a constant ($0 \leq p \leq 1$) representing surface inhomogeneities and ω is the angular frequency of the AC electrical signal. In a Nyquist plot, the angle between the data and the abscissa axis gives p according to $p = (2\theta)/\pi$. When $p = 1$, Z_{CPE} represents a purely capacitive impedance element corresponding to the double layer capacitance. If $p = 0.5$, the Nyquist plot of Z_{CPE} appears as a diagonal line with a slope of 0.5 and the Bode plot exhibits a phase shift of 45°. This represents an infinite length Warburg element and its impedance is defined as:

$$Z_{Wi} = \frac{\sigma(1-j)}{\omega^{1/2}} \qquad \text{(Equation 3.2)}$$

where σ is the Warburg coefficient parameter that depends on the diffusive properties of the electrolytes, and the area and characteristics of the electrodes [97]. This form of the Warburg impedance is only valid if the diffusion layer has an infinite thickness. However, the diffusion layer of actual systems is usually bounded and exhibits a phase shift between 0° and 90°, which represents a finite Warburg element with an impedance defined by:

$$Z_{W_f} = \frac{1}{(j\omega)^{nB}} \qquad \text{(Equation 3.3)}$$

where *n* and *B* are parameters that depend on the properties of the electrolytes and of the electrodes and ω is the angular frequency of the AC electrical signal ($\omega = 2\pi f$).

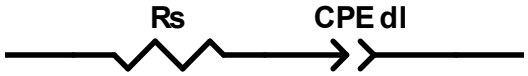

Figure 3.12 Equivalent electrical circuit of the cell confluence detector in cell-free media. This model contains constant phase elements in place of capacitors to take into account any system surface inhomogeneities.

Impedance measurements are performed on living cells because of the electrical properties they exhibit. As shown in Figure 2.5, biological cells are represented as a capacitor and resistor in parallel with each other. However, in Figure 3.13, the capacitor must be replaced by a CPE because it is a non-ideal, inhomogeneous system. CPE_{cell} in the equivalent circuit represents the phospholipid bilayer and intracellular volume of the cell exposed to an applied AC signal. The resistive component, R_{cell}, represents the restriction of current flow due to the narrow cell-substrate junctions and spaces in

between neighboring cells formed from cell adhesion processes. ECM receptor proteins form aqueous gaps between the cell and electrode surface, inhibiting the flow of ionic current between the electrode surface and the cell and into the bulk electrolyte.

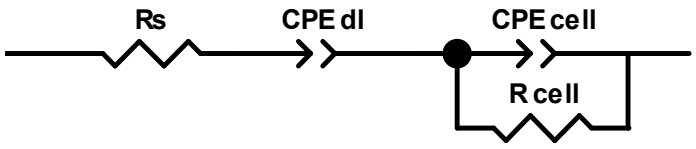

Figure 3.13 Equivalent electrical circuit of the cell confluence detector with the addition of cells in media.

The deposition of PEMs onto the electrode surface leads to the addition of a capacitor and resistor in parallel with each other to the existing equivalent electrical circuit (Figure 3.14). Again, however, the capacitor is replaced with a CPE. The individual layers of PEMs consist of an internal carbon-carbon arrangement, which is terminated by a charged species (Figure 3.5). Therefore, with its hydrophobic interior and hydrophilic end, the PEMs contains dielectric properties [92] and act as a capacitive element, C_{PEMs}. The resistive element, R_{PEMs}, in parallel with the other circuit components takes into account that surface coatings often have very small pores that can allow the electrolyte to leak through the layer, providing a conduction path through the coating. The polyelectrolyte surface is inhomogeneous with respect to electroactive species transport and contains areas where transport is quite favored [99].

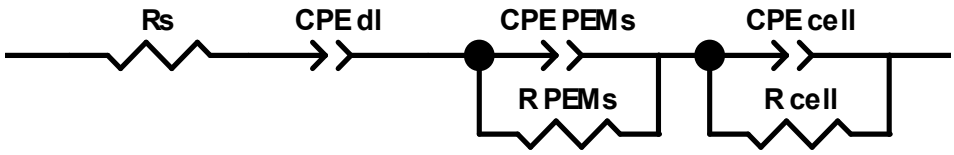

Figure 3.14 Equivalent electrical circuit that takes into account the electrical properties of the addition of PEMs, which facilitates cell attachment and growth on otherwise non-supporting materials for cell adhesion and proliferation.

3.5 Electrode Characterization

Electrode characterization tests were run to compare the performance of the unmodified and PEMs-modified electrodes, as well as to determine the variability of the performance of unmodified electrodes within the same and different fabrication batches. The fabricated electrodes were characterized using impedance spectroscopy at frequencies ranging from 1 Hz to 10^6 Hz. Samples included air, deionized water, saline solutions with various ionic concentrations, and PBS.

In addition to testing electrode performance and variability, electrochemical characterization of the fabricated electrodes was completed with cell culture media (DMEM) as the supporting electrolyte. The resulting current-potential curves provided information about the nature of both the electrode types and the supporting electrolyte. Additionally, it was an indicator of any reactions that may have occurred at the electrode interface. The fabricated gold electrodes were used in a two-electrode electrochemical cell to evaluate the feasibility of using two gold electrodes as the working and reference electrodes.

Cyclic voltammetry (CV) was also utilized to perform the electrochemical characterization of unmodified and PEMs-modified electrodes using PBS as a control electrolyte with no reactive species. This was followed by CV measurements made with a solution of PBS and a standard redox couple, $[Fe(CN)_6]^{3-/4-}$. All measurements were performed using the Solartron 1287A Electrochemical Interface system (Solartron Analytical, Oak Ridge, TN). The impedance spectra and CV curves were measured and recorded using Zplot2/Zview2 and Corrware2/Corrview2 software packages (Scribner Associates, Inc., Southern Pines, NC), respectively.

3.5.1 Electrode Performance versus Ionic Concentration

Three consecutive impedance sweeps were recorded for each measurement sample of each device and the averages of those sweeps were plotted. After measuring the impedance of the device with air and deionized water as controls, each saline solution measurement was completed in the order from lowest to highest ionic concentration. After each measurement, the PDMS reservoir was rinsed with deionized water three times before the next saline solution was added.

The graphs in Figure 3.15 show the magnitude and phase of the measured impedance of a single device as a function of frequency when filled with air, deionized water, and saline solutions of different concentrations. The individual curves were the averages of three frequency sweeps. The magnitude of impedance decreased as the ionic concentration of the solution increased because of the increase in conductivity. In addition, the length of the nearly linear response of the magnitude increased in frequency from approximately 10 Hz to 100 kHz with an increase in ionic concentration. It was at

frequencies higher than 1 kHz where differences in ionic concentrations were easily measured because the effect of the solution resistance dominated at these higher frequencies. At lower frequencies, the impedance of an ionic solution, which is represented simply as the RC equivalent circuit in Figure 3.11, was dominated by the effect of the double layer capacitance. At higher frequencies, the magnitude of impedance was dominated by the solution resistance.

The differences between the impedance of the seven solutions with varying ionic concentrations were statistically significant on both the unmodified and PEMs-modified electrodes. The calculated two-tailed confidence levels (shown in Appendix B) using student t-tests at high frequencies ($f \geq 10$ kHz) showed that the unmodified and modified fabricated devices are capable of discriminating between a minimum of a factor-of-five difference in solution concentration. However, it was more difficult to differentiate between different concentrations of ionic solutions at low frequencies (10 Hz and 100 Hz). This was because at these low frequencies the solution resistance did not play a significant role in the impedance of the system. This was especially apparent in the PEMs-modified electrodes because the polyelectrolyte multilayers contributed to an additional capacitive component in parallel, as shown in Figure 3.14, in the low frequency range.

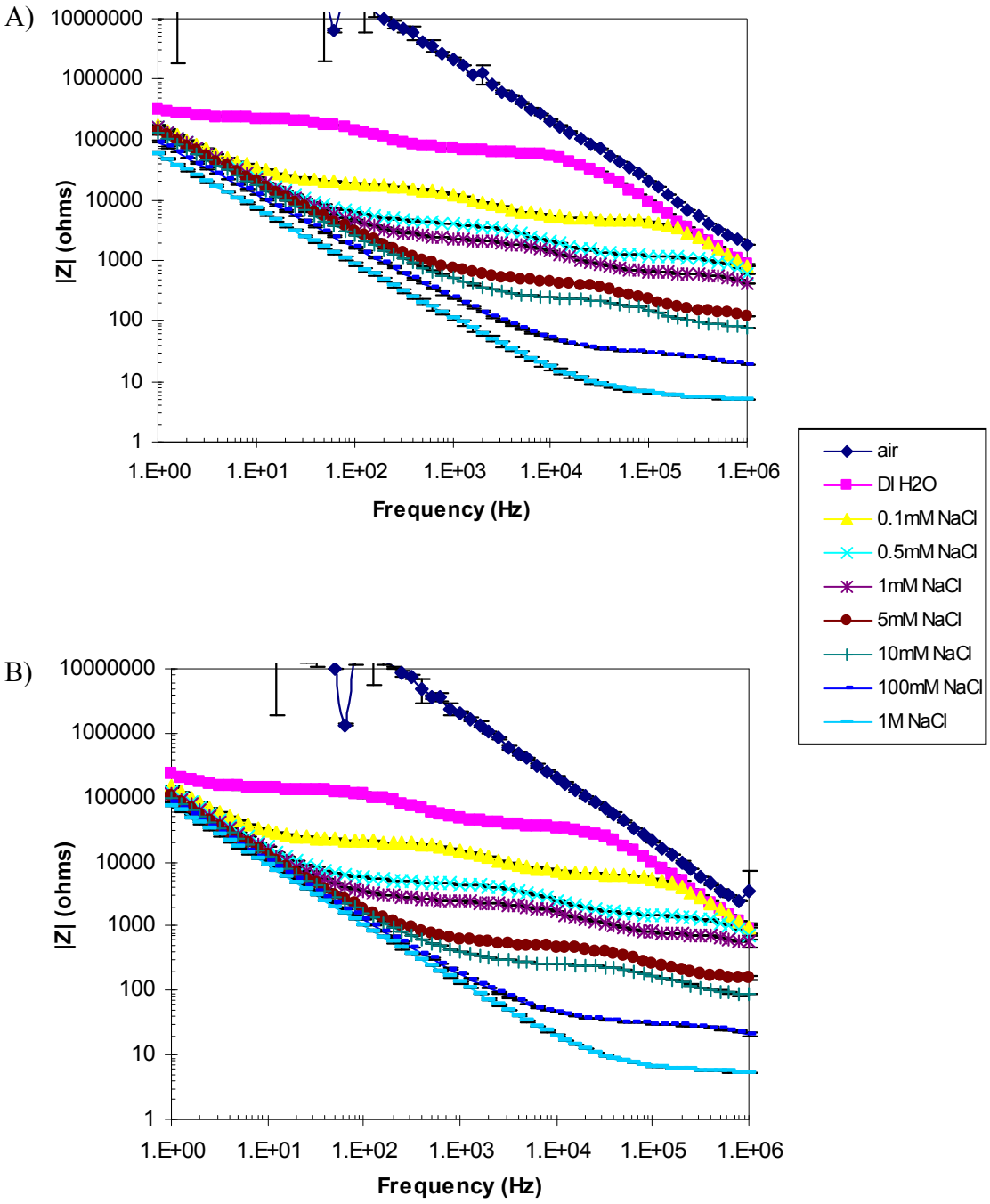

Figure 3.15 Magnitude of impedance of A) unmodified and B) PEMs-modified electrodes as a response to air, deionized water, and solutions with varying ionic concentrations.

3.5.2 Interbatch and Intrabatch Variability

The variation in the performance between different unmodified devices was also examined. This included devices produced within the same fabrication batch as well as those devices fabricated in different batches. The graphs in Figure 3.16 show the magnitude and phase angle of impedance versus frequency of six devices filled with PBS. The magnitudes and phase angles of the impedances of all the devices were similar and varied by less than one order of magnitude from each other.

The calculated two-tailed paired t-test shown in Appendix B revealed that at high frequencies ($f \geq$ 10kHz) and at selected low frequencies (10 Hz and 100 Hz) there is no significant difference (probability level = 0.02 and 0.10, respectively) in the measurement performance of the unmodified devices. Because these measurements did not produce significant variations, there were no substantial fabrication process disparities in electrode and electrode active area dimensions, geometry, and gaps.

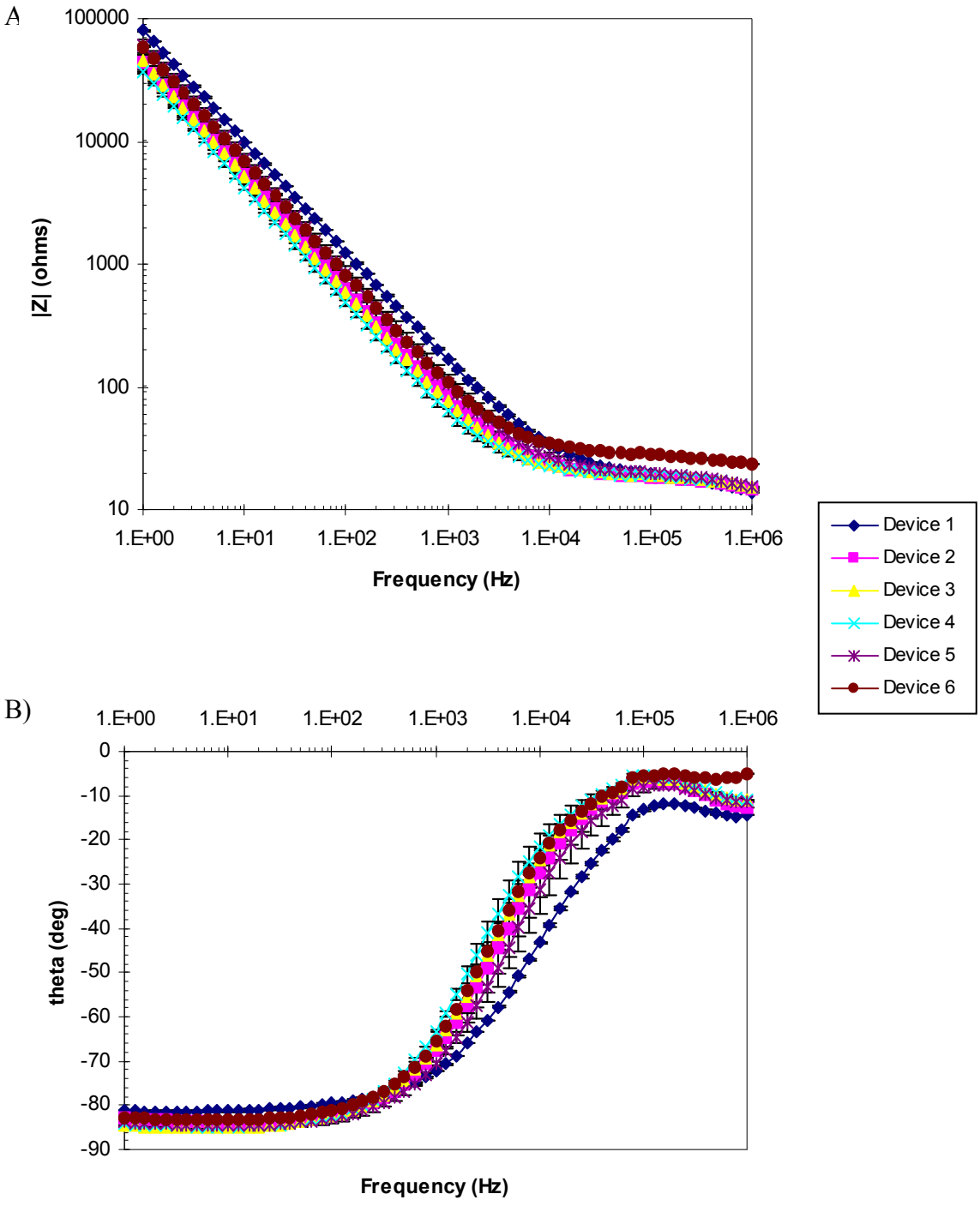

Figure 3.16 A) Magnitude of impedance and B) phase shift of six devices filled with a physiological concentration of PBS to test for interbatch and intrabatch variability.

3.5.3 Cyclic Voltammetry

The quality and state of the unmodified and PEMs-modified electrode surfaces were determined by running cyclic voltammetry with a potential window scan from -0.6 V to +0.85 V. Figure 3.17 shows the CV curves measured at room temperature at scan rates of 5 mV/sec, 10 mV/sec, 25 mV/sec, 35 mV/sec, and 50 mV/sec in DMEM. The fabricated electrodes produced repeating and overlapping CV curves at each scan rate. This demonstrated that the quality and state of the fabricated gold electrodes are excellent and clean. It also confirmed that DMEM acted as a proper supporting electrolyte with no contamination or no redox species present.

When comparing the CV curves of the unmodified and PEMs-modified electrodes, there was a small change in charging current with the addition of PEMs on the electrode surface. There was an increase in the "separation gap" in the steady state area of the curves due to the change in charging current. This was an indication that the deposition of PEMs took place, which affected the value of the double layer capacitance of the electrode. The repeating CV curves for each individual scan rate overlapped each other, indicating no adsorption processes were taking place during the duration of the CV experiment.

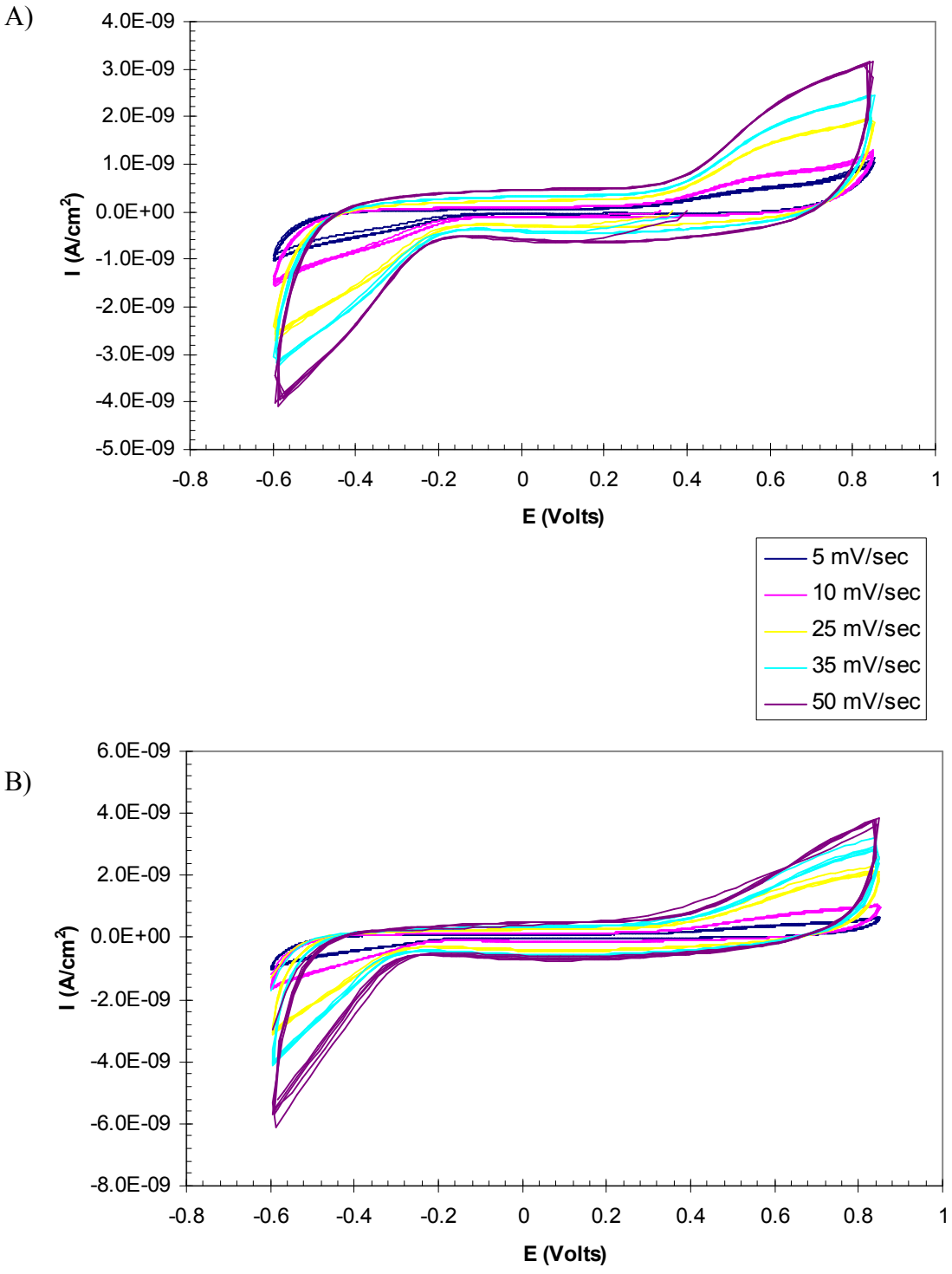

Figure 3.17 Cyclic voltammogram of A) unmodified and B) PEMs-modified TiW/Au electrodes in DMEM at room temperature.

In addition to determining the quality and state of the electrodes and of the supporting electrolyte, it was also possible to determine the capacitive property of the fabricated electrodes by performing cyclic voltammetry at different scan rates in DMEM. According to classical electrochemical theory [100], the relationship between the charging current and scan rate is given by the following equation:

$$i_c = \upsilon A C_d \qquad \text{(Equation 3.4)}$$

where i_c is the charging current (A), υ is the scan rate (V/sec), A is the electrode surface area (cm^2), and C_d is the specific double-layer capacitance (F/cm^2). Therefore, the double layer capacitance, $C_{double} = AC_d$, is the slope of the plot of the charging current versus scan rate. Figure 3.18 shows the plot of the charging current as a function of scan rate. The resulting slope was equivalent to the double layer capacitance of the non-faradaic process. The charging current was different for the forward and reverse scans, therefore two slopes were calculated (Table 3.2).

Table 3.2 Summary of Measured DMEM Double Layer Capacitance Values of Forward and Reverse CV Scans on Unmodified and PEMs-Modified Electrodes

	C_{dl} (F), Forward Scan	**C_{dl} (F), Reverse Scan**
Unmodified Electrode	9.331×10^{-9}	-1.247×10^{-8}
PEMs-Modified Electrode	8.77×10^{-9}	-1.49×10^{-8}

A)

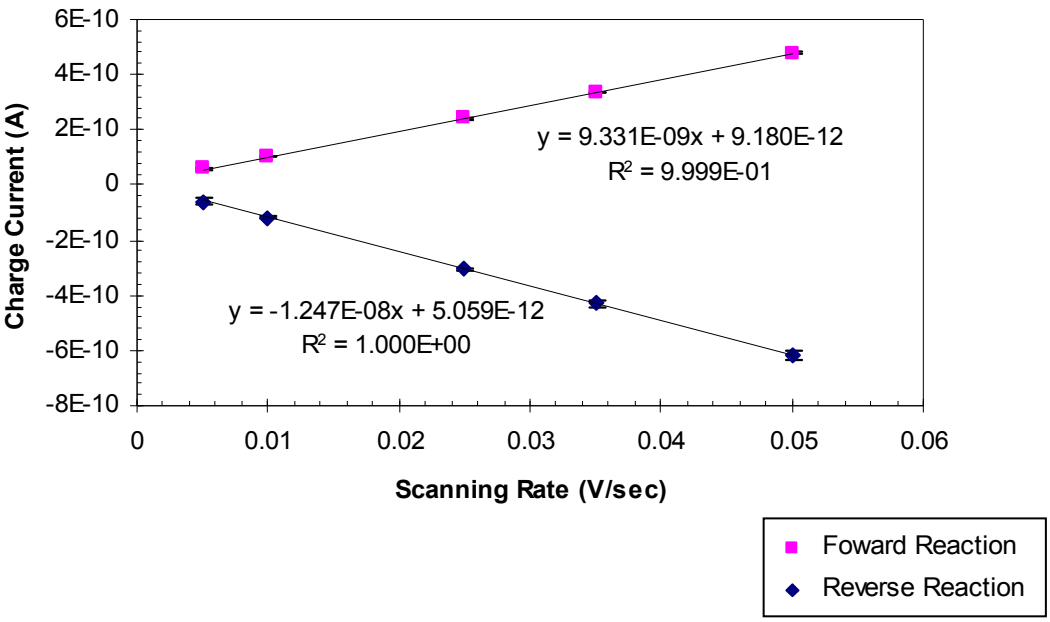

B)

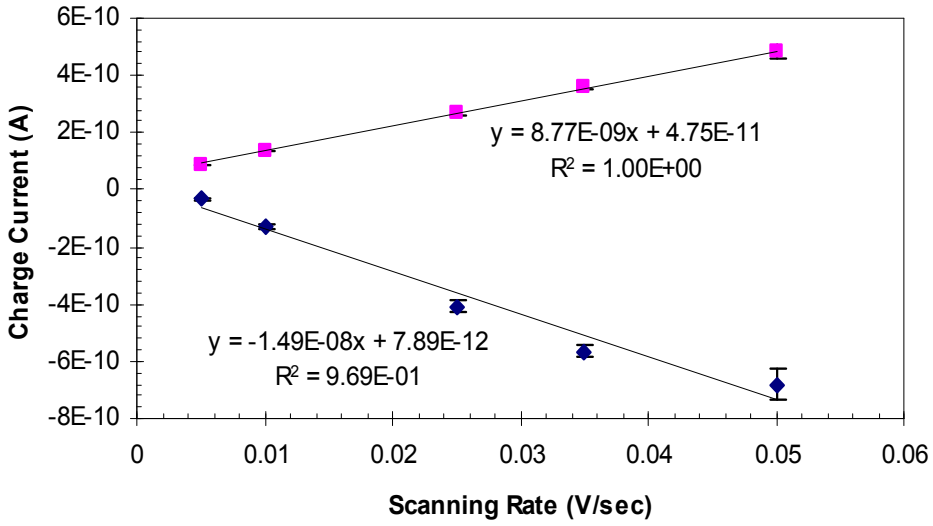

Figure 3.18 Determination of double layer capacitance value of A) unmodified and B) PEMs-modified electrodes in DMEM at room temperature.

The PEMs-modified electrodes showed a decrease in the double layer capacitance for both the forward and reverse scans. This was expected because the PEMs themselves act as a porous blocking layer, thereby decreasing the electrical double layer effect at the electrode surface. PSS/PAH films prepared with 0.1 M NaCl produced a characteristic rigid matrix that lead to the consequent decrease in ionic mobility [92] from the electrolyte-film interface to the film-electrode interface. As the number of deposited layers increased, the electrode regions that were once uncovered by polyelectrolytes began to progressively reduce [101], as shown in Figure 3.19. Therefore, the electrode interface became less and less accessible to the electroactive species in solution.

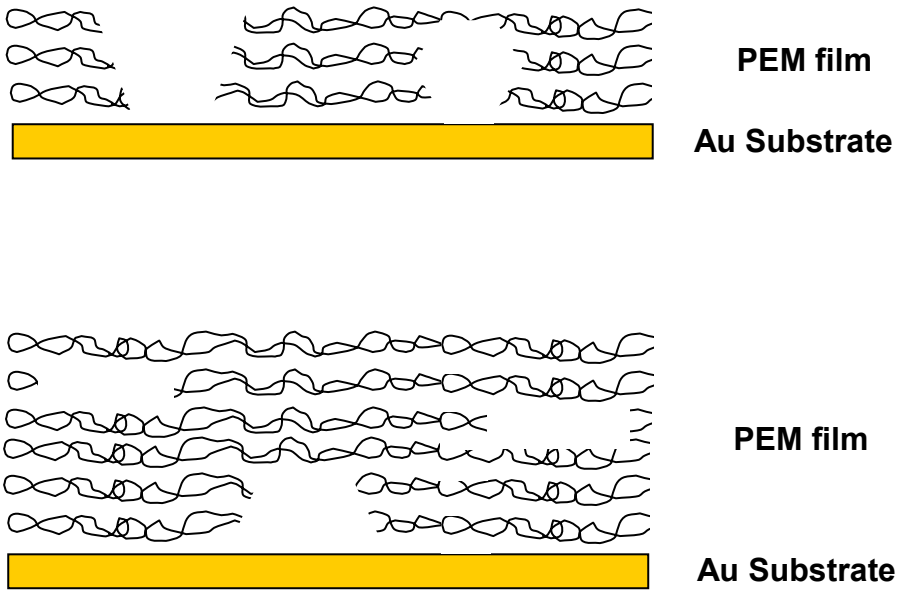

Figure 3.19 Electrode active area region configuration at two stages of PEM film growth. A) Open regions and capillaries present at early film growth stage. B) Partially covered capillaries at a moderate number of polyelectrolyte layers. Adapted from [101].

The electrochemical behavior of both bare gold and PEMs-modified electrodes were evaluated in a solution of either a pure electrolyte of 0.15M PBS or a pure electrolyte with a negative electroactive redox species of 1.5mM $K_3Fe(CN)_6$ in 0.15M PBS. The fabricated gold electrode was used as the working electrode in a two-electrode setup. The reference electrodes (RE) utilized were either an aqueous Ag/AgCl (saturated KCl) electrode or the gold reference electrode found on the fabricated device. Figure 3.20 shows cyclic voltammograms obtained in 0.15M PBS and 1.5mM $[Fe(CN)_6]^{3-/4-}$ for unmodified gold electrodes and electrodes with $PEI(PSS/PAH)_5$ at a scan rate of 50 mV/sec.

The CV response of the unmodified electrode (Figure 3.20A) measured with respect to Ag/AgCl (sat. KCl) in PBS and $[Fe(CN)_6]^{3-/4-}$ in PBS served as a control for the performance of a two-electrode system with a gold WE and a standard RE. When a gold electrode was utilized as the RE, there was a negative shift in the resulting voltammograms. In the CV scan of a reversible electrochemical process, the difference in the anodic and cathodic peak potentials is $57/n$ mV [100], where n is the stoichiometric number of electrons consumed in the electrode reaction. The difference in peak potentials, shown in Table 3.3, in the systems with a Ag/AgCl RE and a gold RE were approximately $290.8/n$ mV and $121.8/n$ mV, respectively. This result showed that the fabricated gold surface allows for a well-defined voltammetric response, but can only produce a quasi-reversible response to electron transfer processes.

A)

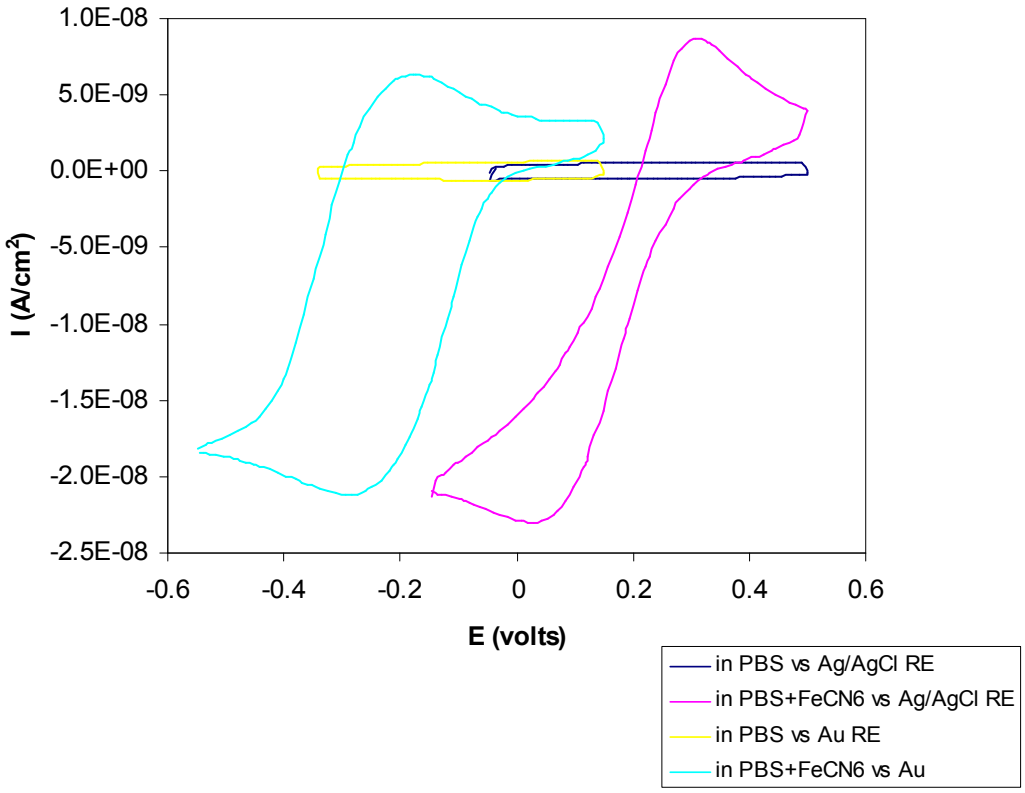

B)

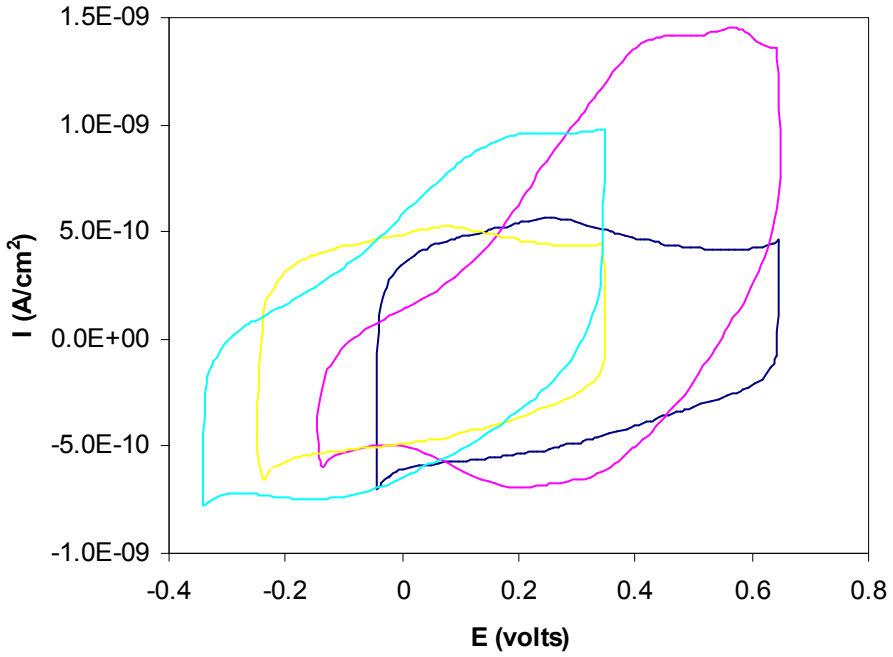

Figure 3.20 Cyclic voltammograms of A) unmodified and B) PEMs-modified electrodes in 0.15M PBS and 1.5mM $[Fe(CN)_6]^{3-/4-}$ in 0.15M PBS with respect to Ag/AgCl (sat. KCl) or gold reference electrodes at a scan rate of 50 mV/sec.

Table 3.3 Anodic and Cathodic Peak Potentials of $[Fe(CN)_6]^{3-/4-}$ For Unmodified and PEMs-Modified Electrodes

	Bare Electrode		PEMs-Modified Electrode	
	vs. Ag/AgCl	vs. Au	vs. Ag/AgCl	vs. Au
E_{anode} (V)	0.31895	-0.17222	0.56545	0.21343
$E_{cathode}$ (V)	0.028111	-0.29397	0.20514	-0.15904

Figure 3.20B shows the CV response of the gold electrodes modified with PEI/$(PSS/PAH)_5$. Well-defined peaks were not present in these graphs because the polyelectrolyte layers acted as blocking layers to electron transfer processes. Although polyelectrolyte multilayers were very permeable to the monovalent or divalent ions of the supporting electrolyte, the permeability toward heavily charged electroactive ions such as $[Fe(CN)_6]^{3-/4-}$ decreased rapidly with the number of layers [99]. The multilayer buildup of PEMs had a marked influence on electrode response, where an increased number of layers resulted in a decreased peak currents [99, 101]. This produced a plateau-shaped CV graph. This was due to the effect of the reduced diffusion ability of the redox species to reach the electrode surface (Figure 3.19). There was also an apparent increase in peak separation (360.31/*n* mV vs. Ag/AgCl RE and 372.47/*n* mV vs. Au RE) because of the large PEMs coverage on the electrode surface. This increase in coverage area as more and more multilayers were deposited on the surface led to an increase in the charge-transfer resistance [99, 101], R_{ct}, shown in Figure 3.10. However, since the cell confluence detector system does not require the unmodified or PEMs-modified electrodes to sense faradaic processes, as shown in Figure 3.11, this altered CV response with a

redox species does not diminish its impedance monitoring capability for monitoring cell growth.

3.6 Conclusion

The fabrication and characterization of TiW/Au electrodes, as well as the surface treatments to facilitate cell attachment through the use of PEMs, was presented in this chapter. The deposition of PEMs was verified by AFM height measurements, as well as by FTIR spectra. Contact angle measurements showed that PEMs led to an increase in the hydrophilicity of the electrode surface. Therefore, the addition of PEMs promoted cell adhesion and supported normal cell growth, which was visualized by viability and cell spreading morphology staining assays.

The performances of the unmodified and PEMs-modified electrodes were investigated with impedance spectroscopy and cyclic voltammetry. It was verified that the use of gold electrodes for both the working and counter electrodes would suffice for impedance studies that monitor cell growth on the surface of electrodes. Impedance spectroscopy revealed that both the unmodified and PEMs-modified electrodes were able to distinguish between a minimum factor-of-five difference in ionic solution concentration. CV measurements with the electroactive species $[Fe(CN)_6]^{3-/4-}$ demonstrated that the addition of PEMs led to a decrease in the ability to allow ions and other molecules to penetrate the layer to come into contact with the electrode surface. However, it is still believed that PEMs can be used as a cell adhesion promoter on the surface of electrodes and allow for successful impedance measurements to probe cell growth. This is because the cell impedance biosensing platform only needs to monitor

non-faradaic processes. The proposed equivalent electrical circuit model did not contain faradaic process elements. Instead, it had parameters to describe solution resistance, double layer capacitance as a constant phase element, and parallel resistance and constant phase elements to represent contributions from either the PEMs layer or adherent cells.

CHAPTER 4

CELLULAR PROLIFERATION MEASUREMENTS

The next phase of research examined the use of the fabricated TiW/Au electrodes modified with PEMs to probe cell growth. As discussed in Section 1.2.1, polyelectrolyte multilayers offer numerous advantages over other cellular adhesive materials, i.e. ECM proteins, which include their inability to degrade over time unlike their biological counterparts. Their functionality, charge, and wettability characteristics can also be modified through the choice of the outermost layer. PEMs layer thickness and surface roughness can be controlled with pH and ionic concentration [102].

Cell proliferation was observed through the analysis of impedance measurements. Cell growth monitoring was first completed with visual inspection of the increase in cell number over time. This estimate was then correlated with an electrical impedance method and an optimal frequency was identified. The impedance measurements and cell counts on PEMs-modified electrodes were compared with cell growth on unmodified gold electrode devices. These results were then evaluated with the electrical equivalent circuit proposed in Section 3.4. Finally, a correlation between cell density and normalized impedance was made.

4.1 Impedance Monitoring

As seen in Figure 4.1, the total impedance of the system is dependent upon frequency. At lower frequencies of < 10 kHz, the impedance is dominated by the diffusive ion transport and capacitive current flow through the double layer electrode

interface. The electrical double layer capacitive region, C_{dl}, illustrates that the double layer capacitance becomes essentially resistive at lower frequencies. As the impedance value increases, it becomes the main source contributing to the total impedance. The medium resistance can, therefore, be ignored in this case.

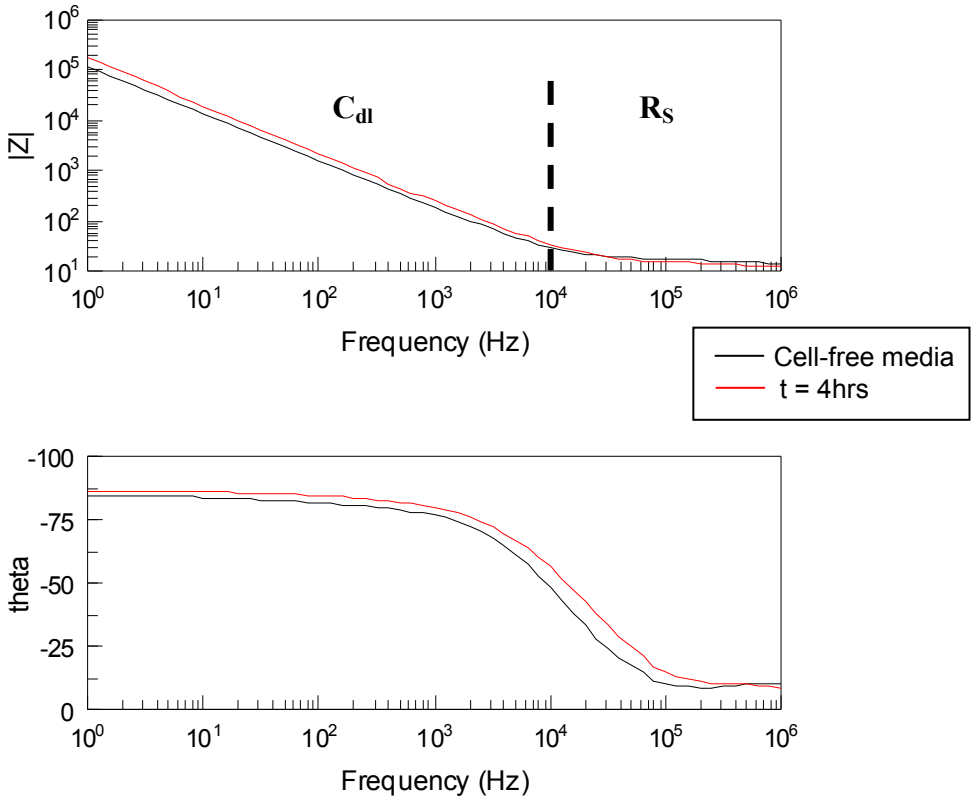

Figure 4.1 Example Bode plot of the impedance of cell-free media (black line) and cells that began to flatten onto the electrode surface 4 hours after inoculation (red line).

At higher frequencies of > 10 kHz, the total measured impedance should be constant because capacitance offers no contribution to impedance. Thus, the impedance is dominated by the conduction of ions in the medium, or medium resistance, while the contribution of the double layer capacitance becomes negligible. This effect is illustrated by the resistive region, R_s, in Figure 4.1.

It is essential to sweep across a frequency range while taking impedance measurements because of the information about the changes in the electrical double layer of the electrode and in the medium during cell growth acquired at different frequencies. Low-frequency impedance measurements provide information about the double layer capacitance, while high-frequency impedance measurements provide information about medium resistance. Therefore, the behavior of either the electrical double layer of the electrode or the resistive nature of the medium can be used to provide information during the detection of cell growth.

4.1.1 Determination of Optimal Frequency

The change in the total impedance between no cells and cells that are confluent on the electrode surface can be seen as a maximum value at a particular frequency. It is at this frequency that the impedance measurements are the most sensitive and mirror the associated changes in cell number and morphology [62]. In particular, these measurements are monitored at frequencies between 10 Hz and 10 kHz, as stated in the above section. The electrical impedance measurements at both ends of the spectrum are independent of cell shape changes and viability.

At the low frequency end (f < 10 Hz), the overall impedance of the system is dominated by the impedance of the electrode/electrolyte interface. This low-frequency impedance is also affected by the ionic concentration close to the interface, which is altered by cell respiration [81]. At the high frequency end (f > 10 kHz), the total system impedance is represented by the sum of the culture medium resistance, the constriction resistance of the working electrode, and the resistance due to all of the wiring. In

addition, at high frequencies, some of the applied AC current can capacitively couple through the cell plasma membrane and flow through the cell layer via transcellular pathways, i.e. transcellular proteins [62]. This does not allow the impedance measurements to be solely based on the phenomenon of cell-substrate interactions.

Therefore, at the intermediate frequencies (10Hz < f < 10 kHz), the effect of the cell bodies dominates the total impedance of the system. The current is altered to flow underneath the cell-substrate junctions, through aqueous gaps formed from focal adhesions, and in between cell-cell junctions. To validate the choice of the working frequency, the Bode plots must be recorded starting with a cell-free media measurement. The impedance measured at the cell seeding, or inoculation, time point must also be plotted, as well as the cellular impedance response to a solution or chemical that promotes cell detachment from the surface. After the addition of the solution, the impedance signal should decrease to a value that is close to the cell-free impedance value. It is at an optimal frequency that the device is most sensitive to the presence or absence of cells on the electrode surface.

4.2 Quantification of Cells

Visual inspection of 3T3 cells growing on unmodified and PEMs-modified devices was made using optical microscopy with phase contrast. Cell number on the detecting electrode and counter electrode was estimated with the use of optical micrographs and a cell counter plugin using the ImageJ 1.38x software (National Institutes of Health, USA).

To check for deleterious responses as 3T3 cells grew on the device, the cells were seeded at comparable densities of ~1.0 x 10^5 cells/mL (~4000 cells/cm^2) for a conventional 25 cm^2 cell culture flask. It was desired for the time of the cells to attain confluency in the 7 mm diameter growth chamber device to be comparable to that exhibited by the cells grown in the culture flask. Figure 4.2 shows 3T3 cells growing on A) unmodified and B) PEMs-modified electrodes. Cell growth on unmodified electrodes was discontinued after 72 hours from cell seeding, while cell growth on PEMs-modified electrodes was stopped after 96 hours.

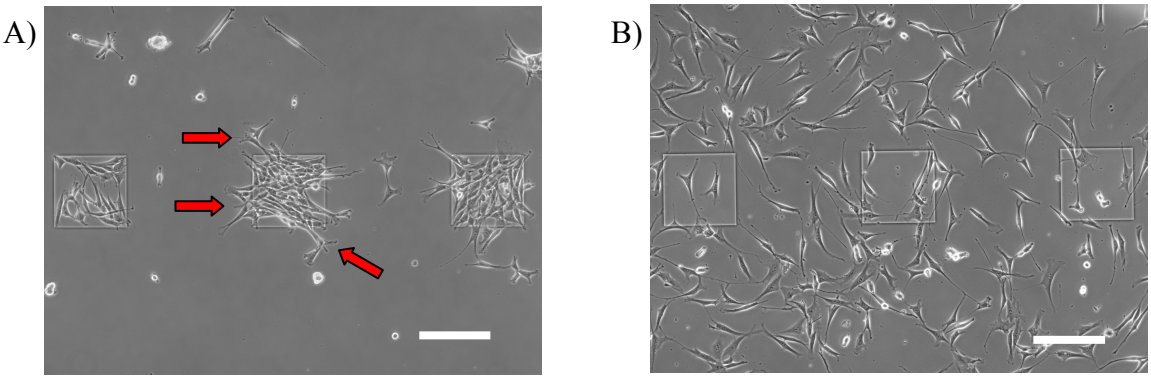

Figure 4.2 NIH-3T3 fibroblast cells growing on A) unmodified and B) PEMs-modified electrodes 48 hours after inoculation. Red arrows denote examples of 3T3 cells migrating onto oxide due to overcrowding on unmodified gold surfaces. All scale bars are 200 μm.

In Figure 4.2A, the 3T3 cells grew preferentially on the unmodified gold surfaces and rarely extended onto the oxide passivation layer. When overcrowding occurred on the unmodified gold surfaces, the 3T3 cells migrated onto the oxide (see red arrows for examples). Some of these migrated cells had continuous contact with those cells attached onto the bare gold surfaces, which played a role in their viability [39]. Figure 4.2B

shows 3T3 cells grown on PEI/$(PSS/PAH)_5$, which covered the unmodified gold areas, as well as the oxide passivation layer. Because of this increased surface area to which the cells proliferated on, the time required for attaining approximately 80% confluency, which was between 72-96 hours from inoculation, was comparable to that of a traditional cell culture flask. On the other hand, cells grown on unmodified devices reached 80% confluency in approximately half the time (48 hours). Figure 4.3 shows the change in cell density over time on unmodified and PEMs-modified devices.

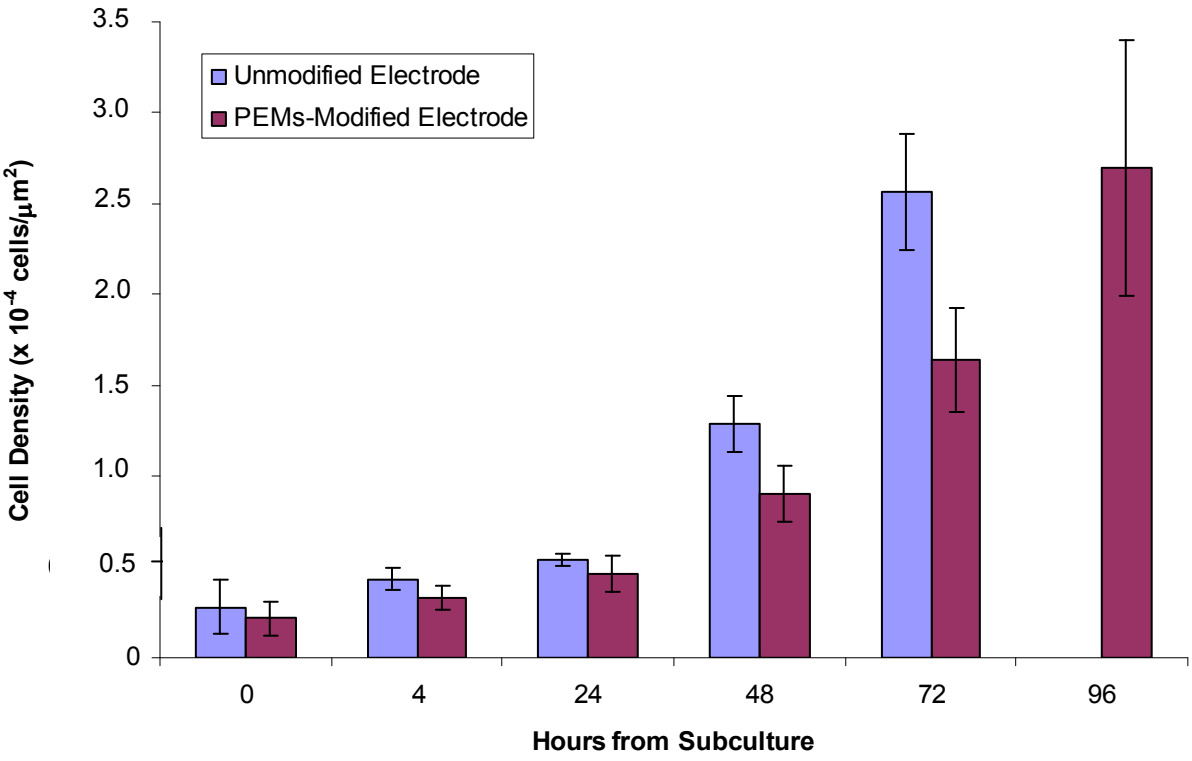

Figure 4.3 Cell density graphs of NIH-3T3 fibroblast cells growing on unmodified and PEMs-modified devices.

From Figure 4.3, the graph of the cell density on the unmodified electrode device shows a deviation from cell growth on PEMs. During the first 24 hours, there was

approximately no change in cell density between the two substrates. However, 3T3 cells reached confluency faster on the unmodified substrate because the growth was supported on a reduced surface area restricted to bare gold. The cells preferred to grow on the unmodified gold areas and not on the oxide passivation layer unless overcrowding occurred, as seen in Figure 4.2A. This constrained growth would be beneficial if a confluent layer of cells is needed quickly because the cells are populating the electrode active area very rapidly. In approximately 48 hours, the cells were approximately 80% confluent. Therefore, cell assays can be performed on these cells more quickly than those cells reaching confluency in 72 hours.

The PEMs-modified device allowed for normal cell growth to occur in a comparable pace as those cells grown in traditional polystyrene cell culture flasks at equivalent cell seeding densities. The final cell density of 2.5×10^{-4} cells/μm^2 on a PEMs-modified device reached at t = 96 hours was approximately the same as on an unmodified device at t = 72 hours.

4.3 Cell Confluency Monitoring

In addition to visual inspection to quantify the number of cells on the electrode surface, time-dependent alternating current impedance was used to evaluate the performance of bare gold and PEMs-modified cell-bearing electrodes under conventional cell culture conditions. The setup used for the impedance testing comprised of the Solartron SI 1287A Electrochemical Interface with the Solartron 1260 Impedance/Gain-Phase Analyzer (Solartron Analytical, Oak Ridge, TN) and is illustrated in Figure 4.4 (top image). The humidity and temperature of the system was maintained at 37 °C, as

well as the CO_2 levels being preserved at 5% (v/v), through the use of an Axiovert 200m inverted microscope (Zeiss, Inc.) equipped with a surrounding incubation chamber. The bottom image in Figure 4.4 displays another setup located within the incubation chamber. This setup consisted of an in-house fabricated poly(methyl methacrylate) (PMMA) chip carrier to hold the cell confluence detector device in place on the microscope stage. A small Petri dish was included to hold ultrafiltrated deionized water (DI H_2O) to avoid DMEM evaporation. A microscope stage cover to maintain the humidity and CO_2 levels within the confined area surrounded this secondary setup.

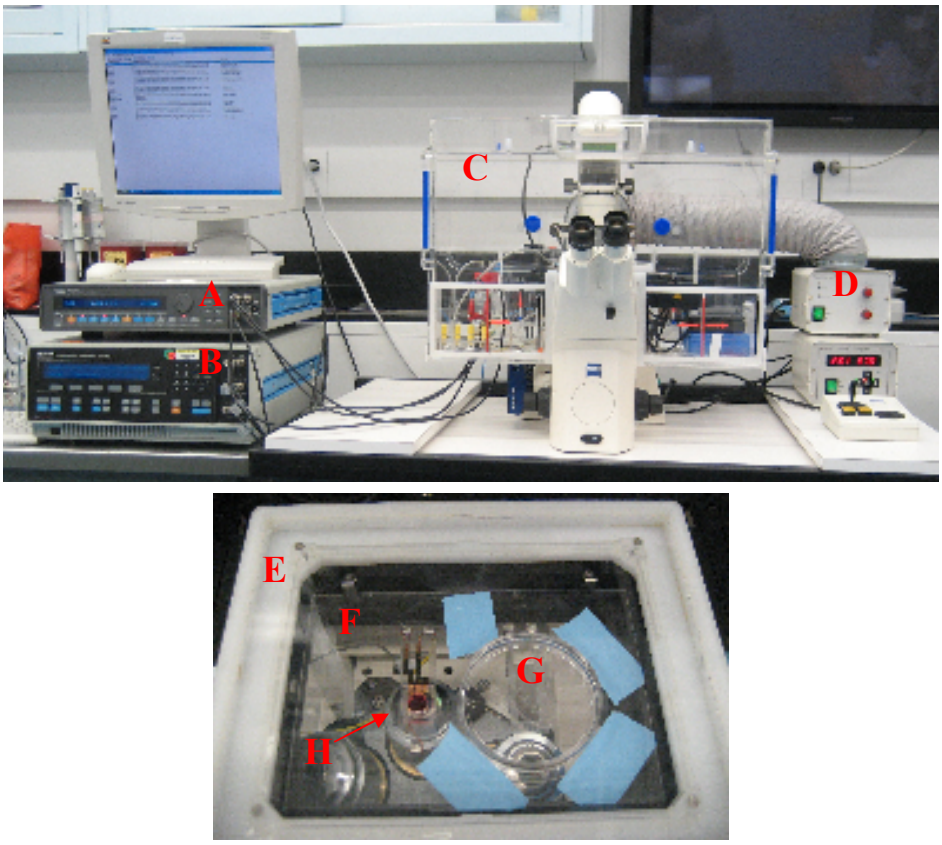

Figure 4.4 Impedance analyzer instrumentation and setup for the characterization of cell confluence detector device. A) Electrochemical interface. B) Impedance/gain-phase analyzer. C) Inverted optical microscope surrounded by an incubation chamber. D) Temperature controller. E) Microscope stage cover to maintain humidity and CO_2 levels. F) PMMA chip carrier. G) Small Petri dish to hold DI H_2O to avoid DMEM evaporation. H) Cell confluence detector device.

The AC probe signal used to characterize the impedance was 1 mV peak-to-peak over the frequency range of 1 Hz to 10^6 Hz. The resulting current never rose above the nA range, which did not cause any detrimental effect on the cells [103, 104]. The impedance spectra were recorded using ZPlot2/ZView2 software package to measure and record the impedance of the system. Three different types of impedance plots, Z" vs. Z', |Z| vs. *f*, and θ vs. *f*, were recorded and used to visualize the raw data and evaluate the quality of data fitting over the entire frequency domain probed.

The cell chamber was filled with warmed DMEM at 37 °C. An initial impedance media control measurement was taken after a 10-minute temperature stabilization period. The microchamber was then seeded with 3T3 cells and impedance measurements were taken continuously over time. The measurements began at t = 0 hours from when the cells were seeded into the system, and in 10 minute increments until either 72 or 96 hours after inoculation for unmodified or PEMs-modified electrode devices, respectively, was reached. Phase contrast images of the cells grown on the device were taken at t = 0 hours, 4 hours, 24 hours, 48 hours, 72 hours, and 96 hours. 3T3 cells were visualized using the AxioCam MRm camera on the inverted microscope and were acquired by the AxioVision software v.4.5.

0.25% trypsin/0.53 mM ethylenediaminetetraacetic acid (EDTA) in Hank's buffered salt solution (HBSS) without calcium or magnesium (ATCC) was introduced to the system to promote cell detachment from the electrode surface (Figure 4.5) after confluency was attained. Cell detachment from the surface was primarily a result of trypsin, a proteolytic enzyme that cleaved the peptide bonds on the carboxyl side of lysine and arginine residues [29]. These amino acids were found in the ECM and

mediated cell adhesion [28, 29]. Cell disaggregation was also facilitated by EDTA. EDTA bound to and chelated Ca^{2+}, which was a promoter of cell-cell adhesion [29]. Figure 4.5A illustrates the presence of a cell monolayer on an unmodified electrode surface. In Figure 4.5B, the morphology of the cells exposed to 0.25% trypsin is visible. The cells show the typical morphology of rounded cells, which were detached from the surface, leaving the electrodes essentially cell-free.

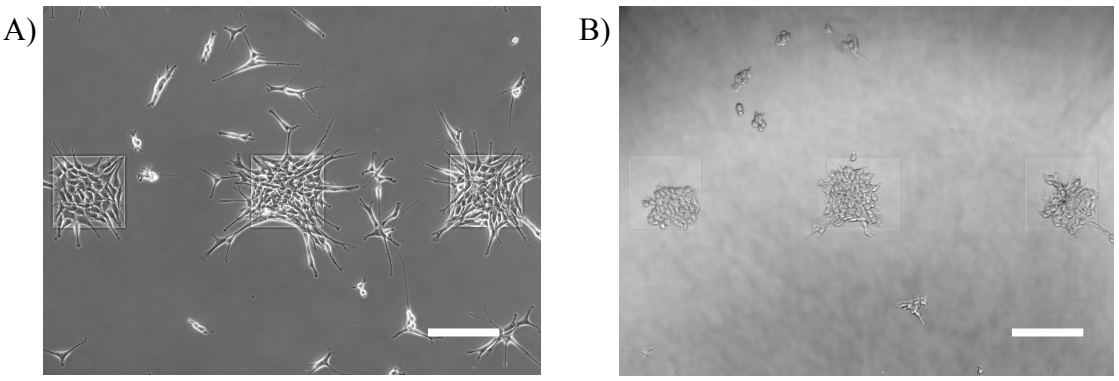

Figure 4.5 Phase contrast images of NIH-3T3 fibroblast cells on the device A) prior to and B) after exposure to 0.25% trypsin. All scale bars are 200 μm.

As stated in Section 4.1, it was essential to determine the proper frequency at which the impedance for cell growth is monitored. For both the bare gold devices and the PEMs-modified devices, the optimal frequency of 1000 Hz was chosen. Figure 4.6 shows the impedance monitoring of 3T3 cells growing on unmodified and PEMs-modified devices at 1000 Hz. The media control measurement was recorded as t = -1 hours from subculture. The magnitude of impedance was recorded until 72 hours and 96 hours from subculture for unmodified and PEMs-modified devices, respectively. At the

specified endpoint, a 0.25% trypsin/EDTA solution was added to the system to promote cell detachment and the impedance was recorded.

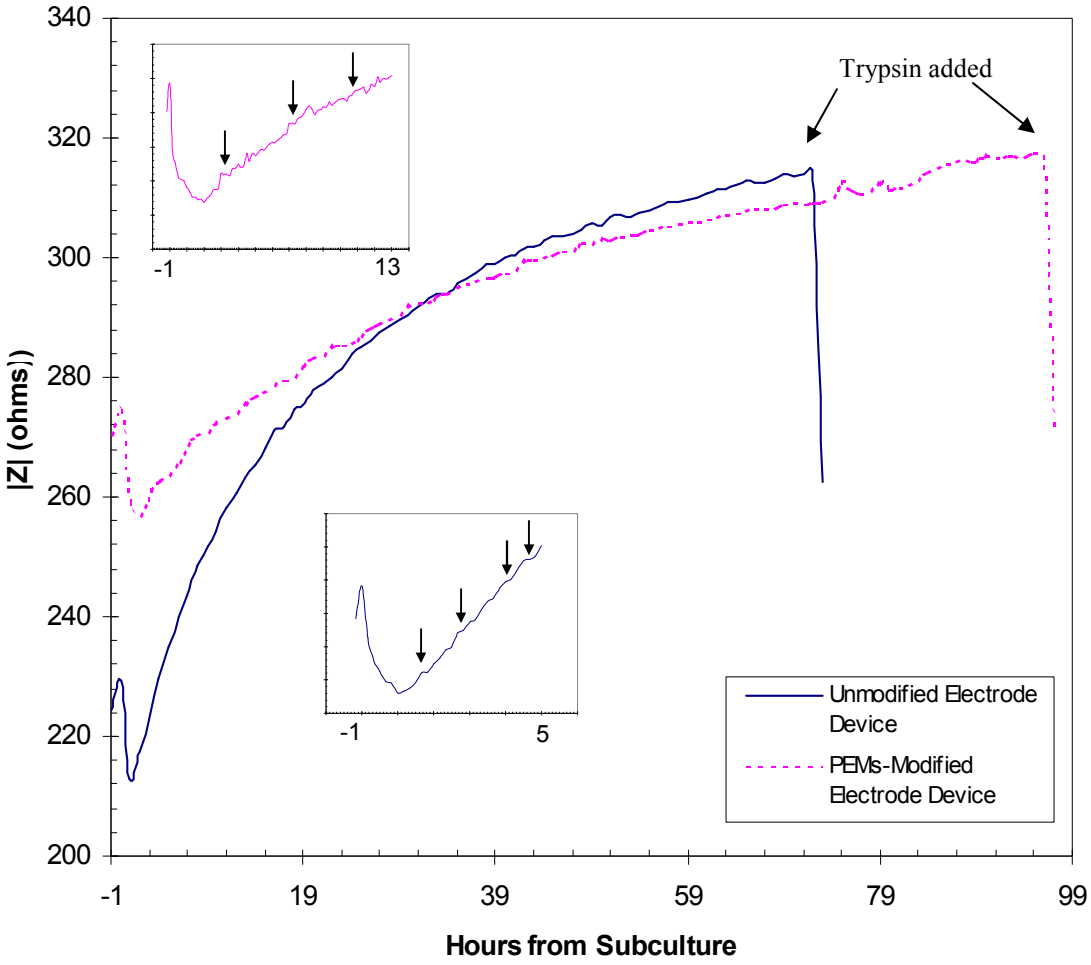

Figure 4.6 Magnitude of impedance of NIH-3T3 fibroblast cell growth on unmodified devices (solid line) and PEMs-modified devices (dashed line) at 1000 Hz. The inset graphs illustrate the change in impedance from cell-free media until 5 hours and 13 hours after subculture for unmodified and PEMs-modified electrode devices. Arrows in the insets denote areas of constant impedance where cells are flat on the electrode surface, moving horizontally across the electrode, and experiencing cell division. 0.25% trypsin/EDTA is added to the system after continuous impedance monitoring is completed.

The impedance of the PEMs-modified devices was measured in DMEM before and after the deposition of PEMs onto the surface of the electrodes. It was determined that the PEMs layer contributed to the overall impedance of the system by increasing the value. The change in impedance from an unmodified to PEMs-modified device was measured to be 75.77 Ω ± 10.23.

In Figure 4.6, the cell suspension was added to the system at t = 0 hours. There was a decrease in impedance at this time point when compared to the cell-free media measurement at t = -1 hour. The addition of the cell suspension caused a decrease in impedance because it was interpreted as a solution with a higher ionic concentration when compared with the media control solution. The cell surface displayed a net negative charge due to exposed charged glycoproteins and glycolipids located on the cell membrane surface [29, 39, 105]. It was also during this time that the cells were adapting to the system, until a constant rate of increase in impedance was reached. When the constant rate of increase occurred, it was interpreted as the beginning of cell spreading and proliferation due to cell adhesion [106].

As time passed, the cells changed from being suspended in solution to migrating downward towards the electrode surface, where cell attachment and spreading occurred. The inset graphs of Figure 4.6 illustrate the change in impedance every 10 minutes from when the cells are seeded until 5 hours and 13 hours for unmodified and PEMs-modified devices, respectively. During this time, constant impedance values were observed when the cells were changing from being a single, flattened cell to a cell experiencing cell division [79]. Small impedance fluctuations were due to the cells crawling along, as well as moving on and off, (i.e. any horizontal motion) the electrode surface. Impedance

increases were also an effect of rounded cells moving from suspension to becoming flat and adherent to the surface.

Impedance fluctuations were also apparent in the later time points, but cannot be contributed to the above explanations. Because the basis of this electrical technique of sensing cell confluency is based upon the ability of the current to flow underneath and in between adherent cells, these later impedance fluctuations were due to interactions of the cells and the electrode surface. Vertical micromotions (i.e. vertical displacements on the order of nanometers, which are significantly beyond the resolution of optical microscopy) of the cells due to changes in cell morphology [57, 61] altered the distance of the aqueous gaps between the cell and the electrode surface, thereby affecting the measured impedance detected by the system. Therefore, the measured impedance continued to fluctuate even after an approximate steady state was reached because of the constant motion of the cells that altered the current flow in subtle ways. It was also expected that the cells continued to change morphology within a single location because of the many chemical processes and reactions taking place internally within the cell [61].

Cell growth continued until the impedance curve began to approach an asymptotic shape. This approximate steady state result was confirmation that the adherent cells became confluent on the electrode surface. The size of the electrode restricted the maximum cell population to be electronically observed. The measured impedance vs. time plot depended upon the cell line, coating proteins, and other physiological conditions, such as pH and temperature [103]. The cells seeded on the unmodified device reached confluency, or an approximate steady state impedance, before the PEMs-

modified devices because of the reduced preferred surface attachment area, which is seen in Figure 4.2.

Once a confluent cell monolayer was obtained, the cells were subjected to trypsin exposure to promote their detachment from the surface and the resulting impedance was followed. The system was successfully able to detect the detachment of the cells after a five-minute exposure to trypsin on both unmodified and PEMs-modified devices. A significant drop in impedance was observed. The measured impedance, however, did not return to the baseline measurement in either case. This was believed to be due in part from cleaved adherent proteins, as well as other serum components from the culture media, that remained on the surface of the electrode, thereby offering a resistive contribution to the resulting impedance. In addition, there may have been some products from cellular metabolism and respiration or from the trypsin solution [60] that contributed to measured impedance not returning to a cell-free value.

4.3.1 Impedance Data Normalization

The raw impedance data for 3T3 cell growth on unmodified and PEMs-modified devices was normalized in Figure 4.7. The normalized impedance $Z_{norm}(t)$ is defined by:

$$Z_{norm}(t) = \frac{Z(t)}{Z(0)} \qquad \text{(Equation 4.1)}$$

where $Z(t)$ is the measured impedance at time t and $Z(0)$ is the measured impedance at the time of cell seeding (t = 0 hours). The data was normalized against this time point because the final measured impedance is dependent upon the initial cell concentration used for inoculation, which could vary due to the small volumes of the added cell

suspension. Figure 4.7 shows the graph of the normalized impedance data of both unmodified and PEMs-modified devices.

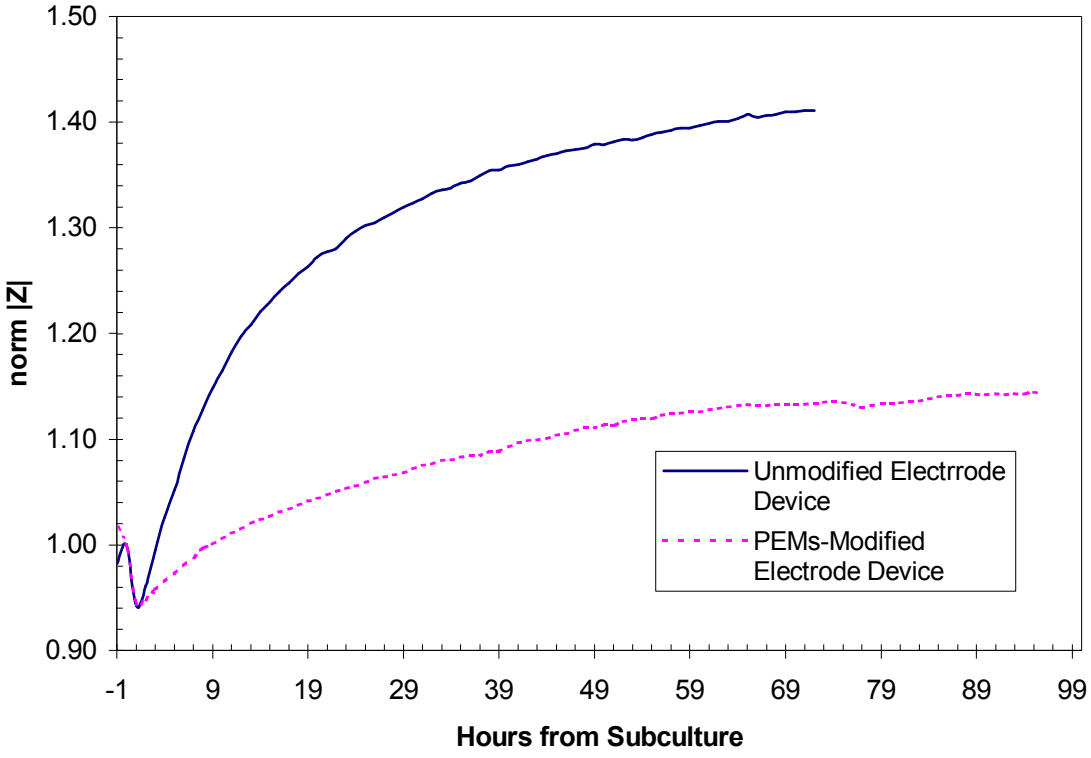

Figure 4.7 Normalized magnitude of impedance against t = 0 hours (time of NIH-3T3 fibroblast cell seeding) of unmodified (solid line) and PEMs-modified (dashed line) devices at 1000Hz.

Figure 4.7 shows that the normalized impedance of unmodified and PEMs-modified electrodes traced each other up until one hour after cell inoculation on the device. It was expected that the impedance of the PEMs-modified device to show a lower sensitivity to cell growth when compared to the unmodified device because of its additional insulating polyelectrolyte layers. However, an approximate steady state level of impedance was still visible when using the device coated with PEMs. The increase in normalized impedance was approximately 40% (1.40-fold difference) and 15% (1.15-fold

difference) for unmodified and PEMs-modified electrode devices, respectively. Despite the small increase in normalized impedance for the PEMs-modified electrode device, examination under a microscope revealed that there was a significant increase in cell number during the course of the experiment. In addition, this data indicated that the PEMs-modified device displayed an excellent efficiency of 82% of detecting cell presence.

Reproducibility of the normalized impedance of both the unmodified and PEMs-modified electrodes was satisfactory since the general behavior of the cell growth was similar in the overall trend (Figure 4.8). However, no correlation between the devices could be made. The most likely explanation for this is because the impedance fluctuations were random in nature due to cell micromotion and viability.

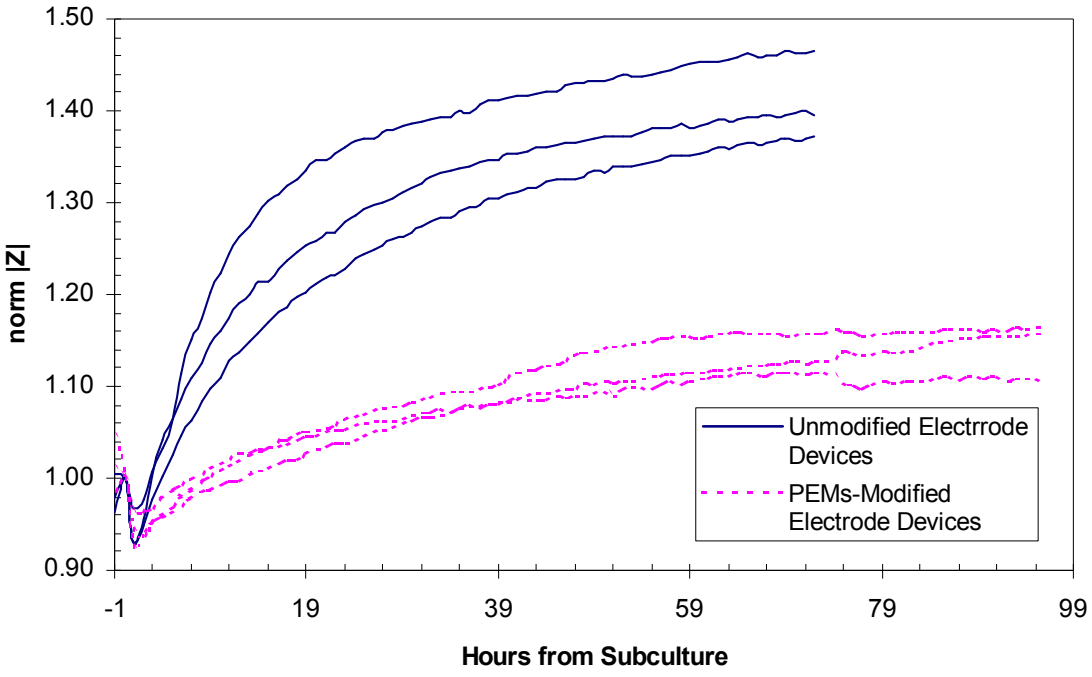

Figure 4.8 Reproducibility of three different unmodified (solid lines) and PEMs-modified (dashed lines) electrode devices each.

4.3.2 Comparison with Equivalent Electrical Circuit Model

Based on the equivalent electrical circuit model proposed in Section 3.4, the recorded impedance data was validated to the theoretical model. This was accomplished with the Zview2 software by applying equivalent circuit and data fitting tools with maximum and optimization iterations of 100 each to all the recorded data points. Using these simulations, the values of R_s, CPE_{dl}, R_{PEMs}, CPE_{PEMs}, R_{cell}, and CPE_{cell} were found, when applicable. Figures 4.9 (unmodified electrode device) and 4.10 (PEMs-modified electrode device) show the recorded and fitted data in cell-free media and with a confluent layer of cells at either 72 or 96 hours after cell seeding.

The |Z| vs. frequency plots in Figures 4.9A and 4.10A show an increase in measured impedance data (open circle data points) when a layer of cells is on the electrode surface. This increase in impedance, illustrated as the difference between the two curves, was due to the resistive and capacitive components of cells. The change, however, was more pronounced in the unmodified electrode system than in the PEMs-modified system. The PEMs added another resistor and capacitor in parallel with each other to the system and acted as an additional coating material on top of the adsorbed proteins from the cell culture media. The capacitive addition of the cells and PEMs layers was also seen in the graph of the phase angle (theta) vs. frequency. The phase angle decreased to a value closer to –90°, which was suggestive of an increase in capacitance.

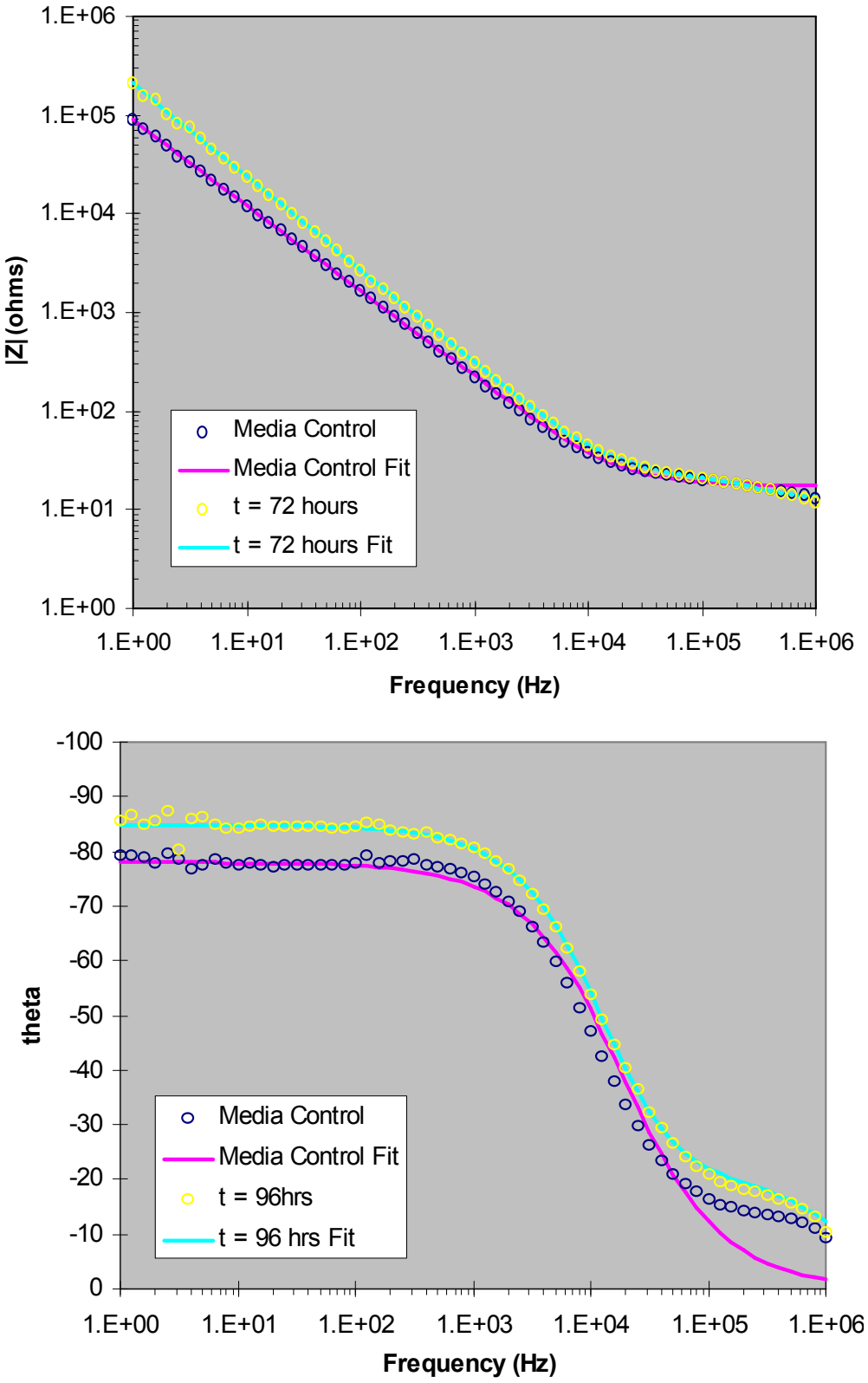

Figure 4.9 Bode plot of theoretical equivalent circuit model data fitted against recorded experimental data of unmodified electrode devices in cell-free media and with NIH-3T3 fibroblast cells at t = 72 hours.

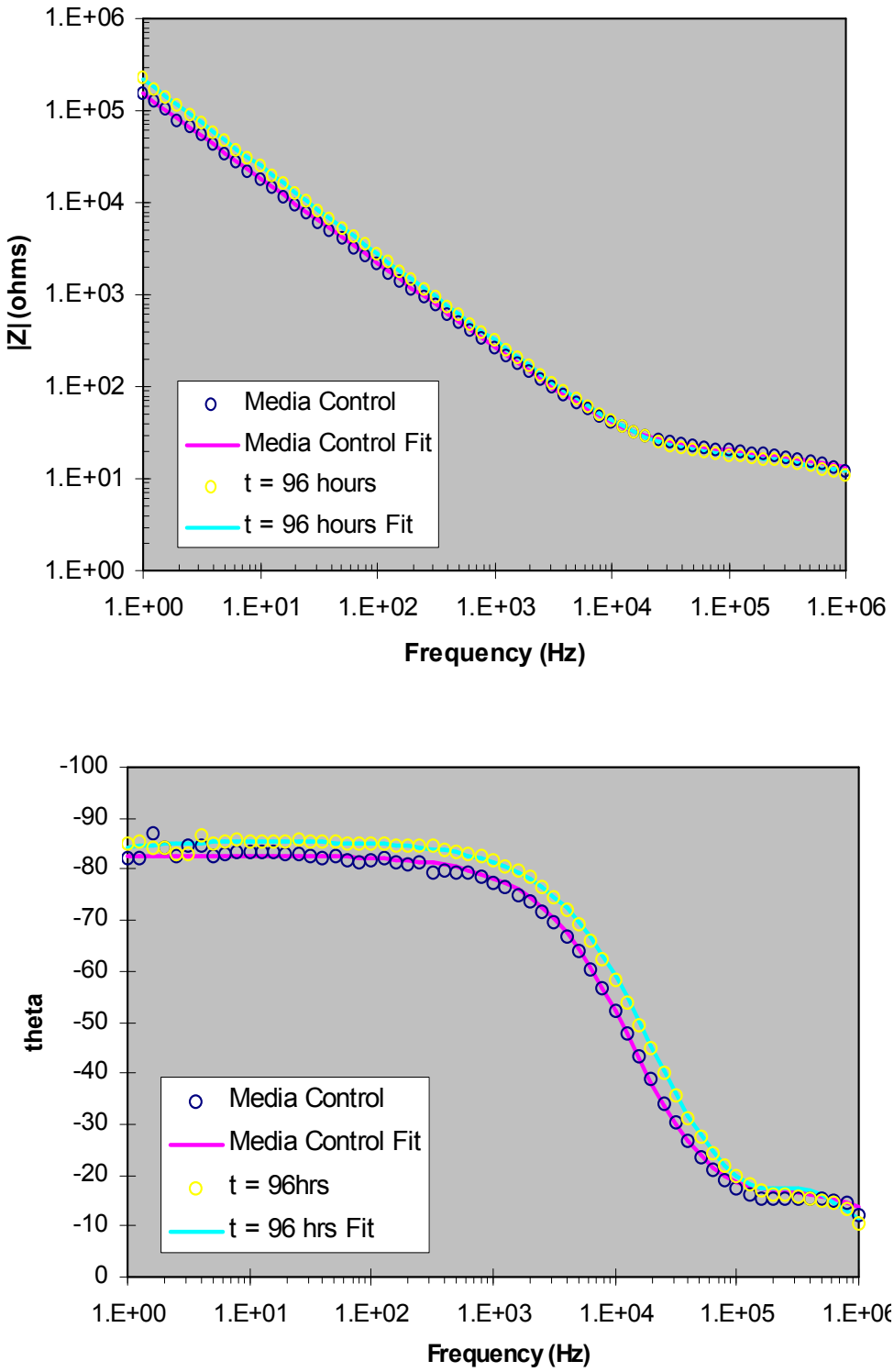

Figure 4.10 Bode plot of theoretical equivalent circuit model data fitted against recorded experimental data of PEMs-modified electrode devices in cell-free media and with NIH-3T3 fibroblast cells at t = 96 hours.

The simulation program was run against the measured impedance data to see how close the equivalent circuit model fit the system. The results are shown as solid lines. The sum-of-squares[4] values calculated by the simulation software for the unmodified electrode device were 0.22599 for cell-free media and 0.34536 for media with cells. The PEMs-modified electrode device displayed sum-of-squares values of 0.28753 for cell-free media and 0.17206 for media with cells. The calculated agreement between the measured data and the fitting spectra was not as high as expected. However, the visual agreement between the measured data and fitting spectra indicated that this proposed equivalent circuit provides a feasible model to describe the performance of unmodified and PEMs-modified electrode devices.

Table 4.1 displays the value of each electrical element in the cell-free equivalent circuit (Figure 3.13) obtained by fitting the equivalent circuit to the measured impedance spectra. When comparing the cell-free media data for both types of electrode devices, the results showed the deposition of PEMs onto the gold electrode surface decreased the solution resistance (R_s) by 40% and the double layer capacitance (CPE_{dl}) by 47%, indicating that those elements were affected by the modification of the electrode surface.

In Section 3.5.3, the values of the double layer capacitance in cell-free media were calculated to be 9.331×10^{-3} μF and 8.77×10^{-3} μF for unmodified and PEMs-modified electrodes, respectively. These values were three orders of magnitude less than the fitted values displayed in Table 4.1. However, considering that the equivalent circuit parameters are inter-correlated and that resistance varies with temperature, the

[4] Sum-of-squares is a concept in statistics to measure the goodness-of-fit and is more accurately called "the sum of the squared deviations." Mathematically, it is an unscaled measure of variability from any point in a collection of data to the mean of the data, otherwise known as the deviation. In general, the larger the sum-of-squares, the better the model performs in its estimation.

capacitance value is also temperature-dependent. The capacitance measurements at room temperature and at 37 °C cannot, therefore, be directly compared. In addition, if the C_{dl} measurements were taken at 37 °C, the simulated value would still not correspond with the calculated values. The values found in Section 3.5.3 represent an ideal capacitor, not a constant phase element, which was the electrical component simulated in the equivalent circuit models of the electrodes in cell-free media (Figures 3.13 and 3.14).

Table 4.1 Parameter Values Obtained by Fitting the Impedance Data of Cell-Free DMEM to the Equivalent Circuit Represented in Figures 3.13 and 3.14

	R_s (Ω)	CPE_{dl}-Q (μF)	CPE_{dl}-p	R_{PEMs} (Ω)	CPE_{PEMs}-Q (μF)	CPE_{PEMs}-p
Unmodified	17.67 ± 0.3	2.292 ± 0.05	0.8664 ± 0.003	—	—	—
PEMs-Modified	10.54 ± 0.6	1.205 ± 0.01	0.9200 ± 0.001	10.91 ± 0.8	2.346 ± 2	0.7282 ± 0.06

The measured impedance data for devices inoculated with cells was fitted against the proposed equivalent electrical circuit to compare the parameter values during cell growth. The time points chosen were four hours after cell seeding onto the device, and then every 24 hours for up to 72 hours (unmodified electrode devices) or 96 hours (PEMs-modified electrode devices) after cell seeding. Tables 4.2 and 4.3 display the values of the CPE corresponding to the cell contribution to impedance. There was no appreciable change in R_{cell} over time, therefore the parameter was left out in the time

course evaluation because of its lack in sensitivity. However, CPE_{cell} showed a variation in the presence of cells and was consequently selected to monitor cell adhesion. The circuit parameters corresponding to the values for R_s, CPE_{dl}, R_{PEMs}, and CPE_{PEMs} were kept fixed to the cell-free values during the simulations. Tables 4.2 and 4.3 show that the CPE_{cell}-Q value decreased over time as cells proliferated and covered the electrode surface. This decrease in CPE corresponded to the increase in impedance as described in Equation 3.1.

Table 4.2 CPE Parameter Values Obtained by Fitting the Impedance Data of Unmodified Electrodes with DMEM + Cells Over Time to the Equivalent Circuit Represented in Figure 3.13

	CPE_{cell}-*Q* (μF)	**CPE_{cell}-*p***
t = 4 hours	3.070 ± 0.4	1.172 ± 0.03
t = 24 hours	1.636 ± 0.09	1.052 ± 0.01
t = 48 hours	1.3089 ± 0.07	1.041 ± 0.01
t = 72 hours	1.209 ± 0.08	1.035 ± 0.01

Table 4.3 CPE Parameter Values Obtained by Fitting the Impedance Data of PEMs-Modified Electrodes with DMEM + Cells Over Time to the Equivalent Circuit Represented in Figure 3.14

	CPE_{cell}-Q (μF)	CPE_{cell}-p
t = 4 hours	7.391 ± 3	1.427 ± 0.1
t = 24 hours	3.259 ± 0.3	1.118 ± 0.02
t = 48 hours	2.352 ± 0.2	1.079 ± 0.01
t = 72 hours	2.042 ± 0.1	1.05 ± 0.01
t = 96 hours	1.973 ± 0.1	1.075 ± 0.01

4.3.3 Correlation of Impedance with Cell Confluency

The correlation between normalized impedance and cell confluency based on cell density of unmodified and PEMs-modified electrodes is shown in Figure 4.11. As the cells began to proliferate on the electrode surface, the magnitude of impedance increased. This continued to occur until the electrode surface area reduced to a point where no more cells could occupy the surface, during which, the magnitude of impedance reached an approximate steady state trend that approached a particular value.

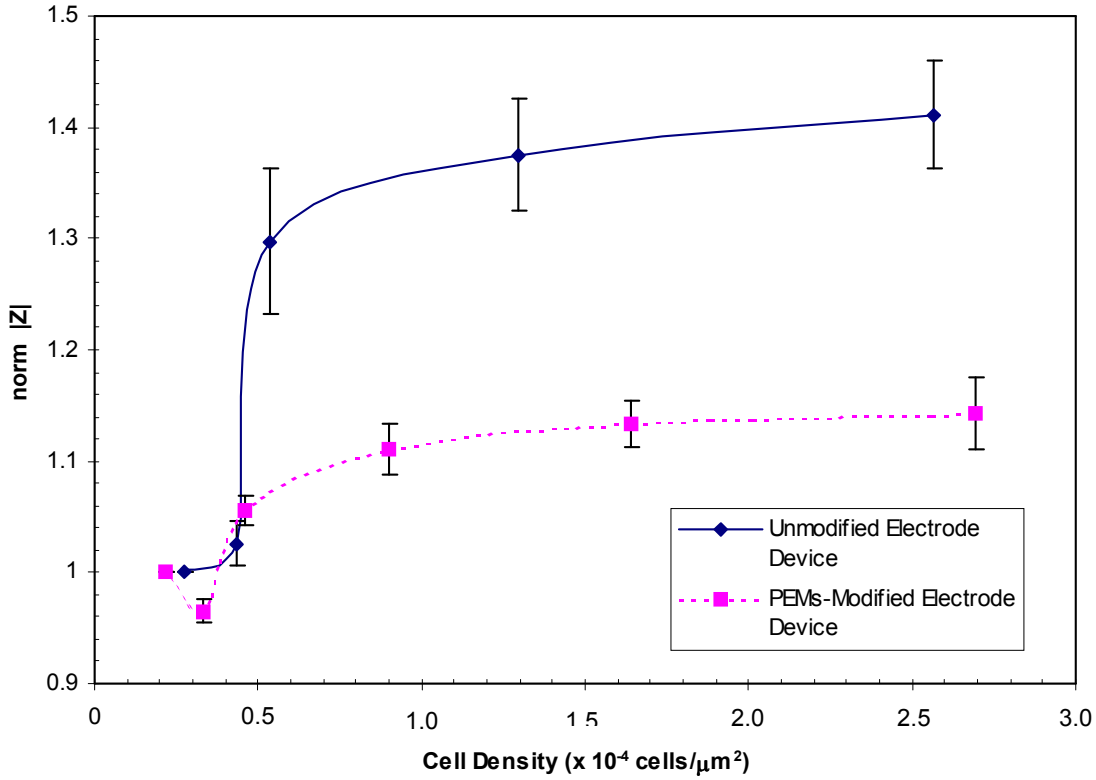

Figure 4.11 Normalized magnitude of impedance as a function of NIH-3T3 fibroblast cell density on unmodified and PEMs-modified electrode devices.

As stated in Section 4.2, the cell population grown on unmodified electrode devices reached approximately 80% confluency 48 hours after inoculation, while the cell population grown on the PEMs-modified electrode devices reached 80% confluency between 72 and 96 hours after inoculation. From Figure 4.10, these time points corresponded to an average normalized impedance magnitude of 1.40 and 1.15 for unmodified and PEMs-modified electrode devices, respectively. Therefore, when the cell population reached the point at which they can be utilized for cell assays (anywhere between 50% and 80% confluency), the corresponding cell density was approximately between 1.0 x 10^{-4} cells/μm^2 and 2.5 x 10^{-4} cells/μm^2.

4.4 Conclusion

Cellular proliferation measurements utilizing visual inspection, as well as recording electronic impedance measurements were presented in this chapter. There was an increase in normal 3T3 cell growth rate on unmodified electrode surfaces because of the decrease in cell attachment surface area. This was due to the cells preferably growing on the unmodified gold surfaces and not on the oxide passivation surface. However, 3T3 cell growth followed a normal confluency rate when they were seeded on PEMs-modified electrodes with PEI/$(PSS/PAH)_5$. Interestingly, at the specified end point of either 72 or 96 hours after cell seeding for unmodified and PEMs-modified electrode devices, respectively, a final cell density of 2.5×10^{-4} cells/μm^2 was observed for both.

Impedance measurements were recorded to follow the adhesion, proliferation, and growth of 3T3 cells. The magnitude of impedance increased as the number of cells on the surface of the electrode increased as well. For both the unmodified and PEMs-modified electrode devices, the magnitude of impedance reached a final value of approximately 320 Ω, which was an indication of maximum cell confluency (80%) at which the cells can be used for cellular assays. Beyond this point, the cells will begin to die by apoptosis due to overcrowding on the surface.

The impedance data was normalized against the measured impedance of the system when the cells are first introduced in the system (t = 0 hours). The unmodified electrode devices experienced a 40% increase in normalized impedance, while the PEMs-modified electrode devices increased by 15%. This displayed the decreased sensitivity of the PEMs-modified devices, but an overall efficiency of 82% to sense changes in impedance due to cell proliferation. Additionally, both types of electrode devices

displayed normalized impedance values that reached an approximate steady state value. Once the curve began to reach this value, it was an indication that the cells have reached 50-80% confluency, which is the optimal time when the cells should be used for any desired experiments. Different devices followed the same trend. Although random impedance fluctuations due to arbitrary cell micromotions were noticeable, all devices displayed a characteristic behavior that was satisfactorily reproducible.

An equivalent electrical circuit model was proposed to model the performance of the cell confluence detector with and without cells present in the system. Simple electrical elements organized into an equivalent circuit represented the supporting electrolyte, device electrodes, PEMs, and fibroblast cells to relate the measured impedance to the electrical behavior of the system. Each type of element had a predominant contribution in the overall impedance at specific frequencies. This allowed for the separation of the effects of the different electrical components. Among these impedance components, the greatest change was in the CPE_{cell} component, which was the variable chosen to monitor during cell growth, while the R_{cell} component did not show any appreciable change with increased cell number. In both the unmodified and PEMs-modified electrodes, the CPE_{cell} value continually decreased. These decreases corresponded to the observed increases in impedance with 3T3 cell growth over time.

Finally, a correlation between the normalized measured impedance values and the cell density was observed. As the cells reached 50% - 80% confluency on the surface of the electrodes, the overall normalized impedance reached an approximate steady state value. At this value there was a 40% change in impedance for the unmodified electrode device and a 15% change in impedance for the PEMs-modified device. For the final

normalized values of both types of electrode devices, the corresponding cell density value for a 50% - 80% confluent cell culture was between 1.0×10^{-4} cells/μm^2 and 2.5×10^{-4} cells/μm^2.

CHAPTER 5

CONCLUSIONS AND FUTURE WORK

In this thesis work, the development and use of PEMs-modified, optically-transparent TiW/Au electrodes for the use in cellular assays were presented. The device fabrication was completed in-house at the National Institute of Standards and Technology Center for Nanoscale Science and Technology Nanofabrication Facility. Polyelectrolyte layers were used to modify the electrode surface to promote cell adhesion and proliferation and the deposition of PEMs was verified. The performances of unmodified and PEMs-modified electrodes were compared by impedance measurements and cyclic voltammetry. Finally, the performance of the unmodified and PEMs-modified devices for cell growth monitoring was investigated. The electrode responses were fitted against the prediction of a proposed electrical equivalent circuit model.

Preparing the fabricated electrode surface for biocompatibility involved the deposition of PEI(PSS/PAH)$_5$. The deposition of PEMs was verified by AFM height measurements and by FTIR spectra. AFM confirmed the height of a single PEI layer to be approximately 2.1 nm in height and a single bilayer of PSS/PAH was 2.5 nm. Contact angle measurements illustrated the increase in hydrophilicity due to the addition of PEMs. A decrease in contact angle from 67.29° with the addition of PEI onto the electrode surface to 46.86° after the deposition of PEI(PSS/PAH)$_5$ onto the substrate was determined. It was essential that the substrate surface be charged to produce a hydrophilic surface for the proper adhesion of cells to take place [28, 30].

The performances of unmodified and PEMs-modified electrodes were investigated with impedance spectroscopy and cyclic voltammetry. Both were able to discern a factor-of-five difference in ionic solution concentration, however, the PEMs-modified electrodes were less sensitive when compared to the unmodified electrodes. Using cyclic voltammetry DMEM was demonstrated it was a proper supporting electrolyte for electronic measurements, as it did not lead to any faradaic processes. The deposition of the PEMs was also confirmed with CV. An increase in charging current was monitored when comparing CV scans for PEMs-modified electrodes and unmodified electrodes. Another proof of PEMs deposition resided in the generated decrease of the double layer capacitance values observed experimentally. The increase in charging current, as well as the decrease in the double layer capacitance values, occurred because the addition of PEMs on the electrode surface hindered the ability of ions to penetrate the layer. Cyclic voltammetry was also used to characterize the behavior of the electrodes. For example, CV with PBS and $[Fe(CN)_6]^{3-/4-}$ demonstrated that unmodified gold electrodes produce a well-defined voltammetric and quasi-reversible response. On the other hand, PEMs-modified electrodes did not show a quasi-reversible or a well-defined voltammetric response, but instead produced increased peak separations. However, PEMs used to promote cell adhesion on electrodes still allow for successful electronic measurements to be performed. It is only essential for the electrodes to be able to probe biological processes, such as cell attachment and growth. These activities are non-faradaic, which means they do not generate the flow of charged particles. Consequently, their detection will not be hindered by the PEMs.

An equivalent electrical circuit of the cell confluence detector system was also proposed. Considering that there were no redox species present in DMEM, the equivalent circuit did not take into account any faradaic processes driving this study. For cell-free media on an unmodified electrode device, the equivalent circuit was modeled as a resistor to represent the resistance due to the solution, coupled with a constant phase element in series to take into account the capacitive contribution from the electrical double layer on the surface of the electrode. When the deposition of PEMs was represented electrically, a resistor and constant phase element in parallel with each other was added to the previous model. This took into account any pores present throughout the entire thickness of the PEMs layer, as well as the insulating property of the PEMs. The addition of cells onto either electrode system corresponded to the serial addition of another resistor and constant phase element in parallel with each other. The resistor parameter represented the altered current flow from the electrode surface due to cellular focal adhesions forming aqueous gaps. The constant phase element took into account the capacitive nature of the cell membrane. It was this specific element that was monitored during the continuous impedance measurements, as it directly correlated to cells attaching and proliferating on the electrode surface.

Impedance spectroscopy was utilized as a technique to monitor adhesion and growth of 3T3 cells on the surface of either unmodified or PEMs-modified electrode devices. The resulting impedance data was extracted for the optimal frequency of 1000 Hz and reached a steady state value of approximately 320 Ω at the desired measurement endpoint of 72 hours or 96 hours after cell seeding for unmodified or PEMs-modified electrodes, respectively. During the cell confluency measurements, small fluctuations

were apparent during monitoring. At the early stages, these fluctuations were due to cells moving horizontally across the electrode surface or experiencing cell division. The later fluctuations were due to the cells undergoing vertical micromotions as a result of biochemical reactions or processes occurring within the cell. These fluctuations, as well as a steady state trend, were also present when the impedance data was normalized. For unmodified electrodes, the impedance increased approximately 1.40-fold, while the PEMs-modified electrodes displayed less sensitivity and showed a 1.15-fold difference in impedance. Even though the PEMs-modified electrodes measured a 20% change in impedance, this data indicated an excellent efficiency of 82% for cell attachment and proliferation detection. Finally, a correlation between normalized impedance and cell confluence was determined. An approximate steady state impedance value indicated that the cells reached a 50%-80% confluency level at which they can be used for cellular assays. During this confluency level, the corresponding cell density ranged between 1.0 x 10^{-4} cells/μm^2 and 2.5 x 10^{-4} cells/μm^2. These values were an indication that the cells reached the optimal growth density for cellular assays before they will begin to die due to overcrowding on the surface.

5.1 Significant Contributions

The work presented in this thesis is novel in the use of PEMs as a cell adhesion promoter for biosensors. The significant contributions of this work are:

- The development of a biocompatible cell confluence detector, which prevents the diffusion of toxic materials from the adhesion layer to be in contact with biological cells.

- The characterization of unmodified and PEMs-modified electrodes for biological applications.
- The validation of an equivalent electrical circuit model that describes the changes in the electrical response of the devices as cells adhere and proliferate on the electrode surface.
- The first demonstration of impedance measurements to monitor cell proliferation on PEMs-modified electrodes.

5.2 Future Work

As impedance measurements depend on electrode geometry, the TiW/Au electrode design must be optimized to maximize the device sensitivity towards cell detection. Currently, the electrodes have sharp, defined corners that concentrate the electric field in those areas. The use of electrodes with rounded corners would allow for a more uniform electric field to be distributed throughout the electrode surface [81]. The uniformity would permit the measured impedance to be a more accurate average of cell spreading and cell morphological changes occurring on the surface of the electrodes. Therefore, with an improved electrode design, the sensitivity of the cell confluence detector can be maximized.

The AC 1 mV peak-to-peak input signal was adequate in sensing changes due to cell-substrate interactions, but this signal could also be optimized to increase device sensitivity. The 1 mV input potential was able to detect the immediate changes occurring at the electrode surface during the first 19 hours for the unmodified electrode device and the first 13 hours for the PEMs-modified device. This was evident with the steep slope in

the beginning of the impedance measurements. However, by optimizing the input potential, it may be possible to be able to further detect more of the changes occurring in the later stages of cell proliferation. A lower input current, *i*, would further reduce the voltage drop (iR_s) of the solution to less than 1-2 mV [100], thereby improving device sensitivity for cell attachment and proliferation events. Along with an optimized electrode device design, this two-electrode setup would not undergo any serious complications associated with the ohmic drop in solution.

After device optimization, it would be possible to demonstrate its use in cellular assays, in particular the ability to probe the cytotoxic effects of substances of interest. This thesis work was towards the development of biocompatible electrode systems with long-term stability for cytotoxicity investigation applications and its integration into a microfluidic network. The development of this microfluidic system will have the ability to continuously culture cells on-chip to probe their viability with electronic means instead of optical techniques after subjecting them to stimuli. This system would be highly beneficial in high-throughput analysis for the fields of medicine, pharmaceuticals, and biological research.

APPENDIX A

BIOCOMPATIBLE ELECTRODE MATERIALS

Materials for electrodes used in probing cell response and sensing cell signaling are important in microsystem design because of cellular biocompatibility issues. This work describes the evaluation of materials and fabrication procedures of metal planar microelectrodes necessary in microfluidic systems for detection methodologies in cellular studies. In particular, metallic chromium (Cr^0) and titanium-tungsten alloy (TiW, 10/90 wt %) are investigated as adhesion layers for gold (Au) electrodes on glass substrates. Cr is a commonly used adhesion layer for planar microelectrodes used in cellular assays, even though hexavalent chromium (Cr^{6+}) is known to cause cell growth arrest through oxidative stress and DNA damage, cell death via apoptosis or necrosis, or malignant cell transformation [107-109]. However, it has not been shown that fabrication processes affect Cr diffusion through the gold electrode surface and produce toxic effects that inhibit the growth of certain cell lines. This work examines the toxic effects of an underlying Cr adhesion layer for Au electrodes and how this is alleviated with the use of TiW as an effective and stable adhesion layer.

Two different surfaces (120 nm-thick layer of sputtered gold with either an underlying 7.5 nm-thick TiW or Cr adhesion layer) were fabricated. These surfaces were then passivated with a 400nm-thick oxide layer using plasma enhanced chemical vapor deposition (PECVD). This PECVD process required the temperature of the substrate to be elevated to 300 °C, which allowed atoms to migrate through layers.

The two different surfaces were analyzed using X-Ray Photoelectron Spectroscopy (XPS). All XPS measurements were made on a Kratos Axis-Ultra DLD spectrometer with a monochromated Al-Kα source at a 0° angle between the sample surface normal and the analyzer lens. For each sample, a survey spectrum was taken with pass energy 160 eV, using the hybrid lens and the slot aperture for a ~300 μm × 700 μm analysis area. For those samples where Cr was detected, high resolution spectra were taken for the Cr 2p, O 1s, C 1s, Au 4f, and Si 2p regions with pass energy 40 eV, using the hybrid lens and the slot aperture.

In Figure A.1A, the XPS survey showed no evidence of TiW diffusion through the Au layer to the surface. However, as shown in Fig. A.1B, samples using Cr as an adhesion layer resulted in Cr diffusion, which allowed the cells to be in contact with the toxic material.

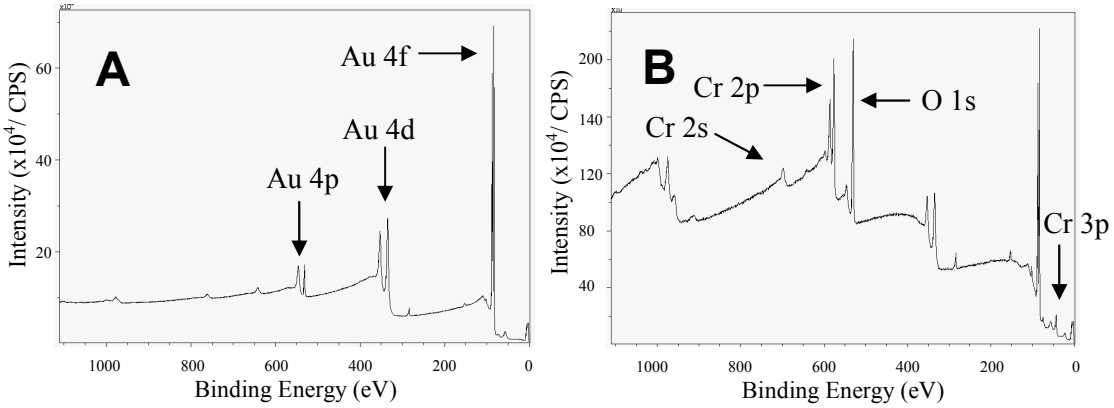

Figure A.1 XPS spectra of sample surface analysis. A) The survey scan shown is for the sample of Au with a TiW adhesion layer. The major peaks shown are for Au, while no peaks resulted from Ti or W. B) The survey scan shown is for the sample of Au surface with Cr adhesion layer. The arrows denote the peaks that represent Cr and O. All other major peaks are for Au.

Figure A.2 shows the comparison of proliferation and morphology of mammalian cells growing on either TiW or Cr. Differential interference contrast images showed that cells grown on Cr did not grow as well as those cells on TiW and eventually became destroyed. This demonstrated the full toxic potential of Cr when cells are in contact with the material.

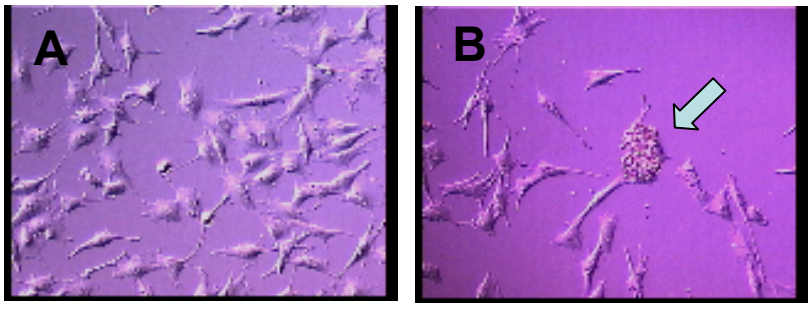

Figure A.2 Differential interference contrast images. Mammalian cells growing on A) a TiW surface and B) a Cr surface at 48 hours after inoculation. Arrow denotes destroyed cells.

In Figure A.3, the numbers of cells growing on both materials were compared and demonstrated that TiW better supports cell proliferation and viability. Cells on TiW grew from 1.5 to almost 5 times more than on Cr from 48hrs to 72hrs.

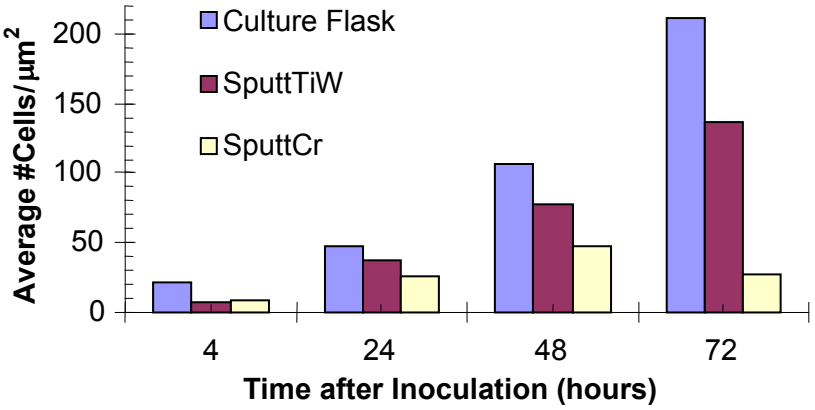

Figure A.3 Effect of metal adhesion layer for Au electrodes. As time increased, the number of cells present on the TiW surface increased, similar to that of the culture flask control. Cell growth decreased after 48 hours on the Cr surface.

Adherent cells, like the ones used in this study, require adhesion onto a surface in order to function normally in culture. Impedance measurements shown in Figure A.4 illustrate the ability of these cells to attach and proliferate on the electrode surfaces. It was expected that with cell growth, impedance will increase [70], however, the gold electrodes with Cr adhesion layers did not show this behavior. Instead, a decrease in impedance was seen over time, demonstrating the cells were not adhering well to the surface, whereas the opposite was observed on TiW.

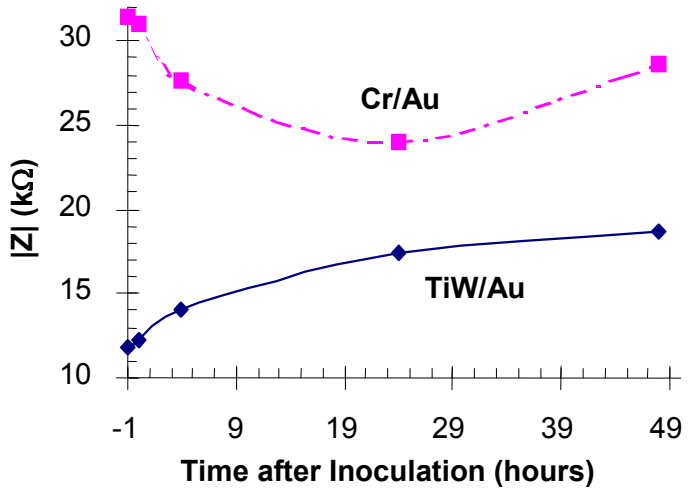

Figure A.4 Impedance measurements at 10 Hz of mammalian cell growth until 48 hours after inoculation. The baseline media control measurement with cell-free media occurred at t = -1 hour. Cells were added to the system at t = 0 hours. Cell growth on TiW/Au electrodes (solid line) displayed an increase in impedance over time as the cells proliferated. Cell growth on Cr/Au electrodes (dashed line) did not increase above the value at t = 0 hours.

In summary, this work examined the evaluation of electrode materials for biocompatibility in microsystems using mammalian cells. Cr was shown to be an unsuitable adhesion layer because it diffused through to the electrode surface, where it

hindered cells from properly adhering to and proliferating onto the electrode surface. This problem was solved with the use of TiW as an adhesion layer for metal electrodes that supported the adhesion and growth of cells.

APPENDIX B

STUDENT's *t*-TEST CALCULATIONS

In general, student's *t*-test calculations are used either for comparing a sample mean with a true mean, or are used to determine whether there is a significant difference between two sets of results [110]. The *t*-test is widely used because it can be applied to a relatively small number of samples. In this work, two-tailed paired student's *t*-tests were calculated to evaluate the performance of fabricated TiW/Au electrodes. Specifically, the tests were used to determine if the fabricated TiW/Au electrodes were able to distinguish between ionic differences in solution. In addition, the *t*-tests were also used to evaluate if there was any variability between devices made within the same or different fabrication batches. A two-tailed *t*-test is one that assesses if a result differs from specific value, which implies the result may be above or below the specified value. A paired *t*-test compares whether there is a significant difference between two values. The null hypothesis usually states that there is not a significant difference between separate methods, values, or groups. Therefore, the two null hypotheses tested in this work are as follows:

1. Varying ionic solution concentrations display no significant difference from each other when measured by unmodified or PEMs-modified electrodes, and
2. Two devices, fabricated either within the same batch or separate batches, do not display a significant difference from each other.

First, the differences (d_i) between each pair of results were calculated, followed by the mean of the differences, $\bar{d}$. An example using a factor-of-two difference in ionic solution measured with PEMs-modified electrodes is shown in Table B.1.

Table B.1 Example Calculations of *t*-Test Difference Values for a Factor-of-Two Change in Ionic Solution Concentration Measured with PEMs-Modified Electrodes at Low Frequencies

Frequency	0.5 mM $\lvert Z \rvert_{Avg}$	1 mM $\lvert Z \rvert_{Avg}$	d_i	$(\bar{d} - d_i)$	$(\bar{d} - d_i)^2$
1000 Hz	4043.633	2327.7	1715.933	-341.611	116698.1512
100 Hz	3275.033	4578.333	1696.7	-493.183	243229.8003
10 Hz	23457.67	22747.33	710.33	493.183	243229.8003
			$\Sigma d_i = 4122.967$	$\Sigma(\bar{d} - d_i)^2 = 661506.8274$	
			$\bar{d} = 1374.322$		

The standard deviation of the differences, s_d were then evaluated using the following equation:

$$s_d = \sqrt{\frac{\Sigma(\bar{d} - d_i)^2}{N - 1}} \qquad \text{(Equation B.1)}$$

where N is the number of replicate analyses. The number of degrees of freedom (*d.o.f.*) is given by (N-1). In the example, $N = 3$, therefore, there is 2 *d.o.f.*

$$s_d = \sqrt{\frac{661506.8274}{3 - 1}} = 575.1117$$

The value of t was then calculated from the equation $t = \frac{\bar{d}\sqrt{N}}{s_d}$. (Equation B.2)

$$t = \frac{1374.322\sqrt{3}}{575.1117} = 4.14$$

Table B.2 summarizes the calculated t-values to determine the minimum difference in ionic concentration that either unmodified or PEMs-modified electrodes could detect. The differences in ionic solution concentration ranged from a factor-of-two difference to a factor-of-1000 difference. The high frequency range included impedance measurements taken between 10^4 Hz and 10^6 Hz. The low frequency range included impedance measurements taken at 10 Hz and 100 Hz.

Table B.2 Summary of Calculated *t*-Values for Unmodified and PEMs-Modified Electrode Performance in Solutions with Varying Ionic Concentration Differences

	Unmodified Electrodes		**PEMs-Modified Electrodes**	
	High Frequency	**Low Frequency**	**High Frequency**	**Low Frequency**
Factor-of-two	2.34	4.23	2.58	4.58
Factor-of-five	0.96	4.08	1.06	4.38
Factor-of-10	—	3.68	—	4.01
Factor-of-20	—	2.93	—	3.52
Factor-of-200	—	1.82	—	2.41
Factor-of-1000	—	—	—	1.90

Table B.3 summarizes the calculated *t*-values to determine intrabatch and interbatch variability of unmodified electrodes. Six electrode devices were immersed and measured in a physiological concentration of PBS. Devices 4 and 6 were chosen to represent the devices fabricated within the same batch run, while devices 1 and 4 were chosen to represent devices fabricated in different batches.

Table B.3 Summary of Calculated *t*-Values for Unmodified Electrode Variability Within the Same (Devices 4 & 6) and Different (Devices 1 & 4) Fabrication Batches

	High Frequency	**Low Frequency**
Device 4 & Device 6	2.75	1.28
Device 1 & Device 4	2.41	2.27

The calculated *t*-values were then compared with that of tabulated *t*-distribution values (Table B.4) to determine what probability, *P*, the null hypothesis was incorrect. Again, the null hypotheses state that there is either 1) no significant difference between specified ionic solutions, or 2) no significant difference between intrabatch or interbatch electrode devices. It was desired to determine what difference in ionic solution concentration produced a significant difference. On the other hand, it was desired to have no significant difference in electrode performance with electrodes fabricated within the same and different fabrication batches.

If the calculated *t* value is less than the tabulated value, the null hypothesis is retained. If, however, the calculated *t* value is greater than the tabulated *t* value, the null hypothesis is rejected. In practice, a probability level of 0.05 is usual. But for the purposes of this thesis, a probability level of 0.20 is adequate to accept the null

hypotheses. It should be noted for a two-tailed test, the value of *P* for a one-tailed test is doubled. Table B.4 displays the *t*-distributions of a one-tailed test for three selected degrees of freedom.

Table B.4 Table of Selected *t*-Distributions

	Probability Level, *P*							
d.o.f.	**0.25**	**0.2**	**0.15**	**0.1**	**0.05**	**0.025**	**0.01**	**0.005**
1	1.000	1.376	1.963	3.078	6.31	12.71	31.82	63.66
2	0.816	1.061	1.386	1.886	2.92	4.30	6.97	9.92
20	0.687	0.860	1.064	1.325	1.725	2.086	2.528	2.845

From the example shown above, the calculated *t*-value was 4.14 for 2 *d.o.f.* The calculated *t*-value is below the tabulated *t*-value of 6.31 for a probability level of 0.10 for a two-tailed test. Therefore, there is a 90% probability that the device cannot distinguish between a factor-of-two difference in ionic solution concentration at low frequencies (1000 Hz, 100 Hz, and 10 Hz).

The calculated two-tailed confidence levels using student's *t*-test calculations at high frequencies ($f \geq 10$ kHz) showed that the unmodified and PEMs-modified fabricated devices are capable of discriminating between a minimum of a factor-of-five difference in ionic solution concentration. The probability of the devices not being significantly different was 0.40 and 0.30 at 20 *d.o.f.* for unmodified and PEMs-modified electrodes, respectively. However, it was more difficult to differentiate between different ionic solutions at the low frequencies of 10 Hz and 100 Hz. To produce a significant difference in the impedance measurements of ionic solutions, it took a factor-of-200

(unmodified electrode device) and a factor-of-1000 concentration difference (PEMs-modified electrode device) for the devices to sense the change.

There was no significant difference in the measurement performance of unmodified electrode devices. The calculated two-tailed paired *t*-test revealed that at high frequencies ($f \geq 10$ kHz) there was a probability level of less than 0.01 for a *d.o.f.* = 20 that there was a significant difference between the performance of electrodes fabricated within the same or different batches. In addition, a probability level of 0.20 for 1 *d.o.f.* showed that there was no significant difference in electrode performance at the low frequencies of 10 Hz and 100 Hz.

BIBLIOGRAPHY

1. Katz, E., *Bioelectronics.* Electroanalysis, 2006. **18**(19-20): p. 1855-1857.

2. Turner, A.P.F., *Biosensors and Bioelectronics 20 Years On.* Biosensors and Bioelectronics, 2005. **20**: p. 2387.

3. Willner, I. and E. Katz, *Bioelectronics: From Theory to Applications*. 2005, Weinheim, Germany: Wiley-VCH.

4. Dittrich, P.S. and A. Manz, *Lab-on-a-Chip: Microfluidics in Drug Discovery.* Nature Reviews Drug Discovery, 2006. **5**(3): p. 210-218.

5. Yi, C.Q., C.W. Li, S.L. Ji, and M.S. Yang, *Microfluidics technology for manipulation and analysis of biological cells.* Analytica Chimica Acta, 2006. **560**(1-2): p. 1-23.

6. Liu, D., L. Wang, R. Zhong, B. Li, N. Ye, X. Liu, and B. Lin, *Parallel microfluidic networks for studying cellular response to chemical modulation.* Journal of Biotechnology, 2007. **131**(3): p. 286-292.

7. Popovtzer, R., T. Neufeld, E.Z. Ron, J. Rishpon, and Y. Shacham-Diamand, *Electrochemical Detection of Biological Reactions Using a Novel Nano-Bio-Chip Array.* Sensors and Actuators B-Chemical, 2006. **119**(2): p. 664-672.

8. Ros, A., W. Hellmich, J. Regtmeier, T.T. Duong, and D. Anselmetti, *Bioanalysis in Structured Microfluidic Systems.* Electrophoresis, 2006. **27**(13): p. 2651-2658.

9. Li, C.W., J. Yang, and M.S. Yang, *Dose-Dependent Cell-Based Assays in V-Shaped Microfluidic Channels.* Lab on a Chip, 2006. **6**(7): p. 921-929.

10. Manz, A., N. Graber, and H.M. Widmer, *Miniaturized Total Chemical Analysis Systems: a Novel Concept for Chemical Sensing.* Sensors and Actuators B, 1990. **1**(1-6): p. 244-248.

11. Reyes, D.R., D. Iossifidis, P.-A. Auroux, and A. Manz, *Micro Total Analysis Systems. 1. Introduction, Theory, and Technology.* Analytical Chemistry, 2002. **74**(2623-2636).

12. Vilkner, T., D. Janasek, and A. Manz, *Micro Total Analysis Systems. Recent Developments.* Analytical Chemistry, 2004. **76**: p. 3373-3386.

13. Harrison, D.J., A. Manz, Z. Fan, H. Ludi, and H.M. Widmer, *Capillary Electrophoresis and Sample Injection Systems Integrated on a Planar Glass Chip.* Analytical Chemistry, 1992. **64**(17): p. 1926-1932.

14. Jacobson, S.C., R. Hergenroder, L.B. Koutny, and J.M. Ramsey, *High-Speed Separations on a Microchip.* Analytical Chemistry, 1994. **68**(7): p. 1114-1118.

15. Burns, M.A., B.N. Johnson, S.N. Brahmasandra, K. Handique, J.R. Webster, M. Krishnan, T.S. Sammarco, P.M. Man, D. Jones, D. Heldsinger, and C.H.B. Mastrangelo, D.T., *An Integrated Nanoliter DNA Analysis Device.* Science, 1998. **282**: p. 484-487.

16. Auroux, P.-A., D. Iossifidis, D.R. Reyes, and A. Manz, *Micro Total Analysis Systems. 2. Analytical Standard Operations and Applications.* Analytical Chemistry, 2002. **74**: p. 2637-2652.

17. Harrison, D.J., K. Fluri, K. Seiler, Z. Fan, C.S. Effenhauser, and A. Manz, *Micromachining a Miniaturized Capillary Electrophoresis-Based Chemical Analysis System on a Chip.* Science, 1993. **261**: p. 895-897.

18. Mourzina, Y., A. Steffen, D. Kalvagin, R. Carious, and A. Offenhausser, *Capillary Zone Electrophoresis of Amino Acids on Hybrid Poly(dimethylsiloxane)-Glass Chip.* Electrophoresis, 2005. **26**(9): p. 1849-1860.

19. Blom, M.T., E. Chmela, R.E. Oosterbroek, R. Tijssen, and A. van den Berg, *On-Chip Hydrodynamic Chromatography Separation and Detection of Nanoparticles and Biomolecules.* Analytical Chemistry, 2003. **75**(24): p. 6761-6768.

20. Neuzil, P., J. Pipper, and T.M. Hsieh, *Disposable Real-Time microPCR Device: Lab-on-a-Chip at a Low Cost.* Molecular Biosystems, 2006. **2**(6-7): p. 292-298.

21. Marentis, T.C., B. Kusler, G.G. Yaralioglu, S.J. Liu, E.O. Haeggstrom, and B.T. Khuri-Yakub, *Microfluidic Sonicator for Real-Time Disruption of Eukaryotic Cells and Bacterial Spores for DNA Analysis.* Ultrasound in Medicine and Biology, 2005. **31**(9): p. 1265-1277.

22. Taylor, P., D.P. Manage, and K.E. Helmle, *Analysis of Mitochondrial DNA in Microfluidic Systems.* Journal of Chromatography B - Analytical Technologies in the Biomedical and Life Sciences, 2005. **822**(1-2): p. 78-84.

23. Kumari, S. and S. Mayor, *ARF1 is Directly Involved in Dynamin-Independent Endocytosis.* Nature Cell Biology, 2008. **10**: p. 30-41.

24. Shikano, S., B. Coblitz, H. Sun, and M. Li, *Genetic Isolation of Transport Signals Directing Cell Surface Expression.* Nature Cell Biology, 2005. **7**: p. 985-992.

25. Butcher, E.C., E.L. Berg, and E.J. Kunkel, *Systems Biology in Drug Discovery.* Nature Biotechnology, 2004. **22**: p. 1253-1259.

26. Bhavsar, A.P., J.A. Guttman, and B.B. Finlay, *Manipulation of Host-Cell Pathways by Bacterial Pathogens.* Nature, 2007. **449**: p. 827-834.

27. Yadava, R.S., C.D. Frenzel-McCardell, Q. Yu, V. Srinivasan, A.L. Tucker, J. Puymirat, C.A. Thornton, O.W. Prall, R.P. Harvey, and M.S. Mahadevan, *RNA Toxicity in Myotonic Muscular Dystrophy Induces NKX2-5 Expression.* Nature Genetics, 2008. **40**(1): p. 61-68.

28. Freshney, R.I., *Culture of Animal Cells: A Manual of Basic Technique*. 2000, New York, New York: Wiley-Liss, Inc. 577.

29. Alberts, B., A. Johnson, J. Lewis, M. Raff, K. Roberts, and P. Walter, *Molecular Biology of the Cell*. 4 ed. 2002, New York, New York: Garland Science. 1463.

30. Koller, M.R., M.A. Palsson, I. Manchel, R.J. Maher, and B.O. Palsson, *Tissue Culture Surface Characteristics Influence the Expansion of Human Bone Marrow Cells.* Biomaterials, 1998. **19**(21): p. 1963-1972.

31. Decher, G., J.D. Hong, and J. Schmitt, *Buildup of Ultrathin Multilayer Films by a Self-Assembly Process: III. Consecutively Alternating Adsorption of Anionic and Cationic Polyelectrolytes on Charged Surfaces.* Thin Solid Films, 1992. **210-211**: p. 831-835.

32. Mendelsohn, J.D., S.Y. Yang, J. Hiller, A.I. Hochbaum, and M.F. Rubner, *Rational Design of Cytophilic and Cytophobic Polyelectrolyte Multilayer Thin Films.* Biomacromolecules, 2003. **4**: p. 96-106.

33. Caruso, F., K. Niikura, D.N. Furlong, and Y. Okahata, *2. Assembly of Alternating Polyelectrolyte and Protein Mulitlayer Films for Immunosensing.* Langmuir, 1997. **13**: p. 3427-3433.

34. Decher, G., B. Lehr, K. Lowack, Y. Lvov, and J. Schmitt, *New Nanocomposite Films for Biosensors: Layer-by-Layer Adsorbed Films of Polyelectrolytes, Proteins or DNA.* Biosensors and Bioelectronics, 1994. **9**(9-10): p. 677-684.

35. Barker, S.L., D. Ross, M.J. Tarlov, M. Gaitan, and L.E. Locascio, *Control of Flow Direction in Microfluidic Devices with Polyelectrolyte Multilayers.* Analytical Chemistry, 2000. **72**: p. 5925-5929.

36. Barker, S.L., M.J. Tarlov, H. Canavan, J.J. Hickman, and L.E. Locascio, *Plastic Microfluidic Devices Modified with Polyelectrolyte Multilayers.* Analytical Chemistry, 2000. **72**: p. 4899-4903.

37. Berg, M.C., S.Y. Yang, P.T. Hammond, and M.F. Rubner, *Controlling Mammalian Cell Interactions on Patterned Polyelectrolyte Multilayer Surfaces.* Langmuir, 2004. **20**: p. 1362-1368.

38. Kumar, G., Y.C. Wang, C. Co, and C. Ho, *Spatially Controlled Cell Engineering on Biomaterials Using Polyelectrolytes.* Langmuir, 2003. **19**: p. 10550-10556.

39. Reyes, D.R., E.M. Perruccio, S.P. Becerrra, L.E. Locascio, and M. Gaitan, *Micropatterning Neuronal Cells on Polyelectrolyte Multilayers.* Langmuir, 2004. **20**: p. 8049-8413.

40. Gomez-Sjoberg, R., A.A. Leyrat, D.M. Pirone, C.S. Chen, and S.R. Quake, *Versatile, Fully Automated, Microfluidic Cell Culture System.* Analytical Chemistry, 2007. **79**: p. 8557-8563.

41. Sniadecki, N.J., R.A. Desai, S.A. Ruiz, and C.S. Chen, *Nanotechnology for Cell-Substrate Interactions.* Annals of Biomedical Engineering, 2006. **34**(1): p. 59-74.

42. Horenstein, M.N., *Microelectronic Circuits and Devices*. 2 ed. 1996, Englewood Cliffs, New Jersey: Prentice Hall, Inc. 25, 1067-1071.

43. Madou, M.J., *Fundamentals of Microfabrication: The Science of Miniaturization*. 2 ed. 2002, Boca Raton, Florida: CRC Press.

44. Vandaveer, W.R., P. S.A., R.S. Martin, and S.M. Lunte, *Recent Developments in Amperometric Detection for Microchip Capillary Electrophoresis.* Electrophoresis, 2002. **23**: p. 3667-3677.

45. Baldwin, R.P., T.J. Roussel, M.M. Crain, V. Bathlagunda, D.J. Jackson, J. Gullapalli, J.A. Conklin, R. Pai, J.F. Naber, K.M. Walsh, and R.S. Keynton, *Fully Integrated On-Chip Electrochemical Detection for Capillary Electrophoresis in a Microfabricated Device.* Analytical Chemistry, 2002. **74**: p. 3690-3697.

46. Ko, J.S., H.C. Yoon, H. Yang, H.B. Pyo, K. Chung, S.J. Kim, and Y.T. Kim, *A Polymer-Based Microfluidic Device for Immunosensing Biochips.* Lab on a Chip, 2003. **3**(2): p. 106-113.

47. Guijt, R.M., E. Baltussen, and G.W. van Dedem, *Use of Bioaffinity Interactions in Electrokinetically Controlled Assays on Microfabricated Devices.* Electrophoresis, 2002. **23**: p. 823-835.

48. Khandurina, J., T.W. McKnight, S.C. Jacobson, L.C. Waters, R.S. Foote, and J.M. Ramsey, *Integrated System for Rapid PCR-based DNA Analysis in Microfluidic Devices.* Analytical Chemistry, 2000. **72**: p. 2995-3000.

49. Lagally, E.T., I. Medintz, and R.A. Mathies, *Single-Molecule DNA Amplification and Analysis in an Integrated Microfluidic Device.* Analytical Chemistry, 2001. **73**: p. 565-570.

50. Smith, E.M., H. Xu, and A.G. Ewing, *DNA Separations in Microfabricated Devices with Automated Sample Introductions.* Electrophoresis, 2001. **22**: p. 318-327.

51. Murphy, W.L., K.O. Mercurius, S. Koide, and M. Mrksich, *Substrates for Cell Adhesion Prepared via Active Site-Directed Immobilization of a Protein Domain.* Langmuir, 2004. **20**(4): p. 1026-1030.

52. Massia, S.P. and J.A. Hubbell, *Covalent Surface Immobilization of Arg-Gly-Asp- and Tyr-Ile-Gly-Ser-Arg-containing Peptides to Obtain Well-Defined Cell-Adhesive Substrates.* Analytical Biochemistry, 1990. **187**: p. 292-301.

53. Asphahani, F. and M. Zhang, *Cellular Impedance Biosensors for Drug Screening and Toxin Detection.* The Analyst, 2007. **132**: p. 835-841.

54. Grob, B., *Basic Electronics*. 8 ed. 1997, New York, New York: Glencoe/McGraw-Hill. 980.

55. Macdonald, J.R., *Impedance Spectroscopy: Emphasizing Solid Materials and Systems*. 1987, New York, New York: John Wiley & Sons, Inc. 4.

56. Keese, C.R. and I. Giaever, *A Biosensor that Monitors Cell Morphology with Electrical Fields.* IEEE Engineering in Medicine and Biology, 1994(June/July 1994): p. 402-408.

57. Giaever, I. and C.R. Keese, *Micromotion of Mammalian Cells Measured Electrically.* Proceedings of the National Academy of Sciences of the U.S.A., 1991. **88**: p. 7896-7900.

58. Cole, K.S., *Some Physical Aspects of Bioelectric Phenomena.* Proceedings of the National Academy of Sciences of the U.S.A., 1949. **35**(10): p. 558-566.

59. Tlili, C., K. Reybier, A. Geloen, L. Ponsonnet, C. Martelet, H.B. Ouada, M. Lagarde, and N. Jaffrezic-Renault, *Fibroblast Cells: A Sensing Bioelement for Glucose Detection by Impedance Spectroscopy.* Analytical Chemistry, 2003. **75**: p. 3008-3012.

60. Ehret, R., W. Baumann, M. Brishwein, A. Schwinde, K. Stegbauer, and B. Wolf, *Monitoring of Cellular Behaviour by Impedance Measurements on Interdigitated Electrode Structures.* Biosensors and Bioelectronics, 1997. **12**(1): p. 29-41.

61. Luong, J.H.T., M. Habibi-Rezaei, J. Meghrous, C. Xiao, K.B. Male, and A. Kamen, *Monitoring Motility, Spreading, and Mortality of Adherent Insect Cells Using an Impedance Sensor.* Analytical Chemistry, 2001. **73**: p. 1844-1848.

62. Arndt, S., J. Seebach, K. Psathaki, H. Galla, and J. Wegener, *Bioelectrical Impedance Assay to Monitor Changes in Cell Shape During Apoptosis.* Biosensors and Bioelectronics, 2004. **19**: p. 583-594.

63. Giebel, K.F., C. Bechinger, S. Herminghaus, M. Riedel, P. Leiderer, U. Weiland, and M. Bastmeyer, *Imaging of Cell/Substrate Contacts of Living Cells with Surface Plasmon Resonance Microscopy.* Biophysical Journal, 1999. **76**: p. 509-516.

64. Huang, X., D. Nguyen, D.W. Greve, and M.M. Domach, *Simulation of Microelectrode Impedance Changes Due to Cell Growth.* IEEE Sensors Journal, 2004. **4**(5): p. 576-583.

65. Giaever, I. and C.R. Keese, *Monitoring Fibroblast Behavior in Tissue Culture with an Applied Electric Field.* Proceedings of the National Academy of Sciences of the U.S.A., 1984. **81**(12): p. 3761-3764.

66. Tiruppathi, C., A.B. Malik, P.J. Del Vecchio, and C.R. Keese, *Electrical Method for Detection of Endohelial Cell Shape Change in Real Time: Assessment of Endothelial Barrier Function.* Proceedings of the National Academy of Sciences of the U.S.A., 1992. **89**: p. 7919-7923.

67. Xiao, C., B. Lachance, G. Sunahara, and J.H.T. Luong, *An In-Depth Analysis of Electric Cell-Substrate Impedance Sensing to Study the Attachment and Spreading of Mammalian Cells.* Analytical Chemistry, 2002. **74**: p. 1333-1339.

68. Maher, M.P., J. Pine, J. Wright, and Y.C. Tai, *The Neurochip: A New Multielectrode Device for Stimulating and Recording from Cultured Neurons.* Journal of Neuroscience Methods, 1999. **87**: p. 45-56.

69. Gross, G.W. and B.K. Rhoades, *The Use of Neuronal Networks on Multielectrode Arrays as Biosensors.* Biosensors and Bioelectronics, 1995. **10**(6-7): p. 553-567.

70. Wegener, J., C.R. Keese, and I. Giaever, *Electric Cell-Substrate Impedance Sensing (ECIS) as a Noninvasive Means to Monitor the Kinetics of Cell Spreading to Artificial Surfaces.* Experimental Cell Research, 2000. **259**: p. 158-166.

71. Hadjout, N., G. Laevsky, D.A. Knecht, and M.A. Lynes, *Automated Real-Time Measurement of Chemotactic Cell Motility.* BioTechniques, 2001. **31**: p. 1130-1138.

72. Ko, K.S., C. Lo, J. Ferrier, P. Hannam, M. Tamura, B.C. McBride, and R.P. Ellen, *Cell-Substrate Impedance Analysis of Epithelial Cell Shape and Micromotion Upon Challenge with Bacterial Proteins that Perturb Extracellular Matrix and Cytoskeleton.* journal of Microbiological Methods, 1998. **34**: p. 125-132.

73. Xiao, C., B. Lachance, G. Sunahara, and J.H.T. Luong, *Assessment of Cytotoxicity Using Electric Cell-Substrate Impedance Sensing: Concentration and Time Response Function Approach.* Analytical Chemistry, 2002. **74**: p. 5748-5753.

74. Connolly, P., P. Clark, A.S.G. Curtis, J.A.T. Dow, and C.D.W. Wilkinson, *An Extracellular Microelectrode Array for Monitoring Electrogenic Cells in Culture.* Biosensors and Bioelectronics, 1990. **5**(3): p. 223-234.

75. Keese, C.R., N. Karra, B. Dillon, A. Goldberg, and I. Giaever, *Cell-Substratum Interactions as a Predictor of Cytotoxicity.* In Vitro and Molecular Toxicology, 1998. **11**(2): p. 183-192.

76. Xiao, C. and J.H.T. Luong, *On-Line Monitoring of Cell Growth and Cytotoxicity Using Electric Cell-Substrate Impedance Sensing (ECIS).* Biotechnology Progress, 2003. **19**: p. 1000-1005.

77. Keese, C.R., J. Wegener, S.R. Walker, and I. Giaever, *Electrical Wound-Healing Assay for Cells In Vitro.* Proceedings of the National Academy of Sciences of the U.S.A., 2004. **101**(6): p. 1554-1559.

78. Wegener, J., C.R. Keese, and I. Giaever, *Recovery of Adherent Cells After In Situ Electroporation Monitored Electrically.* BioTechniques, 2002. **33**(2): p. 348.

79. DeBlasio, B.F., M. Laane, T. Walmann, and I. Giaever, *Combining Optical and Electrical Impedance Techniques for Quantitative Measurement of Confluence in MDCK-I Cell Cultures.* BioTechniques, 2004. **36**: p. 650-662.

80. Nguyen, D., X. Huang, D.W. Greve, and M.M. Domach, *Fibroblast Growth and H-7 Protein Kinase Inhibitor Response Monitored in Microimpedance Sensor Arrays.* Biotechnology and Bioengineering, 2004. **87**(2): p. 138-144.

81. Yu, N., J.M. Atienza, J. Bernard, S. Blanc, J. Zhu, X. Wang, X. Xu, and Y.A. Abassi, *Real-Time Monitoring of Morphological Changes in Living Cells by Electronic Cell Sensor Arrays: An Approach to Study G Protein-Coupled Receptors.* Analytical Chemistry, 2006. **78**: p. 35-43.

82. Brishwein, M., S. Herrmann, W. Vonau, F. Berthold, H. Grothe, E.R. Motrescu, and B. Wolf, *Electric Cell-Substrate Impedance Sensing with Screen Printed Electrode Structures.* Lab on a Chip, 2006. **6**: p. 819-822.

83. Choi, C.K., A.E. English, S. Jun, K.D. Kihm, and P.D. Rack, *An Endothelial Cell Compatible Biosensor Fabricated Using Optically Thin Indium Tin Oxide Silicon Nitride Electrodes.* Biosensors and Bioelectronics, 2007. **22**: p. 2585-2590.

84. Shackman, J.G., G.M. Dahlgren, J.L. Peters, and R.T. Kennedy, *Perfusion and Chemical Monitoring of Living Cells on a Microfluidic Chip.* Lab on a Chip, 2005. **5**: p. 56-63.

85. Brishwein, M., E.R. Motrescu, E. Cabala, A.M. Otto, H. Grothe, and B. Wolf, *Functional Cellular Assays with Multiparametric Silicon Sensor Chips.* Lab on a Chip, 2003. **3**: p. 234-240.

86. Hung, P.J., P.J. Lee, P. Sabounchi, N. Aghdam, R. Lin, and L.P. Lee, *A Novel High Aspect Ratio Microfluidic Design to Provide a Stable and Uniform Microenvironment for Cell Growth in a High Throughput Mammalian Cell Culture Array.* Lab on a Chip, 2005. **5**: p. 44-48.

87. Umehara, S., Y. Wakamoto, I. Inoue, and K. Yasuda, *On-Chip Single-Cell Microcultivation Assay for Monitoring Environmental Effects on Isolated Cells.* Biochemical and Biophysical Research Communications, 2003. **305**: p. 534-540.

88. Tourovskaia, A., X. Figueroa-Masot, and A. Folch, *Differentiation-on-a-Chip: A Microfluidic Platform for Long-Term Cell Culture Studies.* Lab on a Chip, 2005. **5**: p. 14-19.

89. Matsubara, Y., Y. Murakami, M. Kobayashi, Y. Morita, and E. Tamiya, *Application of On-Chip Cell Cultures for the Detection of Allergic Responses.* Biosensors and Bioelectronics, 2004. **19**: p. 741-747.

90. Williams, K.R., K. Gupta, and M. Wasilik, *Etch Rates for Micromachining Processing - Part II.* Journal of Microelectromechanical Systems, 2003. **12**(6): p. 761-778.

91. Delongchamp, D., *personal communication*. January 23, 2007.

92. Durstock, M.F. and M.F. Rubner, *Dielectric Properties of Polyelectrolyte Multilayers.* Langmuir, 2001. **17**(25): p. 7865-7872.

93. Tryoen-Toth, P., D. Vautier, Y. Haikel, J.-C. Voegel, P. Schaaf, J. Chluba, and J. Ogier, *Viability, Adhesion, and Bone Phenotype of Osteoblast-like Cells on Polyelectrolyte Multilayer Films.* Journal of Biomedical Materials Research Part A, 2002. **60**(4): p. 657-667.

94. Sabatani, E., J. Cohenboulakia, M. Bruening, and I. Rubinstein, *Thioaromatic Monolayers on Gold - A New Family of Self-Assembling Monolayers.* Langmuir, 1993. **9**(11): p. 2974-2981.

95. Chang, G.-H., S.-D. Lee, C.-C. Wang, M.H.-I. Shiue, and P.C.-T. Chang, *Plasma-Induced Graft Copolymerization of HEMA onto Silicone Rubber and TPX Film Improving Rabbit Corneal Epithelial Cell Attachment and Growth.* Biomaterials, 1994. **15**(3): p. 163-171.

96. Franks, W., I. Schenker, P. Schmutz, and A. Hierlemann, *Impedance Characterization and Modeling of Electrodes for Biomedical Applications.* IEEE Transactions on Biomedical Engineering, 2005. **52**(7): p. 1295-1302.

97. Gomez, R., A. Sarikaya, M.R. Ladisch, J. Sturgis, J.P. Robinson, T. Geng, A.K. Bhunia, H.L. Apple, S. Werely, and R. Bashir, *Microfluidic Biochip for Impedance Spectroscopy of Biological Species.* Biomedical Microdevices, 2001. **3**(3): p. 201-209.

98. McAdams, E.T. and J. Jossinet, *The Linear and Nonlinear Electrical Properties of the Electrode-Electrolyte Interface.* Biosensors and Bioelectronics, 1995. **10**: p. 67-74.

99. Barreira, S.V.P., V. Garcia-Morales, C.M. Pereira, J.A. Manzanares, and F. Silva, *Electrochemical Impedance Spectroscopy of Polyelectrolyte Multilayer Modified Electrodes.* Journal of Physical Chemistry B, 2004. **108**(46): p. 17973-17982.

100. Bard, A.J. and L.R. Faulkner, *Electrochemical Methods: Fundamentals and Applications, 2nd Ed.* 2001, Hoboken, New Jersey: John Wiley & Sons, Inc. 768.

101. Silva, T.H., V. Garcia-Morales, C. Moura, J.A. Manzanares, and F. Silva, *Electrochemical Impedance Spectroscopy of Polyelectrolyte Multilayer Modified Gold Electrodes: Influence of Supporting Electrolyte and Temperature.* Langmuir, 2005. **21**(16): p. 7461-7467.

102. Salomaki, M., K. Loikas, and J. Kankare, *Effect of Polyelectrolyte Multilayers on the Response of a Quartz Crystal Microbalance.* Analytical Chemistry, 2003. **75**(21): p. 5895-5904.

103. Luong, J.H.T., *An Emerging Impedance Sensor Based on Cell-Protein Interactions: Applications in Cell Biology and Analytical Biochemistry.* Analytical Letters, 2003. **36**(15): p. 3147-3164.

104. Ceriotti, L., J. Ponti, P. Colpo, E. Sabbioni, and F. Rossi, *Assesment of Cytotoxicity by Impedance Spectroscopy.* Biosensors and Bioelectronics, 2007. **22**: p. 3057-3063.

105. Berne, R.M., M.N. Levy, B.M. Koeppen, and B.A. Stanton, *Physiology*. 5 ed. 2004, St. Louis, MO.

106. Ceriotti, L., A. Kob, S. Drechsler, J. Ponti, E. Thedinga, P. Colpo, R. Ehret, and F. Rossi, *Online Monitoring of BALB/3T3 Metabolism and Adhesion with Multiparametric Chip-Based System.* Analytical Biochemistry, 2007. **371**(1): p. 92-104.

107. Rudolf, E., M. Cervinka, J. Cerman, and L. Schroterova, *Hexavalent Chromium Disrupts the Actin Cytoskeleton and Induces Mitochondria-Dependent Apoptosis in Human Dermal Fibroblasts.* Toxicology in Vitro, 2005. **19**: p. 713-723.

108. Gunaratnam, M. and M.H. Grant, *Damage to F-actin and Cell Death Induced by Chromium VI and Nickel in Primary Monolayer Cultures of Rat Hepatocytes.* Toxicology in Vitro, 2004. **18**: p. 245-253.

109. Bagchi, D., S.J. Stohs, B.W. Downs, M. Bagchi, and H.G. Preuss, *Cytotoxicity and Oxidative Mechanisms of Different Forms of Chromium.* Toxicology, 2002. **180**(1): p. 5-22.

110. Morgan, E., *Chemometrics: Experimental Design*. 1991, New York, New York: John Wiley & Sons.